Properties of Sealing Materials in Groundwater Wells

Köser, Claus

Publication date:
2011

Document Version
Accepted author manuscript, peer reviewed version

PROPERTIES OF SEALING MATERIALS IN GROUNDWATER WELLS

PhD Thesis
Defended in public at Aalborg University
(November, 2011)

Claus Köser

ISSN 1901-7294
DCE Thesis No. 29

AALBORG UNIVERSITY
Department of Civil Engineering

Aalborg University
Department of Civil Engineering

DCE Thesis No. 29

PROPERTIES OF SEALING MATERIALS IN GROUNDWATER WELLS

PhD Thesis defended in public at Aalborg University (November, 2011)

by

Claus Köser

July 2011

Scientific Publications at the Department of Civil Engineering

Technical Reports are published for timely dissemination of research results and scientific work carried out at the Department of Civil Engineering (DCE) at Aalborg University. This medium allows publication of more detailed explanations and results than typically allowed in scientific journals.

Technical Memoranda are produced to enable the preliminary dissemination of scientific work by the personnel of the DCE where such release is deemed to be appropriate. Documents of this kind may be incomplete or temporary versions of papers—or part of continuing work. This should be kept in mind when references are given to publications of this kind.

Contract Reports are produced to report scientific work carried out under contract. Publications of this kind contain confidential matter and are reserved for the sponsors and the DCE. Therefore, Contract Reports are generally not available for public circulation.

Lecture Notes contain material produced by the lecturers at the DCE for educational purposes. This may be scientific notes, lecture books, example problems or manuals for laboratory work, or computer programs developed at the DCE.

Theses are monograms or collections of papers published to report the scientific work carried out at the DCE to obtain a degree as either PhD or Doctor of Technology. The thesis is publicly available after the defence of the degree.

Latest News is published to enable rapid communication of information about scientific work carried out at the DCE. This includes the status of research projects, developments in the laboratories, information about collaborative work and recent research results.

Published 2011 by
Aalborg University
Department of Civil Engineering
Sohngaardsholmsvej 57,
DK-9000 Aalborg, Denmark

Printed in Aalborg at Aalborg University

2st edition 2011
ISSN 1901-7294
DCE Thesis No. 29

Preface

This dissertation is submitted in partial fulfillment of the requirements for the degree of Doctor of Philosophy. It is based on a study carried out in collaboration between VIA University Collage, Horsens, and Aalborg University, Department of Civil Engineering. Funding of the project was raised by VIA University Collage and Aalborg University.

The dissertation consists of an extended summary and four supporting papers. The papers have been submitted to the following journals: “Advanced Powder Technology”; “Applied Clays Science”; “Journal of Contamination Hydrology” and “Engineering Geology”.

The work has been carried out in the period June 2008 to May 2011 under the supervision of Associate Professor Michael Rasmussen (AAU), Associate Professor Lars Andersen (AAU) and Associate Professor Lotte Thøgersen (VIA). In addition to that, Søren Hansen who is the leading physicist at the PET-center, Aarhus University Hospital has been of great help regarding the CT work which has been performed during this project. Another thanks should go to Niels Schriver from the geotechnical institute in Aarhus for valuable discussions regarding construction of groundwater wells.

Finally, I would like to thank my colleagues for fruitful discussions, and my dear wife Alice for moral support and helpfulness during the course of the project.

Aalborg, July 22, 2011 Claus Köser

Summary

Denmark is the only country in the world which almost exclusively gets its drinking water from aquifers that are located relatively close to the terrain. There has been a large focus on the quality of drinking water in the last years. Denmark and Greenland Geological Survey (GEUS) has for many years collected data on water chemistry from groundwater wells throughout the country. Based on these data it has been found that the levels of pesticides and their degradation products have been exceeded in many cases. The content of pesticides and degradation products can be the results of leaky boreholes which in some cases can act as direct openings down to aquifers. The reasons for this may include bad or missing seal. In this context, Schmidt (1999) concluded that there is no proven way to make a clay seal with the desired tightness. This thesis deals primarily with the properties of bentonite pellets as sealing material in groundwater wells.

The way and the pattern, in which bentonite pellets are deposited, have been shown to have an effect on the swelling pressure of the bentonite seal. During the transport phase of pellets from the terrain to a given sedimentation depth, a sorting process takes place, which obviously has an influence on the deposition characteristics. Smaller pellets is pack more closely than the larger pellets, gives a greater bulk density. Tests of swelling pressure have been performed and it appears to be clear that two things have a significant influence on the maximum swelling pressure; i) the bulk density of the sample, and ii) whether the sample is sorted or unsorted.

CT scans (Computed Tomography) have been used to evaluate certain properties of bentonite seals in a limited volume. In this context, a set of algorithms to convert CT numbers (HU unit) into densities for clay/water systems has been developed. This method has successfully been used to evaluate e.g., macroporosity, homogenization of the bentonite seal during the hydration of water, hydraulic conductivity and the creation of channels in the bentonite seals.

Based on the results obtained in this Ph.D. thesis, a number of recommendations has been offered; i) a change regarding the production of pellets and ii) how sealing material must be treated in the actual construction of groundwater wells.

Summary in Danish

Danmark er det eneste land i verden der næsten udelukkende får drikkevand fra grundvandsmagasinerne der er beliggende relativt terræn nært. Der har af den grund været stor fokus på drikkevandets kvalitet. Danmarks og Grønlands Geologisk Undersøgelse (GEUS) har gennem en lang årrække indsamlet data for vandkemien fra grundvands-boringer i hele landet. På baggrund af disse data har man fundet ud af at grænseværdierne for bl.a. pesticider samt disses nedbrydningsprodukter er overskredet i en lang række tilfælde. Indholdet af pesticider og nedbrydningsprodukter tilskrives bl.a. utætte boringer der i visse tilfælde kan fungere som direkte åbninger ned til grundvandsmagasinerne. Grunden hertil kan bl.a. være dårlig eller manglende forsegling. I den forbindelse har Schmidt (1999) konkluderet at der ikke er nogen dokumenteret måde at lave lerforsegling med den ønskede tæthed. Denne afhandling omhandler primært egenskaberne for bentonit pellets som forseglings materiale i grundvandsboringer.

Måden hvorpå, samt det mønster hvormed bentonit pellets aflejre sig på har vist sig at have en effekt på det svelletryk, man kan forvente at se i en given aflejring. Under transportfasen af pellets fra terræn og til en given aflejringsdybde sker der en sortering efter størrelse, hvilket selvfølgelig har en indflydelse på aflejringens beskaffenhed. De mindre pellets pakker sig tættere end de store, hvilket giver en større bulk densitet. Der har været udført svelletryksforsøg og det viser sig klart at to ting har en markant indflydelse på det maksimale svelletryk; i) bulk densiteten af prøven, og ii) om prøven er sorteret eller usorteret.

CT scanninger (Computed Tomography) er blevet benyttet til at evaluere visse egenskaber for bentonit forseglinger i et afgrænset volumen. I den forbindelse er der blevet udviklet et sæt algoritmer til at omregne CT tal (HU enhed) til densiteter i for ler/vand-systemer. Denne metode er følgende blevet brugt med succes til at evaluerer bl.a. makroporøsitet, homogenisering i forbindelse med optagelse af vand samt hydraulisk konduktivitet og kanaldannelse i forseglinger.

På baggrund af de opnåede resultater gives en række anbefalinger til ændring vedr. produktionen af pellets samt hvordan forseglingsmaterialet skal behandles i forbindelse med konstruktionen af grundvandsboringer.

List of Supporting Papers

The present thesis is written as a collection of scientific papers. It includes a joint introduction which describes the background for the publications and a presentation of the main results. The publications included in the thesis are the following:

I. Köser, C., Rasmussen, M., Thøgersen, L., and Andersen, L. 2011. Prediction of the depositional pattern of bentonite pellets in groundwater wells by evaluation of particle segregation (submitted to *Advanved Powder Technology*)

II. Köser, C., Andersen, L., Thøgersen, L., and Rasmussen, M. 2011. Swelling behavior of Bentonite pellets in Groundwater wells as a function of the degree of sorting (submitted to *Engineering Geology*)

III. Köser, C., Hansen, S. B., Andersen, L., Rasmussen, M., and Thøgersen, L. 2011. Evaluation of computed tomography as a tool for characterizing homogenization the and hydration process of a bentonite seal (submitted to *Applied Clays Science*)

IV. Köser, C., Andersen, L., Rasmussen, M., Thøgersen, L., and Hansen, S. B. 2011. Evaluation of the hydraulic conductivity and the development of channel systems and internal pathways in a bentonite seal (submitted to *Journal of Contamination Hydrology*)

Supporting papers will be referred to by their roman numbers, e.g., (Paper I). The publications listed above can be found in Appendices 4-7.

Contents

Chapter 1

Introduction

1.1. Presentation of the Problem

Denmark is the only country in the world where drinking water almost exclusively is extracted from groundwater aquifers. It is therefore important that the groundwater is monitored and examined closely. All existing data related to groundwater are recorded by GEUS (The Geological Survey of Denmark and Greenland). During the last 6-7 years, the annual consumption of groundwater in Denmark has been between 600 and 700 million m^3. In 2005, the amount of groundwater extracted from waterworks was estimated to be 65% of the total groundwater supply. Field irrigation and aquaculture accounted for 26% (Thorling, 2007).

As part of the national groundwater monitoring program, GEUS has, in 2007, issued a report which dealt with the status and the development of the groundwater. The report is based on data collected by the counties in the period 1989 to 2006 and data from the waterworks and self-monitoring data from other groundwater studies. The groundwater monitoring program includes 74 survey areas with a total of approx. 1,400 wells (Thorling, 2007). The extent of the monitoring program set out, is outlined in the report "NOVANA – the national monitoring program concerning Water Environment and Nature", DMU (2005). The report concludes that the discovery of pesticides and their degradation products increases. Also the finds which exceed the quality limit in drinking water at 0.1 µg/l have increased continuously. The reason for this is that, since 2004, groundwater samples has only been analyzed for pesticides and degradation products in wells which are screened in relatively high-lying aquifers. This means that groundwater is relatively young (Thorling, 2007). The same conclusion was reached by Brusch (2004) who concluded that the levels of banned pesticides that exceed the threshold values were seen in more than 30% of the cases studied.

From 1991 to 2003 there was found evidence of pesticides and degradation products in up to 35% of the waterworks (including abandoned wells), and in 12% of the cases the limit was exceeded (Brusch, 2004 and Brusch et al., 2004). Thorling (2007) concludes that the incidence of discovery of the pesticides and degradation products in waterworks has declined steadily from 2003. There is still found pesticides or degradation products in 25% of the waterworks wells. This downward trend in the amount of pesticides or degradation products does not give a true picture of the current pollution situation in areas surrounding the waterworks wells. It should only be seen as a result of closing down wells in which contamination is already present.

Contaminants are able to move down through the soil column by two different routes; natural- and anthropogenic routes.

1.1.1. Natural transportation routes

The transport of water and pesticides from the surface to the groundwater reservoir is highly dependent on the geology of the area. In areas where the sediments in the unsaturated zone are mainly composed of fluvial meltwater sand, the surface water and the pesticides can move freely and unhindered down through the formations due to the high porosity and permeability. In areas consisting mainly of till deposits, the movement of water and pesticides is markedly slower. It is known from studies in Denmark and abroad that the clayey till contains large cavities in the form of cracks and holes made of worms and roots (called makropores), which affects the transport conditions. In Denmark there is contamination found in moraine clay containing cracks which reach more than 9 meters below the ground surface (Gravesen et al., 2000).

1.1.2. Anthropogenic transportation routes (pathways associated with leaking wells)

In general, the groundwater in Denmark is placed in reservoirs which consist of sandy deposits. In many cases those water bearing sand layers are sealed on top by impermeable clay deposits, which protects the groundwater reservoir against contamination seeping down from the surface. When groundwater is extracted it is necessary to drill through those protecting clay layers after which the clean groundwater is exposed to a potential contamination risk.

A leaky well can be defined as a well which is contaminated by direct down seeping or down seeping of surface water or by water from the surface near the groundwater reservoirs (Jacobsen, 1999). There are several different scenarios which have to be taking into account regarding leaky wells. Schmidt (1999) has described three kind of possible pathways for contamination which are all in connection with conditional failures of the construction of the well:

1. leakage regarding the construction of the well closing,
2. leakage in the pipe coupling,
3. leakage caused by insufficient or missing sealing materials.

(Figure 1.1 shows a sketch which illustrates the three mentioned pathways)

The sealing is normally used in intervals which consist of an impermeable layer, in order to i) separate water bearing layers and ii) prevent contamination to reach the groundwater reservoir through the well.
In 1978 the law regarding water supply was taking into action and in 1980 the well drilling notice was made. In this notice, a series of instructions and requirements for construction and equipping groundwater wells and raw water stations was mentioned. According to the Danish Standards (DS 442) the cavity between the geological formation and well screen, in an impermeable clay interval, should be filled with 1 meter of watertight material to avoid seepage outside of the well screen.

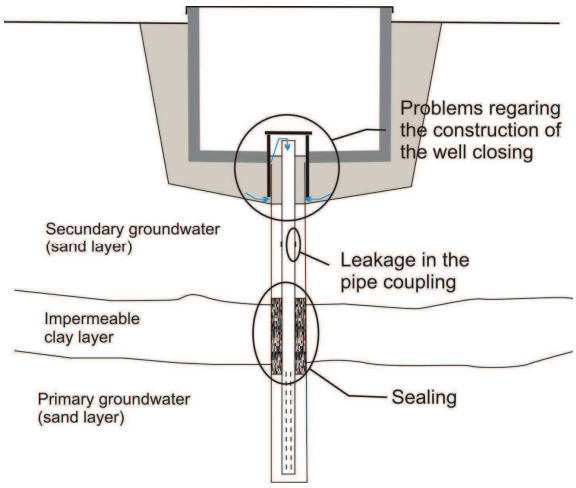

Figure 1.1: Examples of contamination pathways caused by failure of the construction of the well (modified after Schmidt, 1999).

The well drilling notice has since been revised and in July 2007 the latest revision was made. It states that "*the space between the screen and the surrounding soil layers must be sealed by backfilling with material of such a nature that groundwater is not contaminated by seepage along the screen and so that unwanted water exchange between the various magazines does not occure*" (Miljøstyrelsen, 2007).

Regarding item 3, Schmidt (1999) concluded that there has been no documented ways to make clay sealings with a sufficient tightness. This consideration is supported by Jacobsen (1999) who also mentions insufficient sealing as a possible pathway for contamination. Andreasen (1999), Lorentzen (1999), Skovgård et al. (2001), Thorling og Jensen (2002) and Laier (2002) also mention that possibility. At present time no serious attempt to evaluate the properties of bentonite seals in gronudwater wells has been made.

1.2. State of the Art

In the following, a review will be given of some of the methods, which have been proposed in the literature for the analysis of the different properties of bentonite clay. The review has been subdivided into different classes of solution techniques.

1.2.1. Transport, sorting and depositional pattern

There has been done a lot work on how particles with different sizes and shapes move down through a column of water. When a particle is falling through any given liquid in an unconfined environment, its terminal velocity is reached when the gravitational force is exactly equal to the resistance force which includes buoyancy and drag. The drag force depends on determination of the drag coefficient. Many correlations have been developed and presented in the literature relating the

drag coefficient (C_d) to the Reynolds Number (Re) for particles of spherical shape falling at their terminal velocity. See Gibatto and Tsouris (2008) for references. Numerous of correlations have been made on non-spherical particles. Among all the correlations of drag coefficients, Chabra et al. (1999), selected four promising methods that predict drag coefficients and terminal velocities of settling non-spherical particles (Haider and Levenspiel, 1989; Ganser, 1993; Hartman et al., 1994; and Swamee and Ojha, 1991. All these methods entail the use of the equal volume sphere diameter as the characteristic linear dimension. Furthermore the first four methods employ the widely used sphericity to quantify the extent of departure from spherical shape; Swamee and Ojha (1991) preferred the so-called Corey's shape factor. Both sphericity and Corey's shape factor have merits and demerits. First of all it is difficult to evaluate sphericity for irregularly shaped particles. When deciding the drag coefficient for cylindrically shaped particles it is necessary to identify which type of motion the particle is in. The mode of motion is determined by the aspect ratio. This phenomenon has previously been described by Isaacs and Thodos (1967). The same authors also described a correlation of drag coefficient which only depend on aspect ratio (L/d) and density ratio (ρ_s/ρ_f).

In addition to the authors mentioned above, the following authors have worked with drag and should be mentioned as well; Nitin and Chhabra (2006) have worked with the drag on circular disks in power law fluids and Rajitha et al. (2006) have worked with drag on non-spherical particles in non-Newtonian media.

To test the velocity of a single pellet in a water medium, the wall effect should be taken into account. It is customary to introduce a wall factor, f, to quantify the extent of wall effects on the steady-settling motion of a particle (Chakraborty et al., 2004.; Chhabra, 1995 and 1996.; Song and Gupta, 2009). One of the simplest definitions of the wall factor, f, is the ratio of the terminal velocity, V, of a particle in a bounded medium to that in an unbounded medium, V_0:

$$f=V/V_0 \qquad (1.1)$$

The following authors have also worked with wall effect and should be mentioned as well; Lali et al., (1989), Chhabra et al., (2003), and Kaiser et al., (2004). It should be mentioned that this is only a small fraction of all the literature produced which concern the drag coefficients and wall effect on moving particles during transport.

1.2.2. Microstructural evolution of the bentonite clay during hydration

By using a microfocus x-ray computed tomography (μCT, x-ray microscope), Kozaki et al. (1999 and 2001) and Tomioka et al. (2008) have shown a heterogenic hydration pattern in multiple bentonite grains. In both cases Kunipia-F bentonit was used which is commercially available from Kunimine Industries, Japan. The bentonite was an Na^+-type bentonite which contained more than 95 wt.% montmorillonite. The montmorillonite was purified into homoionic Na^+-type montmorillonite, ground by mortar and pestle, and then sieved to obtain a grain size of 75–150 μm, as described elsewhere. The purified montmorillonite samples were then compacted to a dry density of 1.000 kg/ m^3.

By comparing grains in water-saturated samples with grains from a dry sample it were found that the water saturated samples was smaller than those in the dry sample. To compare them quantitatively, the mean diameter distribution of the water-saturated montmorillonite grains was analyzed with a computer code together with that of the dry sample (Tomioka et al., 2008). Realizing that the grain sizes could be overestimated in the image of the water-saturated sample, it is obvious that the grain sizes decreased with the water saturation. Furthermore it was showed, by using x-ray diffraction, that the montmorillonite samples have a dense fragment even after water saturation. It was also showed that the aspect ratio of the dry grains did not change significantly after water saturation. Then, except the region of the open grain boundaries, it can be supposed that the outer montmorillonite sheets of grains swelled and formed a gel, whereas the inner sheets did not change significantly in the water-saturation process, as illustrated in Figure 1.2.

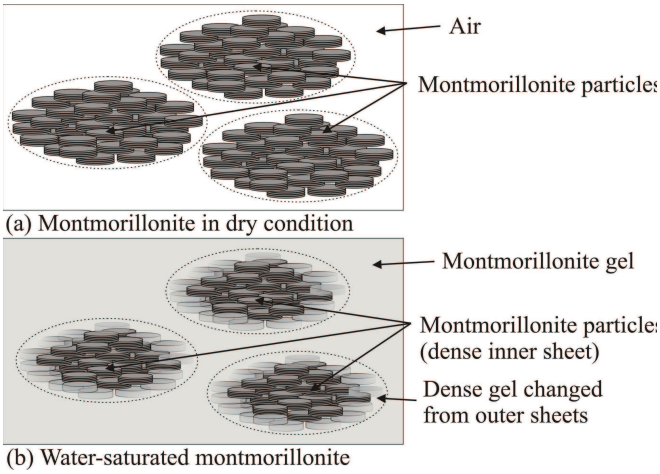

Figure 1.2: Schematic of the structures of montmorillonite: (a) in dry state, (b) in water saturated state (modified after Tomioka et al., 2008)

This general result is supported by Pusch (1999). He worked with MX-80 clay, which is a Na^+-type bentonite. Monte et al. (2003) showed that this bentonite type contained 70,6±2,7 % montmorillonite. The diameter of the big grain was 0.35 mm and 0,1 mm for the small grains. Each grain contains tens of hundreds of millions or even billions of stacks of montmorillonite lamellae. The grains were compacted to a dry density of ca. 1,200 kg/m^3 which corresponds to a density of 1,800 kg/m^3 in saturated form. The stress conditions in the grains and in the contact zone between the grains are shown in Figure 1.3. for a section through the centres. It can be seen that the stress is highest at the inner sheet with decreasing values towards the surface of the grain (outer sheet). In the inner shell (zone with high stress) water will be totally expelled from the interlamellar space. The outermost parts of the grain, which are stress-free, absorb water from the inner part of the grain and the surrounding (Pusch, 1997). The densest parts of the grains have highest hydration potential and become wetted quickly if the cell is free to expand, but hydration is resisted if there is an

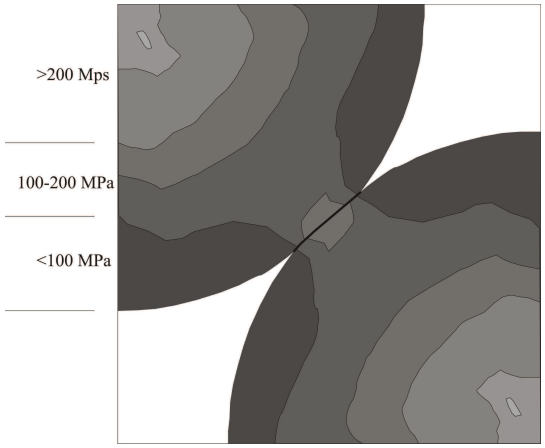

Figure 1.3: Stress distribution in the grain.
Note that the stress increases towards the center of the grain and in the contact zone between the grains. The section is through the center of the grains (modified after Pusch, 1999).

external pressure or confinement. The rate of water uptake is controlled by the capacity of the surrounding clay matrix to provide water, which means that its hydraulic conductivity is a controlling factor of the wetting and expansion process.

During the hydration process, Pusch (1999) concluded that the expansion of the bentonite grains has two forms, primarily growth in thickness of dense aligned aggregates of stacks by ca. 30 %, and the formation of very soft clay gels by coagulation of clay particles that are exfoliated from the dense aggregates. This suggests that the voids between the expanding grains will be occupied by soft clay gels with varying density and degree of filling.

Kawaragi et al. (2009) used X-ray CT technology to observe the bentonite–quartz sand mixtures. It was shown that 'vacant pores' and 'bentonite–water complexes' of the bentonite samples after water permeation are distinguishable in X-ray CT images. The micro-structural differences are closely relating to the sample permeability, and depend on the mixing and saturation conditions. Permeability tests and X-ray CT observations of the bentonite samples show that the permeability and the microstructure are independent to the sedimentary texture developed within the ore samples. In addition, it is characteristic that the bentonite samples with micro-cracks show low hydraulic conductivity, comparable to the compacted powder bentonite, implying that cracks in the sample are filled with 'bentonite–water complexes' formed after permeation.

In addition to the authors mentioned in the examples above, the following authors should be mentioned as well; Bohloli and Pater (2006), made an experimental study on hydraulic fracturing of unconsolidated rocks focusing on mechanisms of fracture initiation and propagation using different injection fluids at various confining stresses. Pusch and Weston (2003) have worked with the microstructural stability that controls the hydraulic conductivity of smectitic buffer clay. Pusch and Schomburg (1999) have worked with the impact of microstructure on the hydraulic conductivity of undisturbed and artificially prepared smectitic clay. Tang et al. (2008) have worked with the influencing factors of geometrical structure of surface shrinkage cracks in clayey soils, and Vogel et al. (2005 I and II) have studied the crack dynamics in clayey soil.

1.2.3. Macrostructural evolution of bentonite clay during hydration

Van Geet et al. (2005) described the nature of hydration of a mixture of FoCa- clay powder and pellets based on microfocus X-ray computed tomography (μCT, x-ray microscope). The FoCa-clay is from the Paris Basin, extracted in the Vexin region. The major component (i.e. 80% of the clay fraction) is an interstratified clay of 50% calcium beidellite and 50% kaolinite. It contains also kaolinite, quartz, goethite, hematite, calcite and gypsum (Coulon, 1987; Lajudie et al., 1994). The pellets are produced by compacting the FoCa powder. Different shapes and sizes of pellets have been tried, in order to obtain a high dry density. The best result was obtained with pellets of approximately 25x25x15 mm^3 of size.

A plexiglass, cylindrical cell (88 mm outer and 38 mm inner diameter) was designed with quick connectors at the bottom for water injection and gas escape routes at the top (Figure 1.4). The cell was filled with a mixture of 50% of pellets and 50% of powder and compacted to a dry density of 1.36 g/cm^3. 56.77 g of pellets and 57.69 g of powder were used. Within the powder surrounding the pellets, a lot of macroporosity, was observed. It was showed that the distribution of the porosity was not homogeneous, which was related to the sample preparation. Indeed, during the filling of the

cylinder with mixture of FoCa-clay powder and pellets, the largest particles tumbled in first, causing more macroporosity at the bottom of the sample. It is therefore concluded that the depositional pattern of the pellets plays an important role when the properties of the final sealing is evaluated.

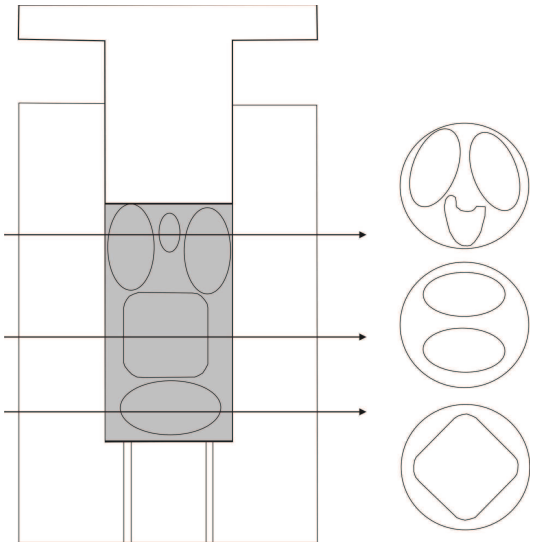

Figure 1.4: Schematic view of the plexiglass cell. The orientation of the pellets is illustrated. The grey colour corresponds with the position of powder and pellets mixture of FoCa-clay (modified after Van Geet et al., 2005).

In order to simulate real condition, water was first injected at very low pressure, so suction of the water by the clay was the dominant process. This was maintained for six weeks. Hereafter, the sample was injected with water at 5 bars during 4 month (22 weeks). Finally, a permeability test at 6 bars was performed during two months (30 weeks). After two weeks of hydration at very low pressure (suction was the dominant process), a distinction between the pellets and the powder could still be made. At this point, there is a clear difference of the powder surrounding the pellets in the top and in the bottom. The mean density of the powder at the bottom has increased from about 1 g/cm^3 to 1.6 g/cm^3. The mean density of the powder at the top of the sample has not changed and is still around 1.3 g/cm^3. After 1 month at low pressure, the pellet can still be distinguished. The mean density of the pellet has not changed, but the mean density of the powder surrounding the pellet at the bottom, has increased from 1.6 g/cm^3 to 1.7 g/cm^3 and the powder at the top has increased from 1.3 g/cm^3 to 1.4 g/cm^3. After 1 month at high pressure (5 bars) the whole sample has obtained a mean density of 1.8 g/cm^3 and 1.63 g/cm^3 in corners. However, homogenisation is not complete, as the bottom of the sample fractures within the mixture can be observed. After 4 month at high pressure (5 bars) the observations has not changed. At the bottom of the sample the fracture outline are still present. After the permeability test at 6 bars, no structural changes have been noticed. The sample now has a mean density of 1.9 g/cm^3. The bottom corners of the sample are still somewhat lower in density, however the fractures were no longer observed. The question rose whether these fractures are related to the original position of a pellet? It was concluded that the previously mentioned fractures occurred at the pellet/powder interface. It was also concluded that the pellet/powder mixture seems to have a memory of the original position of the pellets and the outline of the pellet is a weak point within the mixture along which fractures are more easily developed. When finishing permeability test at 6 bars, the sample was dismantled and dried. A water content of ca. 38% was measured. After drying, the sample was broken in two half cylinders and showed several fractures. The distribution of the fracture pattern was compared with the original position of the pellets. However all fracture seemed to be orientated randomly and no correlation with the original pellet position was found by visual inspection. The overall conclusion is that a homogenisation between pellets and powder only occurs after an injection of water at 5 bars. This means that hydration at very low pressure, where suction was the dominant process, is

not sufficient for a complete homogenisation to take place. By suction alone a heterogenic distribution of densities throughout the sample should be expected. By examining another type of clay (Boom Clay, Belgian), Van Geet et al. (2007 and 2008), concluded that the location of the fractures throughout the whole volume of the sample is limited to the low density zone. This result was indirectly supported by Oscarson et al. (1996). Here the general conclusion was that the hydraulic conductivity in bentonite samples decreases when the dry density increases.

In addition to the authors mentioned in the examples above, the following authors all worked with bentonite pellet mixtures; García-Gutiérrez et al. (2004) have made diffusion experiments with compacted FoCa powder/pellets clay mixtures and Maugis and Imbert (2007) have made experiential and numerical modeling on confined wetting, also with FoCa powder/pellets clay mixtures. Hoffman et al. (2007) and Imbert &Villar (2006) have examined the hydro-mechanical behavior of a bentonite mixture and a bentonite/powder mixture respectively. Pusch et al. (2003) have studied the performance of strongly compacted MX-80 pellets under repository-like conditions. Suziki et al. (2005) have shown that the fraction of macropores among bentonite pellets/aggregates increases with NaCl concentration under highly saline conditions.

1.2.4. Swelling behavior of different expanding clay mixtures

Up until today a lot of work has been done regarding quantification of the swelling pressure for several bentonite types. One common thing is that we are dealing with homogenous samples with no macroscopic pore space.

Langrodi and Yasrobi (2009), have worked with swelling behaviour of unsaturated expansive soils (homogeneous samples). No mathematical model to describe the evolution of swelling pressure was presented. Thus, it was concluded that the structure of compacted clay play an important role in the mechanical behaviour, e.g. swelling pressure. This is supported by Sivakumar et al. (2006).

Agus and Schanz (2006) presented an approach for predicting the swelling pressure of bentonite/sand mixtures based on thermodynamic relationships between swelling pressure and suction. Not surprisingly the sorption curve of the bentonite is found to follow a straight line on the semi-logarithmic plot of water content versus suction for a quite wide range of suction, indicating that the water content of the bentonite is logarithmically related to suction. No mathematical model to describe the evolution of swelling pressure was presented.

Lloret and Villar (2007) have worked with the thermo-hydro-mechanical (THM) behaviour of heavily compacted ‘‘FEBEX’’ bentonite. The main focus was to establish the influence of temperature and water salinity on the THM behaviour of the bentonite. A simple model to describe the evolution of swelling pressure was proposed. A regression curve was derived for the swelling pressure of the FEBEX bentonite at laboratory temperature as a function of dry density. This is expressed by the following equation:

$$P_s = \exp(6.77\rho_d - 9.07) \qquad (1.2)$$

where P_s is the swelling pressure (MPa), and ρ_d is the dry density, in g/cm^3. The deviation of the experimental values with respect to this fitting may be as high as 25%.

Komine and Ogate have made a lot of work regarding swelling characteristic on different types of bentonites and bentonite/sand mixtures. Komine and Ogate (1994) made a experiential study on swelling characteristics of compacted bentonite. The tested material was a commercially produced bentonite from Tsukinuno Mine in Japan. This sodium bentonite contains about 48% montmorillonite. Regarding the swelling pressure, the following conclusions were drawn: The maximum swelling pressure increases exponentially with increasing initial dry density, whereas the maximum swelling pressure is almost independent of the initial water content; furthermore, the maximum swelling pressure of compacted bentonite was found to be strongly dependent on the montmorillonite content and the compaction pressure when the sample is produced.

Komine and Ogate (1999), made an experimential study on swelling characteristics of sand-bentonite mixture. The tested bentonite material was the same as previously mentioned (48% montmorillonite), but this time it was mixed with Mikawa silica sand. Five tests were made. The bentonite content of the mixtures was 5%, 10%, 20%, 30%, and 50%. The results are seen in Table 1.1. Basically the same conclusion were drawn in this paper as in previous papers from Komine and Ogate. No mathematical model to describe the evolution of swelling pressure was presented.

Table 1.1: Show the bentonite content versus the maximum swelling pressure

Bentonite content	Montmorillonite content (48%)	Swelling pressure (kPa)
5%	2.4%	30.9
10%	4.8%	42.9
20%	9.6%	98.2
30%	14.4%	170.5
50%	24%	270.0

In this study they also propose a simplified evaluation of the swelling characteristics of sand-bentonite mixtures using the parameter ”swelling volumetric strain of montmorillonite”. The parameter is defined as; ε^*_{sv} is the percentage volume increase of swelling deformation of montmorillonite. It is expressed by the following equation:

$$\varepsilon^*_{sv} = ((V_v+V_{sv})/V_m) \text{ x } 100 \text{ (\%)} \qquad (1.3)$$

where V_m is the volume of montmorillonite in the sand-bentonite mixture, V_v is the volume of voids, and V_{sv} is the maximum swelling deformation of the mixture at constant vertical pressure ($V_{sv} \geq 0$, $V_{sv} = 0$ in the swelling pressure test).

Made by the same authors, the attention should also be made on the following papers, which all concerns the study on swelling characteristics of different kinds of bentonites and sand-bentonite mixtures; Komine and Ogata (1996a, 1996b, 1997, 2003, 2004).

Komine (2004) studied the swelling pressure for four types of bentonites, all with a different content of montmorillonite. Again it was concluded that the maximum swelling pressure is strongly influenced by the montmorillonite content. No mathematical model to describe the evolution of swelling pressure was offered.

1.2.5. Hydraulic conductivity of bentonite clay

Hasenpatt et al. (1989) discussed the two transport mechanisms which can be distinguished in clay: (1) diffusion, for which the propelling force is the concentration gradient of the diffusing ions; and (2) flow, for which the propelling force is the water pressure gradient. The material of interest

was a calcium-bentonite. The hydraulic conductivity was found to be in the range of $2.8*10^{-9}$ to $1.5*10^{-6}$ m/s.

Oscarson et al. (1996) was working with mass transport through defected bentonite plugs. The Avonlea bentonite used in the buffer is from the Bearpaw Formation of Upper Cretaceous age in southern Saskatchewan. The clay contains approximately 80 wt% smectite (montmorillonite), 10% illite, 5% quartz and minor amounts of gypsum, feldspar and carbonate (Oscarson and Dixon, 1989). The Avonlea bentonite is a component of the buffer material - a 1:1 mix by dry mass of bentonite and silica sand compacted to a dry density, ρ_b, of 1.67 Mg/m ^{3}. In this work they also worked with diffusion and flow as the propelling forces. The main conclusion was that the diffusion processes dominate mass transport through earthen materials when K is less than about 10^{-10} to 10^{-9} m/s. This was also supported by Rowe (1987) and Gillham and Cherry (1982).

Villar and Rivas (1994), have worked with the hydraulic properties of montmorillonite-quartz and saponite-quartz mixtures. The work presented is part of a project of characterization of Spanish clays to be used as backfill and sealing materials in high-level radioactive waste repositories. The hydraulic conductivity of the studied Spanish clays is lower than 10^{-12} m/s for clay dry densities higher than 1.45 g/cm^3 for montmorillonite. The addition of quartz could reach percentages of 40% without changing these properties.

Pusch and Schomburg (1999) have worked with the impact of microstructure on the hydraulic conductivity of undisturbed and artificially prepared smectitic clay. They found that the microstructure, controls most physical properties of clays. This is obvious when comparing natural smectitic clay and clay prepared by drying, grinding and compression of air-dry powder. The hydraulic conductivity of the artificially prepared clay was found to be higher than that of the undisturbed, natural clay. If the latter clay is percolated with distilled water and Ca-rich water, the difference in conductivity is obvious, while percolation of the natural clay with these solutions does not yield a very dramatic change. This is because the microstructure of the natural clay is very homogeneous, while the artificially prepared clay preserves the high density of the powder grains while the gels in the voids between the grains are soft.

Villa et al. (2008) have worked on how to modify of hydraulic properties of bentonite by thermo-hydraulic gradients. The test has been performed with a bentonite from the Cortijo de Archidona deposits (Almeria, Spain). The bentonite has a content of dioctahedic smectite of the montmorillonite type higher than 90% as determined by x-ray diffraction. The main conclusion from this work was that the measurement of saturated hydraulic conductivity performed after the thermo-hydraulic (TH) treatment revealed even an increase of saturated permeability with respect to untreated samples and a strong dependence on dry density.

Komine (2008) have purposed theoretical equations on hydraulic conductivities of bentonite-based buffer and backfill for underground disposal of radioactive wastes. The study proposes a predicting method for hydraulic conductivity of two montmorillonite parallel-plate layers. The method allows for the influence of Na^+, Ca^{2+}, K^+, and Mg^{2+}, the main exchangeable cations of bentonite. Results demonstrate that the theoretical equations proposed in this study can predict hydraulic conductivities of sodium bentonite-based buffer and backfill materials at various dry densities and bentonite contents of 20% or more with high accuracy.

Komine (2010) predicted the hydraulic conductivity of sand–bentonite mixture backfill before and after swelling deformation for underground disposal of radioactive wastes for samples with different bentonite content. The model which was purposed in 2008 by the same auhtor was confirmed in this paper.

1.2.6. The use of computed tomography (CT) in soil science

Anderson et al. (1990) have worked with the evaluation of constructed and natural soil macropores using x-ray computed tomography. Among other things they refer to Petrovich et al. (1982) who claim that the mean bulk density in a soil core is linearly related to the mean x-ray attenuation coefficient of the core. The test material were taken in October 1988 from the A horizon of a Menfro silt loam (fine-silty, mixed, mesic Typic Hapludalf) soil near Rocheport, Missouri. Using the air-dried soil, three soil cores were each packed to bulk densities of 1.3, 1.4 and 1.5 g/cm^3. The soil was packed into 76.2-mm internal diameter. by 76.2-mm high plexiglas rings using a hydraulic press. These packed soil cores were used to calibrate the CT scanner for bulk density determination as indicated by Anderson et al. (1988). Pires et al. (2002) have used gamma-ray computed tomography to characterize soil surface sealing. Variation in gray levels correspond to differences in the attenuation coefficients and consequently, to differences in soil density at each point. Soil samples were collected in cylinders of 3 and 5 cm height at the soil surface. The calibration of the tomograph was obtained through the correlation between linear attenuation coefficients (m) of different materials using the gamma ray transmission method, and the respective tomographic units (TU) (Naime, 2001; Cássaro, 1994). Pires et al. (2005) γ-ray computed tomography to analysis of soil structure before density evaluations. In this work the conclusion regarding dry density was the same.

Wildenschild et al. (2002) start to work with systems, resolutions, and limitations of x-ray computed tomography in hydrology. A combination of advances in experimental techniques and mathematical analysis has made it possible to characterize phase distribution and pore geometry and to delineate air–water interfacial contacts in porous media using non-destructive x-ray computed tomography (CT). Later Ketham et al. (2005) used x-ray computed tomography and digital image analysis (DIA) to improve methods for quantitative analysis of three-dimensional porhyroblastic textures.

Van Geet et al. (2005) have worked with the use of microfocus X-ray computed tomography in characterising the hydration of a clay pellet/powder mixture. This study aimed to visualise and characterise the hydration of a mixture of FoCa-clay pellets and powder. The FoCa-clay is a sedimentary clay from the Paris Basin, extracted in the Vexin region. The major component (i.e. 80% of the clay fraction) is an interstratified clay of 50% calcium beidellite and 50% kaolinite. It contains also kaolinite, quartz, goethite, hematite, calcite and gypsum (Coulon, 1987; Lajudie et al., 1994). The pellets are produced by compacting the FoCa powder. Different shapes and sizes of pellets have been tried, in order to obtain a high dry density. For a quantitative analysis of the images, real density images would be much easier to interpret. For this purpose, a good calibration has to be set up to convert the measured linear attenuation coefficients into density values (Mees et al., 2003 and references therein). The measured linear attenuation coefficient depends on the density (q) and atomic number (Z) of the object and on the used X-ray energy (E) as:

$$\mu = \rho\left(a + b\frac{Z^{3.8}}{E^{3.2}}\right) \quad (1.4)$$

with a and b representing instrument dependent parameters (Rutherford et al., 1976a,b; Avrin et al., 1978; Pullan et al., 1981; Lehmann et al., 1981; Stonestrom et al., 1981; Curry et al., 1990; Gingold and Hasegawa, 1992).

In addition to the above mentioned authors, the following should be mentioned as well. Iassonov et al. (2009) have used segmentation of X-ray computed tomography images for characterization and quantitative analysis of pore structures and Martínez et al. (2010) have worked with multifractal analysis of discretized X-ray CT images for the characterization of soil macropore structures.

1.3. Objectives

As can be seen in section 1.2. a lot of work has been done so far regarding e.g. *transport and sorting of particles, micro- and macrostructural evolution of bentonite clay during hydration, swelling characteristic, hydraulic conductivity*, and *the use of CT technology in soil science*. Never the less, non of the above mentioned works has focused on bentonite pellets as a sealing material in groundwater wells. In this work the focus will be on how bentonite pellets is transported and deposited in a confined space and how swelling- and hydration characteristic is influenced by the a given depositional pattern. To examine that, a new set of algorithme is developed in orter to concerte CT numbers into real densities. This methode is also used to evaluate the hydraulic conductivity of a bantonite sealing.

This dissertation addresses factors controlling the properties of sealing materials in the groundwater wells. The content of the dissertation is based on results presented in **Paper I-IV.** The following chapters describe and discuss:

(i) Prediction of depositional pattern based on the nature of sorting during transport

(ii) Swelling pressure based on the degree of sorting of bentonite pellets

(iii) Computed tomogrephy (CT) as a tool for evaluating clay/water systems

(iv) Prediction of the physical properties of a sealing plug based on CT technology

(v) Creation of channels in the sealing plug.

Part 1

Swelling behavior as a function of size distribution

The main focus in this part will be on the swelling pressure of a bentonite seal.

It has been showed that the higher the bulk density in the bentonite plug, the higher the swelling pressure of the sealing material will be (Komine, 2004; Castellanos et al., 2008). Sealing material (in the form of bentonite pellets) show a large degree of size variations. When multiple pellets are dropped into waterfilled bore holes the pellets will be sorted according to their size which again will affect the depositional pattern. Small pellets will be packed more closely than larger pellets. A closely packed interval will have a higher bulk density than intervals which are not so closely packed.

Chapter 2: Particle segregation and sorting during transport

Chapter 3: Swelling pressure as a function of bulk density

Chapter 2

Particle segregation and sorting during transport

2.1. Introduction

Industrially produced bentonite pellets show a large degree of heterogeneity in size, which means that the velocities of a bundle of bentonite pellets show a great deal of variation. Because of that, a particle segregation of bentonite pellets which travel in a bundle will take place during the transport phase (Schalla and Walters, 1990; Escudié et al., 2006). The bentonite pellets are segregated according to their size which has an important impact on the final depositional pattern. Smaller particles will be packed more densely than larger particles. A densely packed interval in the sealing plug will have a higher bulk density than intervals which are closely packed (Figure 2.1). It has been shown that the higher the bulk density in a bentonite clay, the higher the swelling pressure will be (Komine, 2004; Castellanos et al., 2008). It has also been shown that if the bulk density increases, the hydraulic conductivity of the bentonite clay will decrease (Cuevas et al. 2002; Villar & Rivas, 1994). The behavior of multiple sized bentonite pellets during transport is therefore of great interest with regard to the depositional pattern.

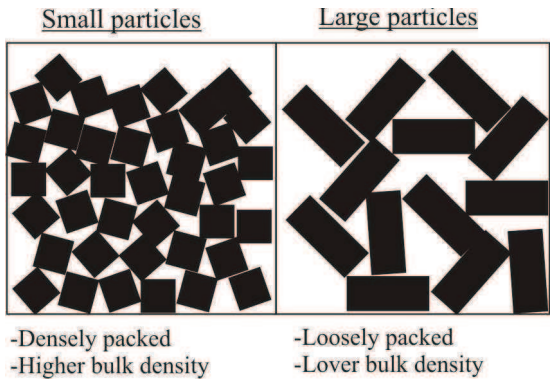

Figure 2.1: View of a principal depositional pattern of bentonite pellets. The left figure shows an interval with small and densely packed pellets and the right figure shows an interval with bigger and loosely packed pellets. By comparing the two figures it is obvious that the bulk density is highly affected by the type of deposition.

The main objective in this chapter is to investigate how the nature of sorting of multi-sized pellets is affected when particle segregation during the transport phase takes place and what effect the sorting has on the final depositional

pattern. It is to be expected that the variation in size of the bentonite pellets affect the depositional pattern in a way which can be predicted.

In order to recover a model which describes the depositional pattern for non-spherical bentonite pellets with a heterogeneous size distribution, it is necessary to test the degree of sorting of bentonite pellets during the transport phase. Basically two sets of test were performed. The first set is to determine the differences in falling velocity for single pellet in an unconfined environment. The second test was to see how a bundle of pellets interacted with each other during the transport phase. In order to see how this interaction affects the depositional patterns, the velocity pattern of the pellets from each test are compared.

2.2. Velocity tests for single pellets

2.2.1. Methodology

The pellets used as sealing material in groundwater wells represent a great variation of grain sizes and shapes. The grain size distribution has been determined. The method is described in Appendix III, page 2-4. The results are summarized in Table 2.1.

Table 2.1: Size distribution with respect to mass.

Size interval (cm)	Mass [%]
$0.2 < d_F \leq 0.4$	1.39
$0.4 < d_F \leq 0.6$	2.85
$0.6 < d_F \leq 1.0$	8.5
$1.0 < d_F \leq 1.5$	34.74
$1.5 < d_F \leq 1.8$	27.56
$1.8 < d_F \leq 2.0$	15.81
$2.0 < d_F \leq 2.5$	9.15

To test the velocity of a single pellet, two things was considered. The first thing was to find a method which was able to account for the wall effect from the fall tube during the test, so that pellets with the biggest Feret diameter were not slowed down relative to the pellets with a smaller Feret diameter. The pellets were subdivided into seven size intervals according to Table 2.1. Twenty seven pellets were picked within each size interval. An appropriated fall tube was chosen and water was loaded into it. The bentonite pellets were introduced below the surface of the liquid and as close to the centre as possible. The terminal velocity of each particle was measured by timing its descent using a stopwatch reading up to 10 ms. Using the fall times, the terminal velocity, V, of each particle was calculated as a function of the length of the fall tube.

It is customary to introduce a wall factor,f, to quantify the extent of wall effects on the steady-settling motion of a particle (Chakraborty et al., 2004; Chhabra, 1995 and 1996; Song and Gupta, 2009). One of the simplest definitions of the wall factor, f, is the ratio of the terminal velocity, V, of a particle in a bounded medium to that in an unbounded medium, V_0:

$$f=V/V_0 \qquad (2.1)$$

To design a system for simulating the effect of a confined system it was decided to use cylinders as test bodies because this shape is visually the nearest approximated shape which describes the shape of bentonite pellets which is of interest in this study. The data of the test cylinders is summarized in Table 2.2.

Table 2.2: Material used in settling studies

Material	Density ρ (g/cm^3)	Cylinder Diameter (mm)	Feret diameter (cm)
Aluminium	2.65	8	3.1, 2.87, 2.66, 2.42, 2.18, 1.96, 1.72, 1.49, 1.32, 1.14, 0.95
PTFE	2.27	10	3.32, 2.97, 2.71, 2.50, 2.29, 2.04, 1.83, 1.63, 1.44, 1.28, 1.16
POM	1.39	10	3.20, 2.94, 2.70, 2.42, 2.25, 2.02, 1.83, 1.61, 1.44, 1.25, 1.12
Plexiglas	1.2	10	3.16, 2.69, 2.24, 1.80, 1.41, 1.12

In order to cover a wide range of particle-to-tube diameter ratios and to explain its role in relation to wall effects, the terminal settling velocity of each particle is measured in six cylindrical fall tubes with different inner diameters: 26, 34, 51, 72, 99 and 139 mm. Each fall tube is at least 1.25 m long with one end sealed by a rubber bung. Water was used as test liquid (density, ρ=1000 kg/m^3; viscosity, μ=0.0013 Pa·s).

Dimensional considerations suggest the wall factor, f, to be a function of the particle-to-tube diameter ratio, $\lambda = d_F/D$, where d_F is the Feret diameter of the particle and D is the inner diameter of the fall tube. The falling velocities are then measured from all the test tubes and the wall factor is determined for each tube diameter, D. Five sets of test has been conducted for each test tube diameter and the average velocity has been calculated. It was shown that a test tube with an inner diameter of 99 mm was sufficient in order to avoid any wall effects during the actual velocity test (Figure 2.2.). It was in this case that the value of V was approximately equal to the value of V_0. The results can be described as a linera function and is expressed in the following way;

$$f = 1\text{-}0.0764\lambda \qquad (2.2)$$

2.2.2. Results

To account for the difference in shapes a total number of 27 pellets within each size interval was picked. Figure 2.3 shows the size interval with respect to Feret diameter versus falling velocity. The black curve shape shows the velocity, V_0, without considering the wall effect, f. By applying *Eq. 2,* to the velocity results the wall effect is considered (black curve on Figure 2.3.). The gap between the red and the black curve

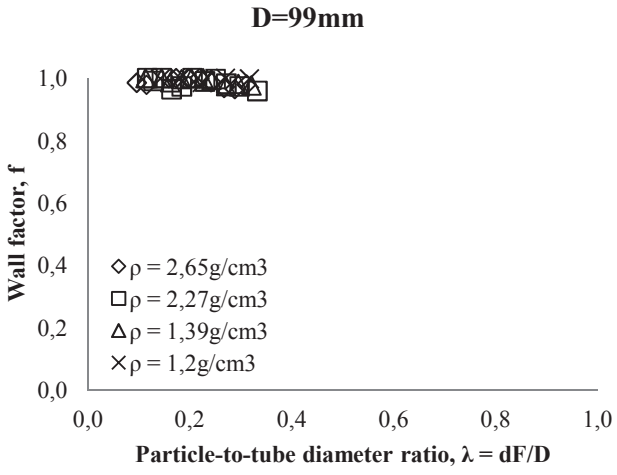

Figure 2.2: Particle-to-tube diameter ratio $\lambda = d_F/D$ versus the wall factor, f. Six test tubes were used, all with different inner diameter. Four different materials were used.

increasing with pellet size (Feret diameter, d_F), which mean that the effect of confining walls increase with pellet size.

A simplified model for the velocity of the pellets is determined. When the size of the pellet is above 1.25 cm there is a linear relationship between the velocity of the pellet and the Feret diameter, d_F, of the pellet. This relationship can be expressed:

$$V = -0.0017\, d_F + 0.37 \qquad (2.3)$$

In the interval where d_F is smaller than or equal to 1.25 cm and bigger than 0.3 on the curve shape can be showed as a logarithmic function, which can be expressed:

$$V = 0.1323 \mathrm{Ln}(d_F) + 0.3394 \qquad (2.4)$$

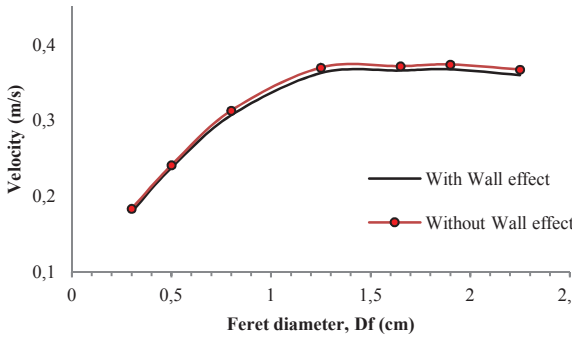

Figure 2.3: Feret diameter versus the velocity of pellets when falling through a test tube with water. The black curve shows the velocity of pellets in a confined environment (D=99mm). The red curve represent the estimated velocity when there has not been accounted for wall effect.

Figure 2.4. show the models expressed in Eq. (2.3) and (2.4) visually. The overall trend of the curve which describes the velocity of single pellet with a Feret diameter above 1.25 cm, shows that velocities decreases very little when the Feret diameters increase. On the other hand it must be noticed that the difference in velocities within this size range is almost negligable.

The intersection between the two curves which is seen at a Feret diameter equal to 1.25 cm, represents the boundary between two types of motion regimes. The change in motion appears when the aspect ratio L/D is approximately 1.2. During the velocity tests mentioned previously, the nature of motion for each pellet down through the test tube was studied visually. Six size intervals with respect to the Feret diameter were considered. Within each interval at least 27 observations were made. It was decided to make a rough distinction between two types of motions. The distinction was set whether or not the pellets were turned around themselves (tumbling) during the downward vertical motion. A high degree of oscillation was allowed.

Going from large Feret diameters and down to a Feret diameter close to 1.25 cm, the oscillation of the particles increases until the particle starts to tumble and rotate in an unpredictable pattern. When the Feret diameter lies in the interval between approximately 0.3 cm and 1.25 cm it is observed that the particle has no preferred orientation and the motion has an unstable

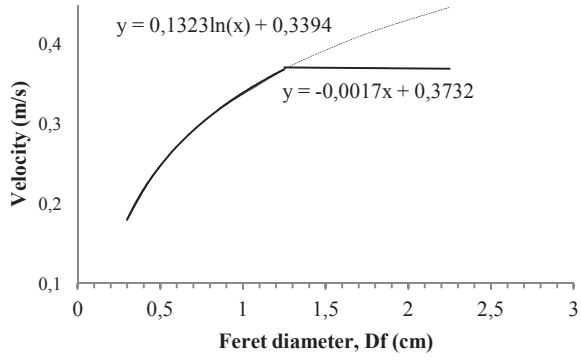

Figure 2.4: Show the models which describs the velocity above and belove a Feret diameter of 1.25cm. Belove that value the velocity cen be expressed as a logaritmic function. Amove that value the velocity cen be expressed as a lineary function.

nature. Due to the tumbling motion, the pellet does not fall vertically. It appears to travelling obliquely across the test tube and follows a path consistent with the direction of tumbling. The ratio between the amount of tumbling particles and the total amount of observations was made. The results are summarized in Figure 2.5.

As can be seen the ratio of tumbling particles compared with the total amount of observations increases dramatically when the Feret diameter d_F decreases below 1.25 cm. For comparison the velocity curve mentioned previously is also showed in Figure 2.5. It is obvious that the type of motion has a pronounced effect on the terminal velocity of the pellet. In general it can be showed that the velocity of a pellet moving downward in a rotating and unpredictable pattern can be expressed as a logarithmic function, of Eq. (2.4). In the case where the pellet is moving downward in a stable predictable manner (thus with a high degree of horizontal oscillations), the velocity can be expressed as a linear function.

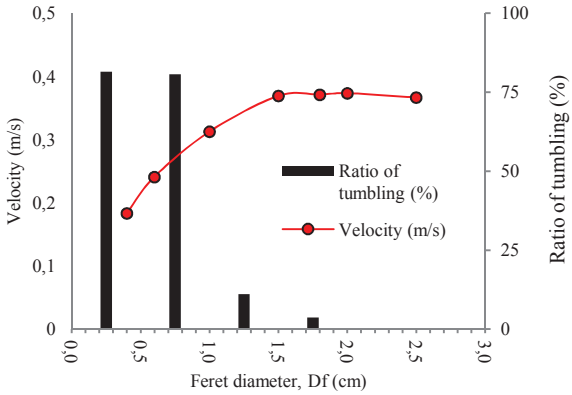

Figure 2.5: Show the Feret diameter versus the ration of tumbling motion of pellets (in %).

2.3. Interaction of Multiple Pellets

2.3.1. Methodology

In the second test the interaction between multiple pellets doing the transport phase is observed, and the depositional characteristic is monitored closely. One fall tube is used with an inner diameter of 110 mm and a height of 3.8 m. One sample of approximately two kg and one samples of approximately one kg of randomly picked pellets were prepared. The pellets are subdivided into four size intervals with respect to the Feret diameter, d_F. Each interval was given its own colour and all pellets within each size interval were painted according to this colour code (Table 2.3).

Table 2.3: Show the four size intervals. Each interval is assigned its own color.

Size interval (cm)	Colour code
$0.2 < d_f \leq 1.0$	Blue
$1.0 < d_f \leq 1.5$	Red
$1.5 < d_f \leq 2.0$	Green
$2.0 < d_f \leq 2.5$	Yellow

After painting the pellets they were mixed completely in a bowl. A high resolution video camera was placed at the bottom of the fall tube to film the deposition of pellets after having travelled 3.8 m in a bundle of other pellets. Test liquid was loaded into the cylindrical fall tubes. The mixed sample of pellets was dropped into the fall tube instantaneously and the depositional pattern was photographed.

2.3.2. Results

Before the test started, each sample was mixed completely. During the transport down through the test tube, the pellets interacted with each other in a way which caused a certain degree of segregation. This fact will be accounted for in the following section. Four images were produced: One for each colour. Due to the DIA technique (described in Appendix III) it was possible to calculate the area which was occupied by each colour in the final deposition (Figure 2.6).

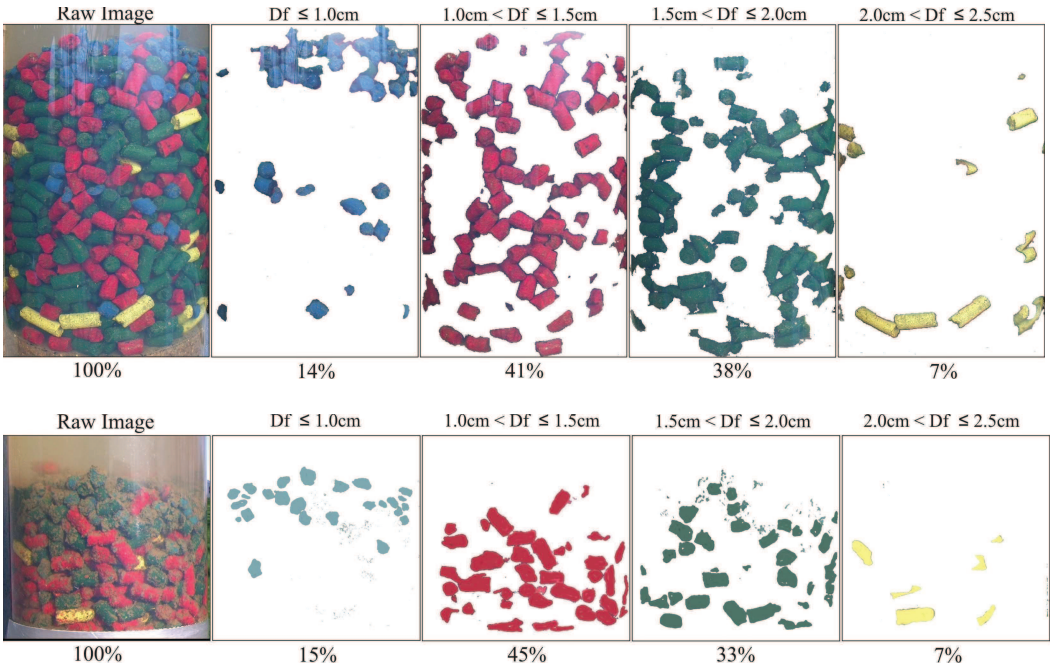

Figure 2.6: Results of the DIA analysis. The first image in each row shows an image of the whole deposit. The four following images, each represent a given size fraction which is denoted by its own color. The upper row represents a sample of approximately 2 kg and the lower row represents a sample of approximately 1 kg.

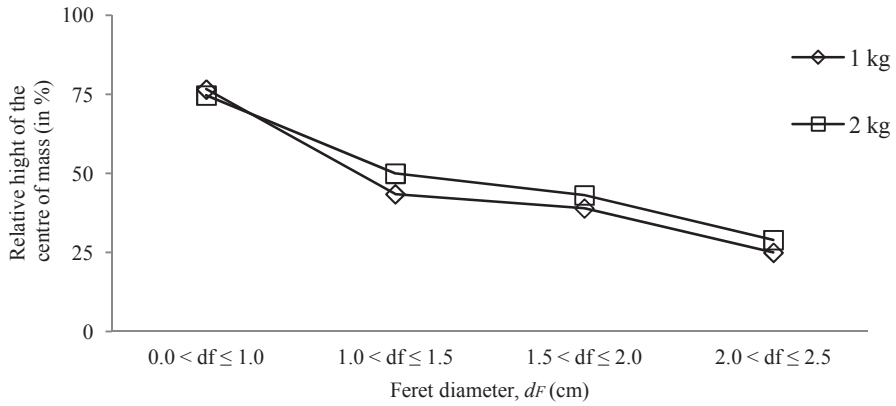

Figure 2.7: The four size intervals of Feret diameter versus the relative height of the center of mass.

The ratio between the area occupied by the pellets and the total area (the raw image of the whole deposition of the bentonite pellets) was then found. The result of the DIA analysis of the two samples is summarized in Figure 2.6. On the top row the results of the two kg sample are showed and the one kg sample is showed below. Starting from left to right; the first image shows the raw image of the final deposition of bentonite pellets. The next four images show the four separated colours, one for each size interval. Above each image, the size interval with respect to the Feret diameter is written, and below is the area percentage shown.

Using the DIA technique it is also possible to find the centre of mass in both x and y direction. In this study, only the vertical y component is of interest. On Figure 2.7, the relative height of the vertical y component of the centre of mass is shown. As can be seen there is a clear tendency that the smallest size fraction ($0.0 < d_F \leq 1.0$) is deposited at the top, and the largest size fraction ($2.0 < d_F \leq 2.5$) is deposited at the bottom. On the other hand there is only a small distinction between the two size fractions in the middle ($1.0 < d_F \leq 1.5$ and $1.5 < d_F \leq 2.0$). It is also seen that the overall trend of the graphs follows almost the same path. This observation indicates clearly that it is possibly to predict the depositional pattern of a given sealing plug.

2.4. Concluding Remarks

Two sets of tests have been performed. The first set showed how single pellets behaved when falling through a liquid in an unconfined environment. The second set showed the depositional pattern of multiple pellets when settling through a test tube with a length of approximately 3.8 m and an inner diameter of 11 cm.

When testing the settling behaviour of multiple pellets it was seen that the pellets with a Feret diameter below 1 cm (blue colour code) have a clear tendency to settle with a low velocity relative to pellets with a Feret diameter above 1 cm (red, green and yellow colour code), which cause the blue pellet to settle last and on top of the deposits. This result corresponds very well with the results obtained from the velocity test of single pellets which clearly indicate that velocities of pellets in the small fractions can be expressed by a logarithmic function, Eq. (2.4). Not surprisingly this marked decrease in velocity can be explained by the tumbling way of movement which has been accounted for previously (Figure 2.5). From Eq. (2.3), which was derived from the velocity test of single pellets, it is obvious that pellets from the interval $1.0 < d_F \leq 1.5$ and bigger with respect to Feret diameter travel with almost the same velocity, thus with a small decrease in velocity when the Feret diameter increases. Based on that, it should be expected that the yellow pellets will reach the bottom after the green and red pellets, which is the case for single pellets. When multiple pellets are mixed and dropped instantaneously, it is shown that the opposite pattern is the case (Figure 2.6. and 2.7.).

The question is what mechanisms acts on the pellets during the transport phase which cause this opposite velocity pattern to dominate. A possible suggestion to this opposite velocity pattern is given in Paper I. The suggestion is based on the simple fact that the degree of oscillations increases when the Feret diameter of pellets decreases. This is valid in the interval where the velocity can be expressed as a linear function Eq. (2.3). The increase of oscillations when the Feret diameter decreases, has two important impacts on the nature of movements of pellets when they are

travelling in a swarm of multiple pellets. The first one is a marked increase in mobility in three dimensions and the second a greater variation in the projected area perpendicular to the direction of motion. An increase in mobility means that a given pellet has a higher possibility to fit into open spaces (mobile pore spaces) which means a higher ability to move around inside the swarm of multiple pellets. A high mobility also leads to a greater variation in the projected area perpendicular to the direction of motion (Figure 2.8). When a given pellet is orientated with its central axis in a vertical position then the projected area must be assumed to occupy a minimum of area. On the basis of that it is obvious to assume that its ability to slip through mobile cavities in the pellet swarm in the vertical direction is bigger than if its central axis is orientated horizontally (Figure 2.8). If the discrepancy in size between large and small particles is great, and because buoyancies have a relatively bigger effect on smaller particles than on bigger ones, the small particles will be sieved up through the pore spaces between larger grains. When a pellet of a given size with respect to the Feret diameter is traveling downward in a bundle with multiple pellets with a larger Feret diameter, it will tend to be replaced upward in the bundle relative to the surrounding pellets.

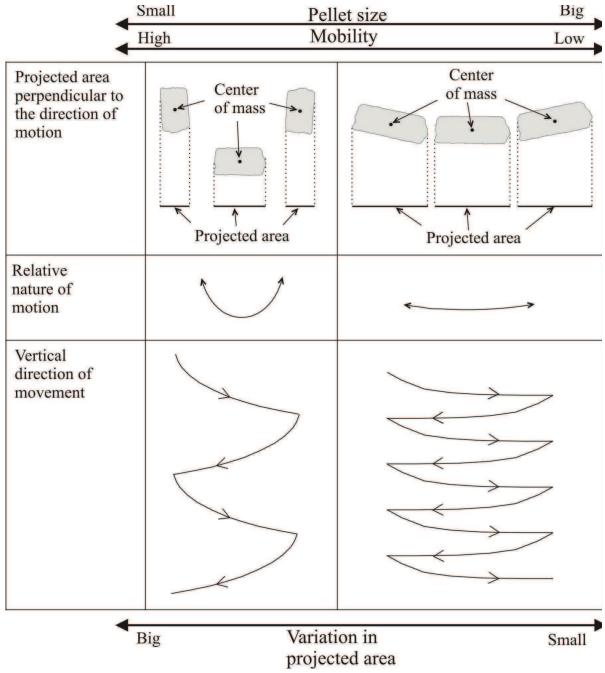

Figure 2.8: Show a diagram of the nature of motion and the projected area as a function of mobility.

Due to the constant and larger projected area of large pellets they will not have the same ability to move upward relative in the bundle in the same way as smaller pellets because mask size of the free pore space which acts as a sieve.

The main objective in this chapter was to investigate how the nature of sorting of multi-sized pellets was affected when particle segregation during the transport phase takes place and what effect the sorting had on the final depositional pattern. The overall conclusion of this work is be that the variation in size of the bentonite pellets affects the depositional pattern in a way which can be predicted. The different size fractions of the bentonite pellets will be deposited according to the pattern described in figure 2.6 and 2.7.

Chapter 3

Swelling pressure as a function of bulk density

3.1. Introduction

The main concern in this chapter is to envestigate the swelling behaviour og bentonite pellets in groundwater wells as a function of the degree of sorting. For this porpuse a swelling-pressure apparatus with an inner diameter of 70 mm was used.

As stated in the previous chapter, a typical sample of bentonite pellets contains a large range of particle sizes. During the transport and settling phases of the pellets, the huge size difference plays an important role regarding the final depositional pattern. The pellets will be sorted during the transport phase and deposited according to their size. The degree of sorting of the pellets plays an important role regarding the bulk density of the deposits. It has been shown that the higher the bulk density in the bentonite sample, the higher the swelling pressure will be (Komine, 2004; Castellanos et al., 2008; Mesri et al., 1994; Sridharan et al., 1986). Even for compacted bentonite-sand mixtures, the magnitude of swelling pressure is a function of bentonite dry density in the mixtures (Agus and Sreepada, 2005; and Sitz, 1997), It has also been shown that if the density increases, the permeability of the bentonite clay will decrease (Cuevas et al. 2002; Villar & Rivas, 1994).

Up until the present time, only the swelling pressure for relatively small, homogeneous bentonite samples has been investigated. No attempt has been done to investigated the swelling pressure for loosely packed bentonite pellets, and no consideration regarding how the degree of sorting of the pellets affects the swelling pressure has been done. Two types of samples will be investigated: sorted samples and unsorted samples. The main focus is to investigate how the degree of sorting affects the swelling pressure of the sample.

3.2. Methodology

3.2.1. Apparatus

Figure 3.1 shows the swelling-pressure test apparatus for the pressure swelling experiment, which can measure the swelling pressure of bentonite pellets in the vertical direction. During each experiment the volume of the inner cell chamber is kept constant by the confining stainless ring and the pistons. The inner diameter of the cell chamber is 70 mm. The preparation of specimens is described in the following section. After the specimen has been mounted in the apparatus, distilled water from the tank was added from the bottom of the specimen. The vertical swelling pressure was measured by the load transducer which was connected to a logging device and a computer. The logging was started the moment water came out at the top of the sample. It took a few minutes to fill the acryl cell completely with water up to the same level which was seen in the water tank. In this period, a constant water flow through the sample was expected. When the water level inside the acryl cell had reached the same level which was in the water tank, the flow through the sample stopped and the only water which was entering the specimen was the water which was sucked into it by the force of the pellets. When the value of swelling pressure reached steady-state condition the test was terminated. In this study test periods vary from approximately 4320 to 17280 minutes.

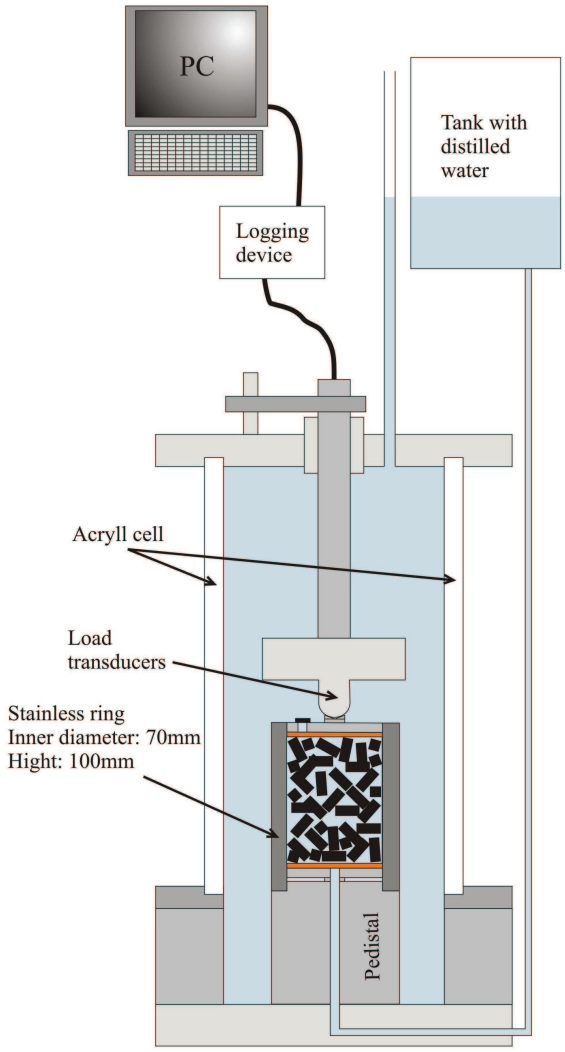

Figure 3.1: Schematic drawing of swelling-pressure apparatus

3.2.2. Sample preparation

The samples are prepared as: i) unsorted samples and ii) sorted samples.

The grain size distribution of the unsorted samples is described in Appendix III. Samples wereprepared and packed into the confined cell chamber. The mass of each bentonite sample was noted. The pore space between the individual pellets was filled with water. Based on that, the bulk density for the whole pellet/water system was calculated. The way the samples were packed plays an important role. In some of the cases the confined cell chamber was filled with water before adding the sample. The pellets were then dropped down into the cell chamber. The transport

through the water column resulted in a more loosely packed depositional pattern of the bentonite pellets. Those samples also show the lowest bulk densities. In the other cases, bentonite pellets was dropped and purred around in the cell chamber in order to get closely packed samples with higher bulk densities than the previously mentioned.

A schematic composition of the sample is shown in Figure 3.2. It is important to note that the overall ratio of montmorillonite (swelling clay minerals) in the final sample is remarkably lower than in the pellets described previously.

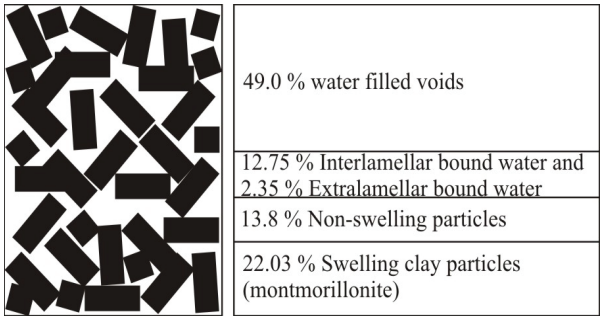

Figure 3.2: Example of the schematic composition of a sample. The values mentioned in the figure, varies from sample to samples.

In the second set of tests the samples were sorted according to the intervals described in Table 3.1. It is seen that there is a general relationship between pellet sizes (with respect to Feret diameter, d_F) and the bulk density of the sample. The tightest packing is seen in samples which consist of pellets from the smallest size fraction. This packing also shows the highest bulk densities. The process of packing the bentonite pellets into the cell chamber is similar to that of the unsorted samples.

Table 3.1: Show the size distribution with respect to mass.

Size interval (cm)	Mass [%]
$0.0 < d_F \leq 1.0$	12.75
$1.0 < d_F \leq 1.5$	34.74
$1.5 < d_F \leq 2.0$	43.37
$2.0 < d_F \leq 2.5$	9.15

There is a clear tendency that the unsorted samples show higher bulk densities than the sorted samples. This is not surprising because all the smallest pellets and debris which is found and unsorted sample will fill up a bigger ratio of the voids between the bigger pellets then in a sorted sample.

3.3. Results

3.3.1. Theoretical considerations

From all the data points obtained during the tests, it can be seen that the increase in swelling pressure is very fast the first 10 minutes which is approximately the time in which it take to fill up the acryl cylinder to the top of the sample. The curves describing the swelling pressure (kPa) versus the time (minutes) for the samples can be approximated by a hyperbola in Eq. (3.1).

$$\sigma(t) = \frac{t+t_0}{a+b(t+t_0)} \qquad (3.1)$$

where t is the time (min) from the start of the experiment, t_0 is the time it takes to fill up the acryl cylinder (t_0 = 10 minuts), $\sigma(t)$ is the swelling pressure at time t whereas a and b are fitting constants

(see Paper II). It can be seen that the curve and equation fits very well with the experimental swelling data. Figures 3.3-3.10 show the approximations for four different samples, all with a different initial bulk density. The model used to fit the swelling pressure vs. time, is well correlated with the experimental data since the regression coefficients (r) estimated in each test are close to 1. The maximum swelling pressure is estimated from the equation of the hyperbola and is expressed in the following way:

$$\sigma_{max} = \lim_{t\to\infty} \sigma(t) = \lim_{t\to\infty} \left(\frac{1}{a/(t+t_0)+b}\right) = \frac{1}{b} \qquad (3.2)$$

Komine and Ogata (1994, 1996a, 1999) have used the same approximation, but only for swelling strain. In this article it is shown that with small modifications, the same approximation is applicable in determination of the swelling pressure of sealing materials.

3.3.2. Swelling pressure for unsorted samples

Within the test series of unsorted samples, seven tests have been executed. The values of the bulk densities are within the range of 1.437 g/cm^3 to 1.556 g/cm^3. Figures 3.3-3.6. show the relationship between swelling pressure and time for four representative unsorted samples with different initial bulk densities.

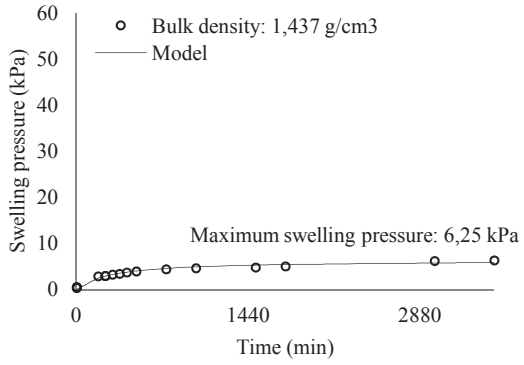

Figure 3.3: Curve of swelling pressure vs. time for unsorted sample with initial bulk density of 1.437 g/cm^3.

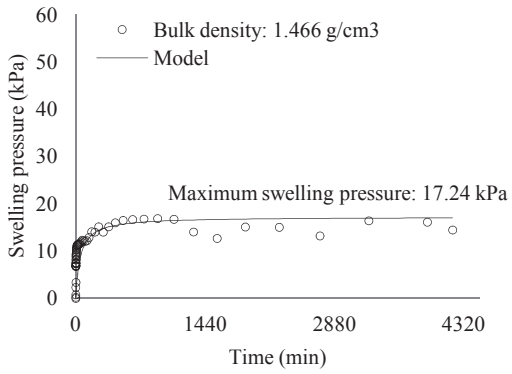

Figure 3.4: Curve of swelling pressure vs. time for unsorted sample with initial bulk density of 1.466 g/cm^3.

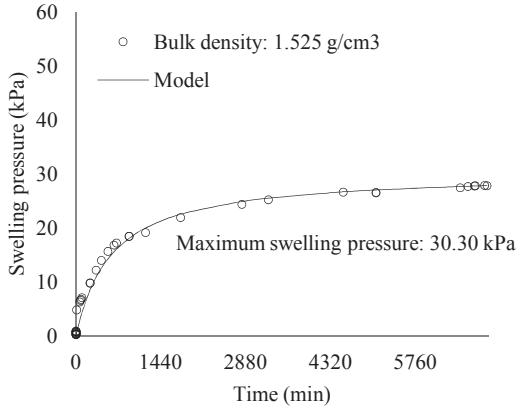

Figure 3.5: Curve of swelling pressure vs. time for unsorted sample with initial bulk density of 1.525g/cm^3.

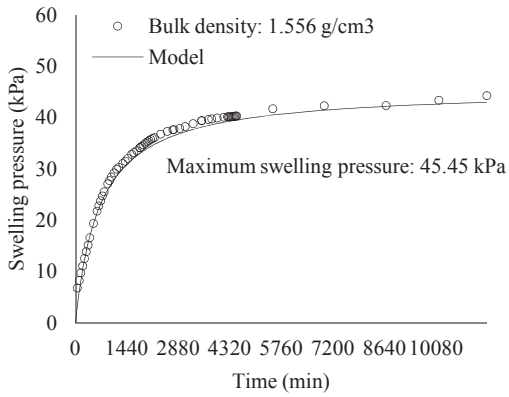

Figure 3.6: Curve of swelling pressure vs. time for unsorted sample with initial bulk density of 1.556 g/cm^3.

3.3.3. Swelling pressure for sorted samples

Within the test series of unsorted samples, seven tests have been executed. The values of the bulk densities are within the range of 1.432 g/cm3 to 1.577 g/cm3. Figures 3.7-3.10 show the relationship between swelling pressure and time for four representative unsorted samples with different initial bulk densities.

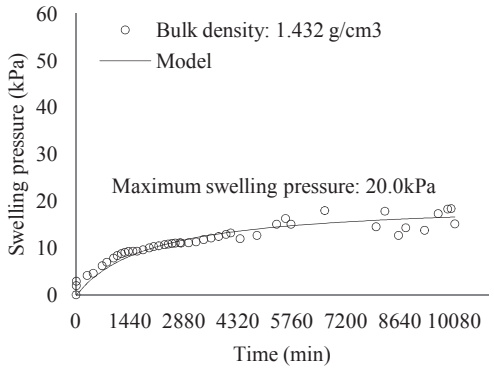

Figure 3.7: Curve of swelling pressure vs. time for sorted sample with initial bulk density of 1.432 g/cm^3.

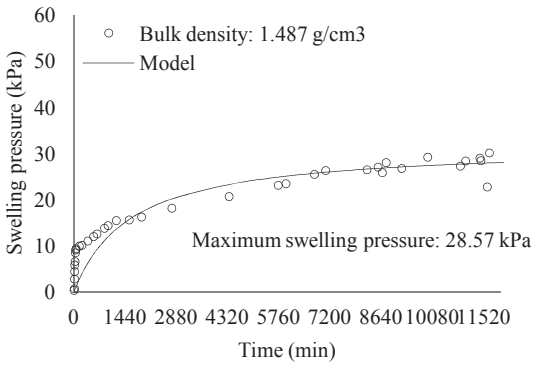

Figure 3.8: Curve of swelling pressure vs. time for sorted sample with initial bulk density of 1.487 g/cm^3.

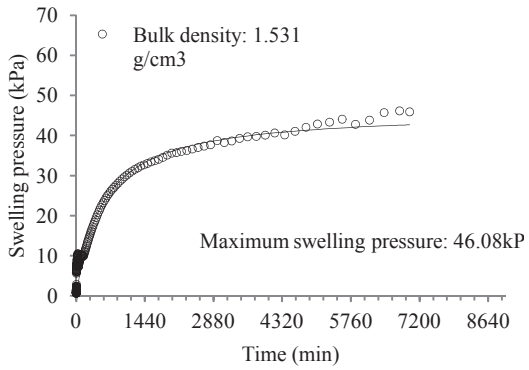

Figure 3.9: Curve of swelling pressure vs. time for sorted sample with initial bulk density of 1.53 g/cm^3.

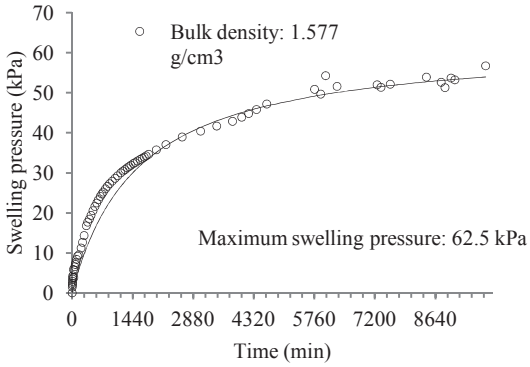

Figure 3.10: Curve of swelling pressure vs. time for sorted sample with initial bulk density of 1.577 g/cm^3.

3.3.4. Maximum swelling pressure

Figure 3.11 shows the relationship between the maximum swelling pressure and the initial bulk density of the sample. In the cases where the swelling pressure of the unsorted and sorted samples were tested, it was found that the maximum swelling pressure depends on the initial bulk density of the sample and the amount of montmorillonite.

The same trend is seen for both the unsorted samples and the sorted samples. The maximum swelling pressure increases with increasing bulk density and montmorillonite content of the samples. Both the unsorted samples and the sorted samples can be expressed as power functions.

This relationship can be described in the following way:

$$SP_{max} = Ss * \left(\frac{D_s - D_w}{D_b - D_w}\right)^a \qquad (3.3)$$

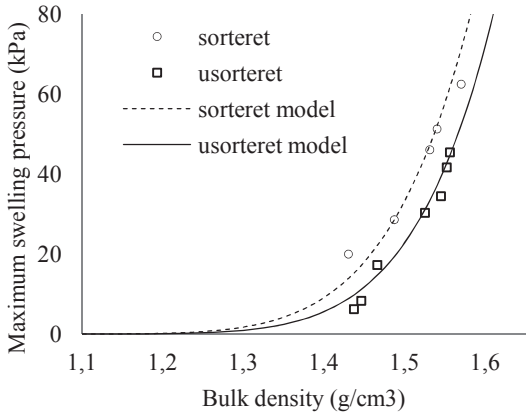

Figure 3.11: Exponential relationship between initial bulk density and the maximum swelling pressure for sorted- and unsorted samples.

where *SPmax* is the maximal swelling pressure, *Ss* is the maximal obtainable swelling pressure at the maximum clay density (the value has been shown in (Komine and Ogata, 2003), *Dw* is the density of water, *Db* is the density of homogeneous bentonite (2.06 g/cm^3), *Ds* is the bulk density of sample, and *a* is the exponent which changes in value from the sorted to the unsorted samples (see Table 3.2).

The models which are used to fit the maximum swelling pressure vs. time for the sorted and the unsorted samples are well correlated with the experimental data, since the regression coefficients (*r*) estimated in each test are close to 1. Those results support the assumption that the data from the unsorted and the sorted sample in fact can be divided into two groups.

Many researchers have performed similar test and obtained the same trend on the maximum swelling pressure vs. bulk density curve (Agus and Schanz, 2008; Komine et al. 2009; Komine and Ogata, 1994, 1996, 2003, 2004) as in this paper. There seems to be a general agreement that the value of maximum swelling pressure is closely related to the montmorillonite content in the sample.

Table 3.2: show how the exponent *a* changes from the sorted to the unsorted samples

Samples	*a*
Sorted	5.8
Unsorted	6.3

3.4. Concluding Remarks

From the data points (Figures 3.3-3.10) it can be seen that the increase in pressure is very fast within the first 10 minutes which approximate the time it takes to fill up the acryl cylinder to the top of the sample (Figure 3.1). In this period, water is flowing through the sample relatively fast and increases the pressure in the sample. When the water level in the acryl cell has increased above the top of the cylinder, a counter pressure will build up and hinder the same water flow through the sample. When the water level in the acryl cylinder has reached the same level as in the water supply tank, the flow through the sample will stop completely. At this point the only water which enters the

sample is the water which is dragged or sucked into the cell by the osmotic forces from the clay itself.

The trend on the density vs. swelling pressure curve (Figure 3.11), which is applicable for both the sorted samples and the unsorted samples, is easily explained.

As can be seen, the pressure increases accelerate with increasing bulk densities. In the cases with relatively low bulk density samples, it must be expected that the ratio of cavities is larger. The swelling potential will first reach its maximum in the moment where the gaps have been filled out (Figure 3.12). Because of the relatively larger ratio of cavities in the relatively low bulk density samples, a larger proportion of the swelling potential will be lost by filling out the cavities.

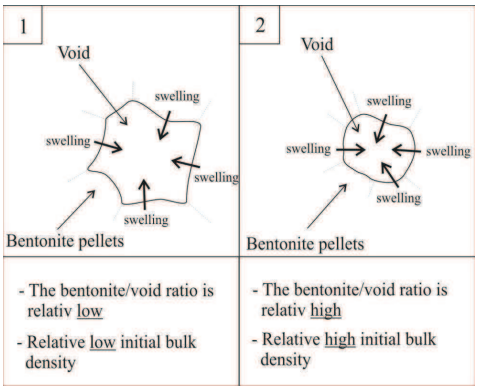

Figure 3.12: Bentonite/void ratio for samples with relative low initial bulk density (1), and for samples with relative high initial bulk density (2).

In the samples with relatively high bulk densities, the opposite is the case. Here we have a relatively small ratio of voids which means that a larger amount of the swelling potential will actually contribute to the overall swelling pressure.

As can be seen from Figure 3.11, the maximum swelling pressure for sorted samples is higher than the maximum swelling pressure for unsorted samples. Two things are of great importance in this matter: Firstly the depositional pattern, or the arrangement of the pellets; secondly the permeability of the sample.

In a sorted sample it must be expected that the overall pore space between the pellets show a great deal of homogeneity regarding volume and shape. Each pellet will be part of the lattice which contributes to the overall pressure increase within the swelling process.

The first column in Figure 3.13 shows an ideal 2-D arrangement of a sorted sample. The argumentation is believed to be applicable for a 3-D arrangement as well. At t=0 the force by which the pellets act on each other at their contact points is shown. It is clear that this force is relatively small before the swelling starts. At this stage the contact forces are only due to the weight of the pellets, i.e. gravity. When the pellets get into contact with water and the swelling starts, the forces at the contact points increase successively with time (t=1 in Figure 3.13). In this arrangement, all the pellets play an active part in the swelling pressure. The volume and the shape of the pore space in an unsorted sample are less homogeneous. Due to the great variation in grain size, smaller grains may be arranged in a way, between larger pellets, so that they only have very few contact points with the surrounding pellets. The second column in Figure 3.16 shows this arrangement. The small pellets

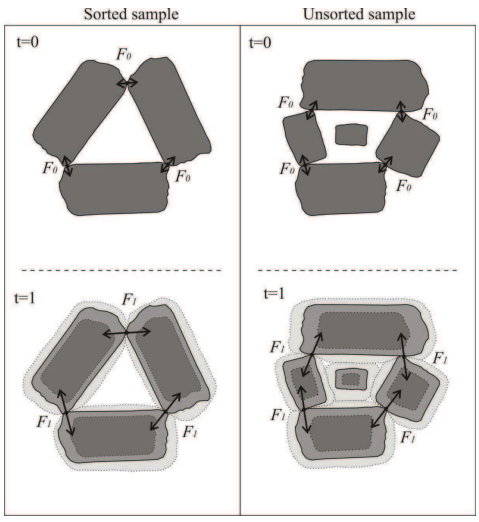

Figure 3.13. Ideal 2-D arrangement of sorted- and unsorted samples.

that are in this way not initially part of the main structure will not play any active part in the contribution to the overall swelling pressure. Another thing which has to be considered is the amount of water available for the swelling process. Consider two samples, one sorted and one unsorted, but with the same initial bulk density. The two samples have the exact same initial amount of water available, before swelling starts. In the case of the unsorted sample (Figure 3.13), a large proportion of the water available in the pore space will be absorbed by the small fragments/pellets which do not contribute to the overall swelling pressure. This means that the amount of water available for the pellets which actually contribute to the swelling pressure is relatively limited compared to the sorted samples.

In order to increase the swelling pressure, water must be dragged or sucked into the sample. By looking at Figure 3.16, it is intuitively obvious that the permeability is higher in the sorted samples. This fact is well documented and reported by Okagbue (1995). This means that a larger amount of water can be transported into the middle part of the sample. The unsorted samples contain a lot of small fragments which mean that they have a much larger surface area compared to the sorted sample. The absorption of water will happen much faster in the unsorted samples as long water is available. In the middle part of the sample, the only water available is the water in the voids between the pellets/fragments.

In the case of unsorted samples it can be expected that the areas around the water inlet will expand relatively fast and thereby hinder the transport of water into the middle part of the sample. Based on that, a much more homogenous water distribution can be expected in the sorted sample. As mentioned previously, there seems to be a general agreement among many researchers that the value of maximum swelling pressure is closely related to the montmorillonite content in the sample. This is only true for the homogeneous samples. In the case of heterogeneous samples (clay, water systems) we have showed that the nature of grain distribution and the depositional pattern plays a much more important role than expected.

The following conclusions were drawn from this experimental study:

- It was showed that the approximation developed by Komine and Ogata (1994), to estimate swelling strain is also applicable in the determination of the swelling pressure of sealing materials.
- A mathematical model has been derived to calculate the maximum swelling pressure based on the initial bulk density of a sample. The maximum swelling pressure increases as a power function with increasing initial dry density for both sorted and unsorted samples. The shape of the curve is explained by the pellet/void ratio which increases toward increasing bulk densities.
- There is clear evidence that the swelling pressure of the sorted samples is approximately 10-12 % higher than the unsorted samples. By comparing the sorted samples and the unsorted samples it was possible to demonstrate that the amount of montmorillonite has a minor impact on the swelling pressure compared to the layering pattern of the pellets/fragments.
- It was shown that the sorted samples have a more effective layering which has a pronounced effect regarding swelling pressure.

Part 2

Evaluation of computed tomography as a tool in soil science

In soil science CT scanning technihques have previously been used to evaluate the density in soil volumes. Anderson et al. (1990 and 1988), Petrovich et al. (1982), Pires et al. (2002) and Van Geet et al. (2005)

In this part the main focus will be on how to modify existing methods.

Chapter 3: Improved methods for qualitative analysis of bulk density with the use of computed tomography (CT)

Chapter 4

Improved methods for qualitative analysis of bulk density with the use of CT

4.1. Introduction

To evaluate the properties of bentonite plugs, x-ray computed tomography (CT) will be used. A new set of algorithms is developed to convert CT numbers (Hounsfield's Units, HU) into reliable densities.

As stated previously Anderson et al. (1990, 1988) have worked with the evaluation of constructed and natural soil macropores using X-ray computed tomography. Among other things they refer to Petrovich et al. (1982) who claim that the mean bulk density in a soil core is linearly related to the mean X-ray attenuation coefficient of the core. To calibrate the CT scanner for bulk density determination they have used packed soil cores with a known density. Pires et al. (2002) have used gamma-ray computed tomography to characterize soil surface sealing. In this paper it is also claimed that the differences in the attenuation coefficients correspond directly to the differences in soil density at each point. The calibration of the tomograph was obtained through the correlation between linear attenuation coefficients (m) of different materials with known densities.

Van Geet et al. (2005) have worked with the use of microfocus X-ray computed tomography in characterising the hydration of a clay pellet/powder mixture. For a quantitative analysis of the images, real density images would be much easier to interpret. To transform the CT values into real densities they go a step further. The measured linear attenuation coefficient depends on the density (q) and atomic number (Z) of the object and on the used X-ray energy (E) as:

$$\mu = \rho\left(a + b\frac{Z^{3.8}}{E^{3.2}}\right) \qquad (4.1)$$

with *a* and *b* instrument dependent parameters (Rutherford et al., 1976a,b; Avrin et al., 1978; Pullan et al., 1981; Lehmann et al., 1981; Stonestrom et al., 1981; Curry et al., 1990; Gingold and Hasegawa, 1992).

In the following a new method to find the average bulk density of a small area on a CT image is proposed. This method is applicable for clay/water systems in the density range from 1.0 to 2.1 g/cm^3.

4.2. Methodology

4.2.1. Preparation of samples

A cylindrical PVC pipe (55 mm inner diameter and 250 mm height) with perforated seal at both ends is used. The density of PVC is 1.39 g/cm^3. The first step was to fill approximately 25 mm well-sorted gravel into the bottom of the cell in order to achieve a good hydraulic contact with the inner part of the cell. Unsorted pellets are then dropped into the middle part of the cell. The grain size distribution was described in more detail in appendix III. Finally, well sorted gravel is filled into the top 25 mm of the cylinder. Figure 4.1. show a CT-scan of the a sample. The sample has been prepared so that the bulk density in the middle part of the sample is approximately 1.5 g/cm^3 when the experiment starts. In this calculation it is assumed that the average density of the pellets is very close to 2.0 g/cm^3 and that the voids between the pellets are filled with water. The porosity of the sample before water is added is approximately 48 %.

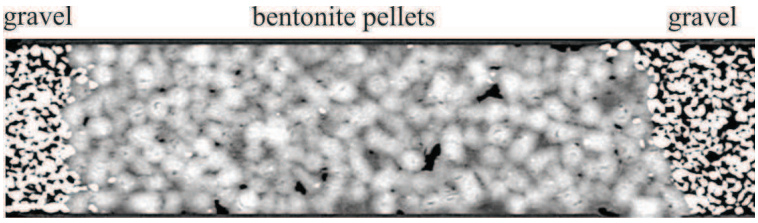

Figure 4.1: CT-scan of a sample. Course grained gravel enclose the bentonite sample in the ends. A high permeability of the gravel ensures a sufficient water supply from the ends.

To simulate the real conditions in a borehole the pellets are only exposed to water from the ends of the cylinder and the water available in the pore space. The swelling of the pellet is confined in the sense that they can only expand into the water-filled pore space between the pellets. Water is free to move into the sample from both ends and not from the sides.

4.2.2. Computed tomography and scanning system

To examine the hydration characteristics of bentonite pellets in a confined space and with a limited amount of water available, the samples are scanned with a high-resolution X-ray CT system.

X-ray CT is based on the interaction process that occurs when this type of radiation penetrates different materials (Wang et al., 1975). When an X-ray beam passes a homogeneous material of thickness *x* (cm), the photons are transmitted according to the Beer–Lambert law:

$$I = I_0 \exp(-\mu x) = I_0 \exp(-\mu^* \rho x) \qquad (4.2)$$

where I_0 and I are, respectively, the rates of the incident and the emerging photon beams, μ (cm^{-1}) is the linear attenuation coefficient that measures the photon absorption or scatter probability per unit length while interacting within the sample, ($\mu^* = \mu/\rho$) ($cm^2\ g^{-1}$) is the mass attenuation coefficient, and ρ ($g\ cm^{-3}$) is the density of the material penetrated.

Each voxel in the reconstructed image corresponds to a point in the field of view, and the pixel value directly reflects the linear attenuation coefficient μ (cm^{-1}) in that point. In order to compensate for variation in photon energy spectra between various CT scanners, the voxel values are usually normalized in Hounsfield units and reported as CT numbers H:

$$H = 1000\ (\mu - \mu_{water})/\mu_{water} \qquad (4.3)$$

Variation in H correspond to differences in the attenuation coefficients and, consequently, to differences in soil density. It is therefore possible to obtain images that present the density distribution of the sample within the volume investigated (Bushberg et al. 2001; Pires et al. 2002).

The CT number associated with each point of the soil matrix is associated with a grey level and visualized. Usually white regions correspond to regions with higher CT numbers and dark regions to lower values. Variation in gray levels correspond to differences in the attenuation coefficients and consequently, to differences in soil density at each point.

The scanner used for this study is a clinical Biograph Truepoint 64 manufactured by Siemens. The scans are acquired as spiral CT at 120 kV tube voltage and an exposure of 300 mAs. The data are reconstructed using filtered back projection on a 512 x 512 matrix with 0.39 mm pixel size and a slice thickness of 0.6 mm (see Photo 4.1).

Photo 4.1. The scanner used for this study is a clinical Biograph Truepoint 64 manufactured by Siemens

4.3. Density calibration

For the quantitative analysis of the images, real density images would be much easier to interpret. It is therefore of great importance to recalculate the CT numbers which are retrieved from the image into reliable densities. For this purpose, however, an additional assumption is needed, since a single CT scan does not in general allow determining the density and elemental composition independently.

Hydration of the bentonite samples are assumed to take place in a confined environment where the only expansion possible for the bentonite pellet is into the water filled pore space. An unlimited water supply is available from the ends of the sample.

As mentioned in Appendix III, the dry density of the pellet, ρ_{pellet}, has been measured to 2.06 g/cm^3. When packed into a test tube with a fixed volume and an air filled pore space, the bulk density, ρ_{dry}, has been measured to 1.06 g/cm^3. During hydration, the air in the pore space is replaced by water which increases the bulk density, ρ_{wet}, of the sample to 1.5 g/cm^3. At this stage the relative weights of the water, w_{water}, and the pellets, $w_{pellets}$, are 0.314 and 0.686 respectively. During the hydration process these numbers will change as a function of water supply over time.

To express the change in bulk density as a function of water supply, the following equation is used:

$$\rho_{wet} = \rho_{dry}\left(1 + \frac{w_{water}}{w_{dry}}\right) \tag{4.4}$$

In order to find the relative weight of the dry part of the sample, w_{dry}, which consists of bentonite pellets (clay), the following expression is used:

$$\mu_{wet} = \rho_{wet}\left[\left(\frac{\mu}{\rho}\right)_{dry} w_{dry} + \left(\frac{\mu}{\rho}\right)_{water} w_{water}\right] \tag{4.5}$$

The first step is to substitute eq. (4.3) into eq. (4.4).

$$\mu_{wet} = \rho_{dry}\left(1 + \frac{w_{water}}{w_{dry}}\right) \times \left[\left(\frac{\mu}{\rho}\right)_{dry} w_{dry} + \left(\frac{\mu}{\rho}\right)_{water} w_{water}\right] \tag{4.6}$$

In the second step, the expression $w_{water} + w_{dry} = 1$ is rearranged into $w_{water} = 1 - w_{dry}$ and then substituted into Eq. (4.6). The following expression then appears:

$$\mu_{wet} = \rho_{dry}\left(1 + \frac{1-w_{dry}}{w_{dry}}\right)\left[\left(\frac{\mu}{\rho}\right)_{dry} w_{dry} + \left(\frac{\mu}{\rho}\right)_{water}\left(1 - w_{dry}\right)\right] \tag{4.7}$$

By rearranging Eq. (4.7) through the following steps:

$$\mu_{wet} = \rho_{dry}\frac{1}{w_{dry}}\left[\left(\frac{\mu}{\rho}\right)_{dry} w_{dry} + \left(\frac{\mu}{\rho}\right)_{water} - \left(\frac{\mu}{\rho}\right)_{water} w_{dry}\right]$$

$$\frac{\mu_{wet}}{\rho_{dry}} = \left(\frac{\mu}{\rho}\right)_{\text{dry}} - \left(\frac{\mu}{\rho}\right)_{\text{water}} + \frac{\left(\frac{\mu}{\rho}\right)_{\text{water}}}{w_{\text{dry}}}$$

$$w_{dry} = \frac{\left(\frac{\mu}{\rho}\right)_{water}}{\left(\frac{\mu_{wet}}{\rho_{dry}}\right) - \left(\frac{\mu}{\rho}\right)_{dry} + \left(\frac{\mu}{\rho}\right)_{water}} \tag{4.8}$$

The linear attenuation coefficient μ_{wet} of the sample is derived from rearranging Eq. (4.3) to the following expression:

$$\mu_{wet} = \mu_{water}\left(\frac{H}{1000} + 1\right) \tag{4.9}$$

By substituting Eq. (4.8) into Eq. (4.9) and using w_{dry} in Eq. (4.4), a direct method is obtained to convert CT numbers into densities.

One condition for performing this calculation, however, is that the effective energy of the x-ray beam is known, since all attenuation coefficients are energy dependent. For this purpose dry bentonite pellets are CT scanned and the CT number for massive bentonite was determined to be 1540. Assuming a number of different energies in the range 60-80 keV, this CT number is converted to linear attenuation coefficients that are compared to mass attenuation coefficients found for dry bentonite using mineral composition (Snyde & Bish) and tabulated attenuation data (NIST X-ray attenuation database). An effective energy of 76 keV is found and used subsequently for determining the density of the hydrogenated samples.

4.4. Further work

In this work bulk densities for whole samples have been determined from single CT images. This method is based on the assumption that hydration takes place in a confined volume, thereby allowing to setup a relationship between bulk density and water content. This relationship is necessary, since measurements of attenuation coefficients alone is not sufficient for independent determination of density and elemental composition. A natural development of the method would be to use dual energy CT, where the sample is CT scanned at two different tube voltages. This approach makes it possible to determine the density and relative water content independently at any position in the sample.

Part 3

Homogenization and hydraulic conductivity in a bentonite seal

There are two focus points in this part. The first is how the hydration of a bentonite seal affects the evolution of macroporosity and homogenization process. The second is how the change in pressure gradient through a bentonite plug affects the hydraulic conductivity

Chapter 4: Evaluation of macro-porosity and homogenization of a bentonite seal

Chapter 5: Evaluation of hydraulic conductivity and the creation of channel systems

Chapter 5

Evaluation of macroporosity and homogenization of a bentonite seal

5.1. Introduction

When the bentonite pellets are deposited in the right place and get into contact with water or drilling mud, the swelling process starts. The pellets are confined in the horizontal directions by the filter tube and the geological formation and in the vertical direction by filter sand/gravel or other bentonite pellets. The bentonite pellets have only a limited possibility to expand into the pore space between the pellets which was created during settling. At this point the density variation throughout the seal is very high.

To evaluate the change in macroporosity and the development of the density contrast over time within a bentonite seal, x-ray computed tomography (CT) will be used. The model to convert CT numbers into bulk densities, which was purposed in chapter 3, is used to evaluate the homogenization process.

Two things will be addressed in this chapter. The first thing is to evaluate the change in macroporosity as a function of hydration over time. The second thing is to investigate how the hydration process affects the homogenization of a pellet/water system over time. In addition to this, the overall density change over time will be investigated. The methodology has been discussed in the previous chapter and will not be further treated here.

5.2. Macroporosity

5.2.1. Hydration scheme

The hydration of the sample is performed by submerging each cylinder into a pool of water. The cylinder is flipped around several times in order to let all the air in the voids be replaced by water. The water is not forced into the sample so the only force which has an influence of the hydration (water going into the sample) is the suction force of the bentonite clay itself.

The ten samples are submerged for different amounts of time (Table 5.1.). After 27765 minutes (which corresponds to approximately 20 days) all the ten samples are scanned at approximately the same time.

Table 5.1: Duration of exposure to water for each sample before CT scanning.

Sample no.	Time (min)
1	27765
2	24898
3	19105
4	14773
5	9042
6	4672
7	2925
8	1175
9	535
10	210

5.2.2. Digital Image Processing (DIA) and analysis

The samples where then CT scanned according to the method described in Chapter 3. One scan was made for each of the ten samples mentioned previously.

In order to make a quantitative evaluation of the porosity of the samples, ten slices from each sample are analysed. In the CT data set, the slice thickness is 0.6 mm. It is only every fifth slice which is picked out for further investigation. This means that there is 3 mm between each analysed section. The total height of the analysed part of the sample is 27 mm.

In order to simulate a real bentonite plug in a borehole, the middle part of the sample is analysed (Figure 5.1.) so that the water intake from the ends only has a minor influence on the analysed part. A total number of 100 slices is analysed using digital image analysis (DIA). Figure 5.2 shows the single steps during the image processing using a representative 2-D grey scale image of bentonite pellets during the hydration process. Macropores are clearly visible (black spots). The second step in the image processing procedure (2) is to mark the

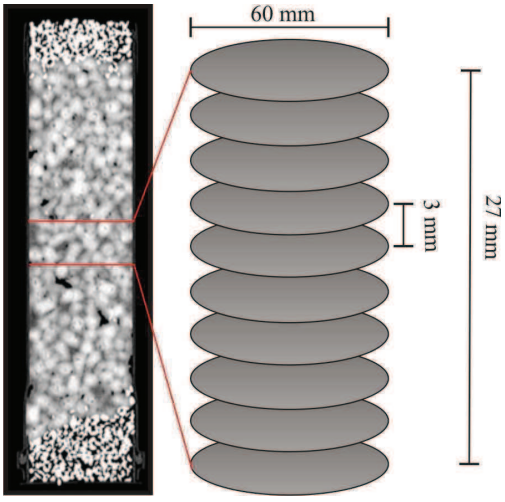

Figure 5.1: Position and orientation of slices within the sample. Note the different scale in the vertical and horizontal direction.

region of interest (ROI) and clear the area outside the ROI. In image 3, a simple brightness/contrast adjustment is performed. The colour mode which is used is a greyscale (0-255). The lower value is set to 0 and the upper value is set to 25. The next step was to make an 8-bit binarization (4) followed by an area analysis. Both the amount of pores, pore size and the total size of the area was measured. Image processing, analysis and measurement are carried out using the free software, ImageJ ver. 1.43s.

Each slice will be approximated to a cylindrical body with a given volume. The area of ROI is in all the image analyses 3849 mm^2. With a thickness of each slice of 0.6 mm, the volume is 2309 mm^3. The total area of voids was found by using DIA. It will be assumed that this area is the same through the slice (0.6 mm). The volume of voids can then be calculated and from this result it is a trivial task to find the porosity by using the following equation:

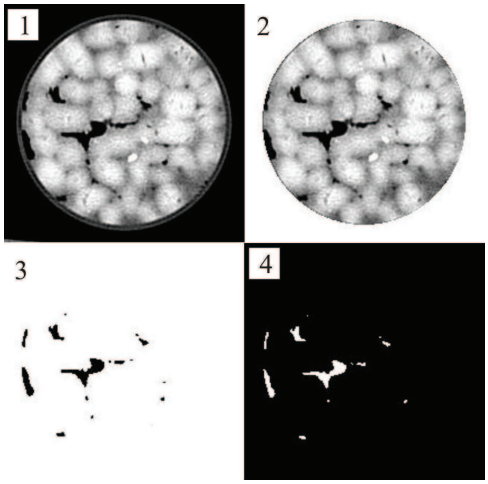

Figure 5.2: Steps in image processing and analysis process: 1) 2-D greyscale image of bentonite pellets; 2) identification of the region of interest; 3) brightness/contrast adjustment; 4) 8-bit binarization followed by area analysis.

$$Porosity\ (\%) = (Volume_{voids}/Volume_{total})*100 \qquad (5.1)$$

This approach is used for each of the ten analysed slices in every sample, and an average value is found.

5.2.3. Results

Table 5.2. shows the results of the digital image analysis of the ten scanned samples. As can be seen from the table, three parameters are listed: 1) average number of macropores per slice; 2) average size of macropores; 3) total area covered by macro pores. Each value in the table represents an average value of the ten slices mentioned previously.

First of all it should be noted that there is no significant relationship between the amount of pores and time. On the other hand, it is seen that there is a very clear relationship between

Table 5.2: Characterization of macropores.

Sample no.	Time (min)	Average number of macropores per slice	Average size of macropores (mm^2)	Total area (mm^2)
1	27765	22.2	1.27	27.69
2	24898	25.9	1.22	31.29
3	19105	27.5	1.03	28.25
4	14773	26.2	1.46	36.13
5	9042	24.7	1.02	24.77
6	4672	26.4	2.42	59.01
7	2925	25.3	2.12	52.42
8	1175	29.5	2.86	83.44
9	535	31.3	3.43	106.32
10	210	27.5	5.34	140.76

the size of pores and time. The less time the sample has been exposed to water the bigger the average size of macropores. This means that the pore pressure increases with time. The total area covered by macro pores shows the same trend. It is important to note that the total area decreases in size until approximately 9000 min. After this point, the values show relativly constant values. The average porosity of the samples 1-10 is calculated based on the description given in subsection 4.2.3.

Figure 5.3 shows a clear relationship between the time where the sample is exposed to water and the porosity. A mathematical model which describes this relationship is found and can be represented by:

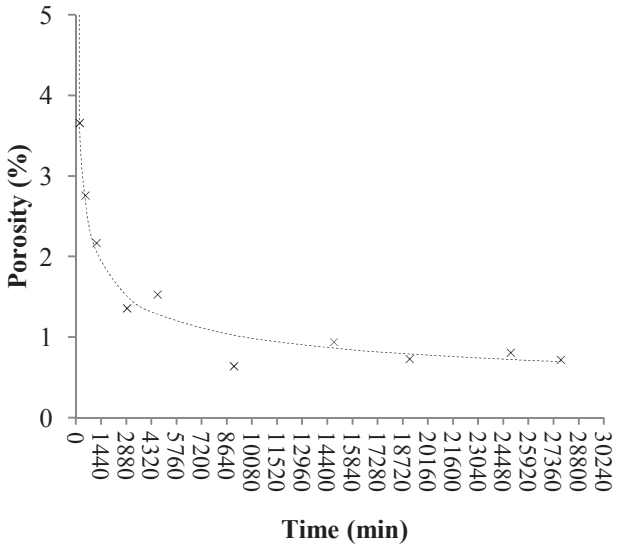

Figure 5.3: Relationship between macroporosity and the time over which the sample has been exposed to water.

$$n(t) = n_0 \cdot \left(\frac{t+t_0}{t_0}\right)^{-b} \qquad (5.2)$$

where t is the time (min), t_0 is the initial time (in this case t_0 = 0.115 minuts), $n(t)$ is the macroporosity at time t, n_0 is the macroporosity before swelling occur, b is a fitting constants (in this case it has been approximated to 0.345). The mathematical model used to fit the time vs. porosity, is well correlated with the experimental data with a regression coefficient (r) 0.997.

The macroporosity before the pellets start to swell, n_0 (at t = 0) has been estimated to approximately 50%. After a period of 210 minutes, the porosity has decreased significantly to less than 4%. This pattern lasts the first two days after which the slope of the curve becomes gentler and after approximately one week it has reached a level of approximately 1%. Based on the CT values of the macro porosity in the middle part of the sample, it can be seen that the pore space is air filled. This indicates that a limited amount of air is present at the surface area of the pellets during settlement.

During the swelling process, the air bubbles gather in the water-filled pore space. During this period, the amount of macropores does not change significantly (Table 5.2.). Only the size of the pores decreases, which means that the air captured in the macropores experience a significant pressure increase.

5.3. Homogenization

5.3.1. Methodology

See Subsection 4.2.2 and section 4.3

5.3.2. Quantitative visualization

Figure 5.4. illustrates the changes in the degree of hydration over time by the visualization of a vertical slice through the center of the cylinder. The black spots are macropores. Based on the CT values it can be seen that these macropores are air filled and no water is present.

The sizes of the pores decrease over time. The colour code is directly related to density. The dark purple colour indicates densities of approximately 2.0 g/cm^3 which is the dry density of bentonite pellets. The orange/red color (density around 1.1 g/cm^3) indicates clay gel. The white regions indicate gravel which has a significantly higher density than hydrated bentonite clay.

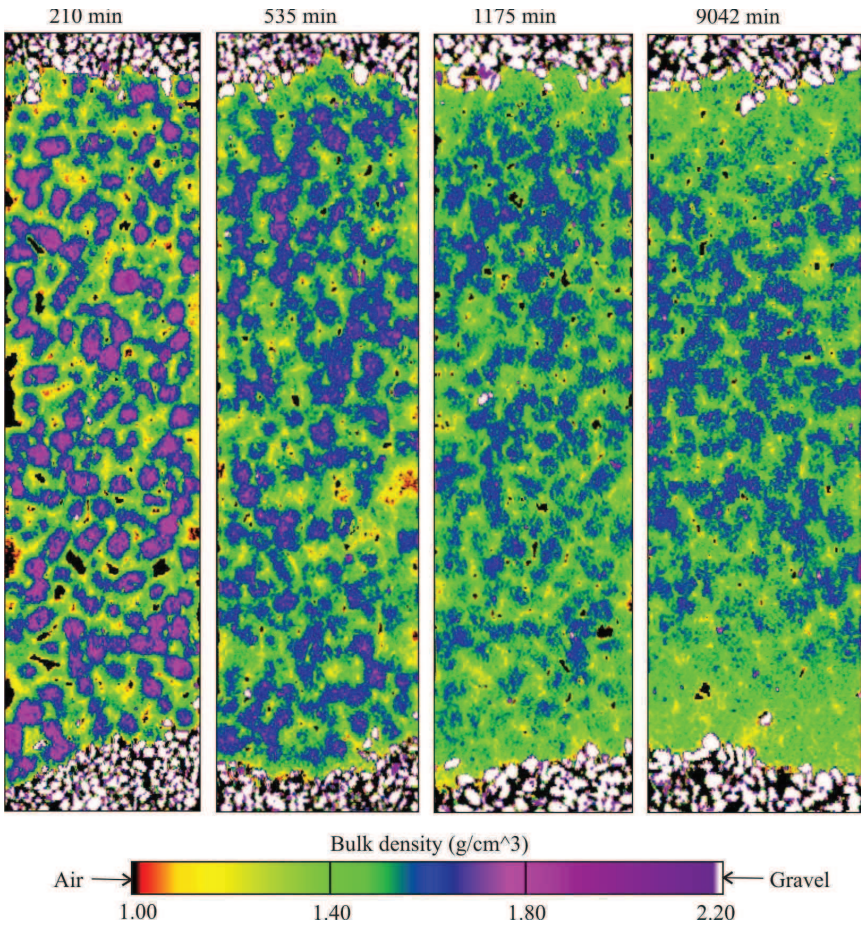

Figure 5.4: Recomputed vertical slices through the center of samples at four different stages. The figure illustrates the change in hydration and homogenization over time. On top of each vertical slice, the time by which the specific sample has been exposed to water is written. The black regions indicate air filled macro pores and the white regions indicate gravel which has a significantly higher density than hydrated bentonite clay.

By comparing the four stages in Figure 5.4, it is clearly shown that all the pellets have a decreased density as a consequence of swelling. In the dry stage, the mean densities of the pellets are approximately 2.0 g/cm^3 (the geochemical analysis indicates a wide range of components, all with different densities). After the first stage of hydration (after 210 min) the pellets are clearly outlined. However, a beginning gradation in color within the outline of each pellet is seen, which means that the pellet has started to hydrate leading to a decrease in density. As mentioned previously, the porosity of a sample (with different degree of compaction) before water has interacted with the clay mineral, varies from approximately 45% to 55%.

By inspection of Figure 5.3, it can be seen that the porosity after 210 min has decreased to 3.7%. At this stage, much of the pore space is occupied with clay gel. In general a great variation in densities throughout the sample is seen. After almost 1 day (1175 min) the variation in densities has decreased and a larger degree of homogenization is seen. The porosity has decreased to 2%. After almost 7 days (9042 min) it is still possible to recognize the overall outline of the pellets. However, the border is much more diffuse compared with the sample which has only been exposed to water for a short period of time.

One very important thing to note is the degree of homogenization in the sample which has been exposed to water more than 9000 min. It is seen that there is almost no density contrast in the sample very close to the water inlet. On the contrary, a larger density contrast is seen in the middle of the sample. This could indicate that the water supply into the middle of the sample has not been sufficient.

5.3.3. Quantitative density variations

The degree of homogenization of the middle part of the sample can be expressed as a function of standard deviation of the density contrast through a profile versus the time. A profile from the centre of one pellet to the centre of another pellet is made. Figure 5.5 illustrates how the density variation through the centre of two pellets is expressed (profile A – A´). The greyscale value which is extracted from this profile is converted into density values according to the method described in Section 3.5. In this example the CT image has been chosen from a sample which only has been exposed to water for a period of 210 minutes.

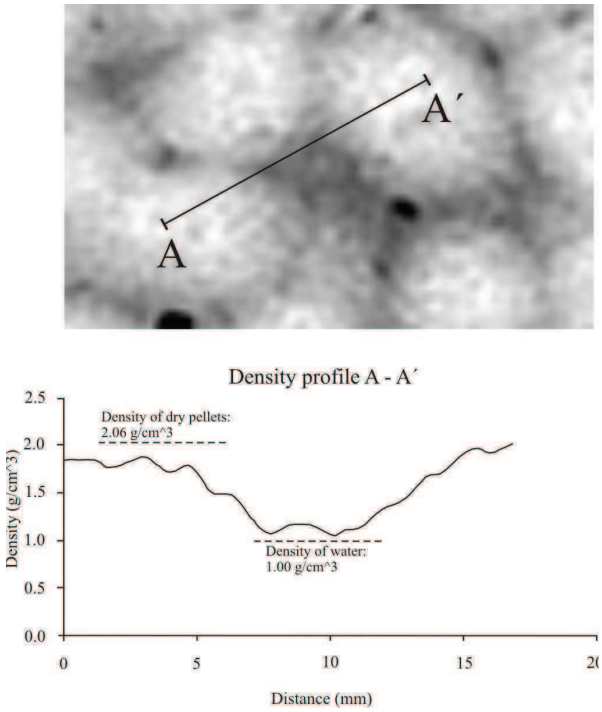

Figure 5.5: Example of a density profile (A – A´) between two pellets which has been exposed to water for a period of 210 minutes. The light grey area indicates relatively high densities and darker grey areas indicate relatively low densities. From the graph it is clearly seen how the densities vary within the sample. At the center of the pellets, the density is still close to 2.0 g/cm^3.

The light grey area indicates relatively high densities and darker grey areas indicate relatively low densities. From the graph it is clearly seen how the densities vary without the sample. At this stage the density at the centre of the pellets has decreased from 2.06 g/cm^3 (dry density) to approximately 1.85 g/cm^3. The pore space between the pellets (dark grey regions), which was filled with water before the swelling started, has increased its density from 1.0 g/cm^3 to approximately 1.1 g/cm^3.

Density profiles have been constructed in this way for each of the samples 1-10. Each profile contains approximately 50 data points and based on that the standard deviation has been calculated. From Figure 5.6 it is evident that the biggest part of the homogenization takes place during the first day. The reason for that is that the density contrast between the pellet and the surrounding water is greatest in the beginning. Over time this contrast decreases in size, which leads to a drop in the velocity of the process of homogenization.

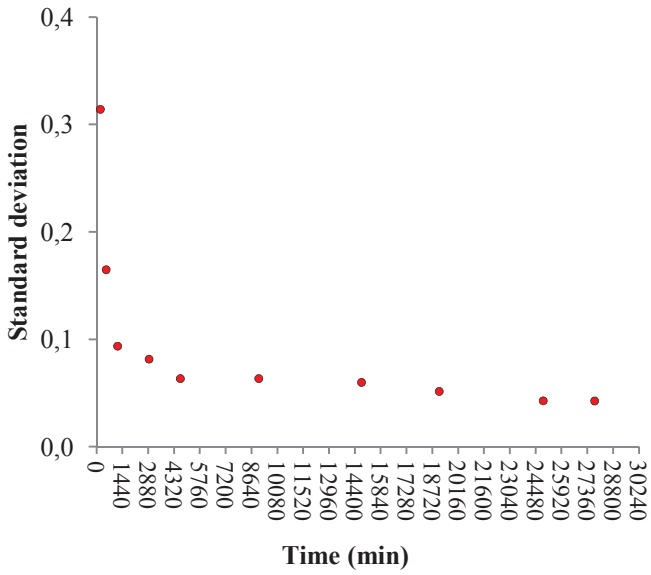

Figure 5.6: Variation in density within the sample expressed as standard deviation in pixel values in a profile through the sample. A marked decrease in values in the first day is seen, which means a high degree of homogenization is happening in this time window.

5.3.4. Bulk densities

The change in the overall bulk density of the sealing plug has been investigated. All the pixel values (in HU units) have been investigated in a volume of approximately 115.470 mm^3. With a pixel size of 0.39 mm it gives a total amount of data points of approximately 2*10^6 pixels. Histograms have been constructed based on the densities. Based on Eq. (3.5), (3.9) and (3.10) which were derived in Section 3.5, the HU units have been converted into bulk densities. Figure 5.7 shows the histograms for the same four samples that were shown in Figure 4.4. By examining the histograms more closely, it is obvious that the diversity in densities is much bigger when samples only have been exposed to water for a short period of time. Over time the width of the histogram becomes more narrow, which indicates a higher degree of homogenization. This also means an absence of the high-density area. This observation is supported by a closer visual inspection of Figure 5.4. Here it is clear to see the absence of the high-density area when the sample has been exposed to water for a period of 1175 minutes.

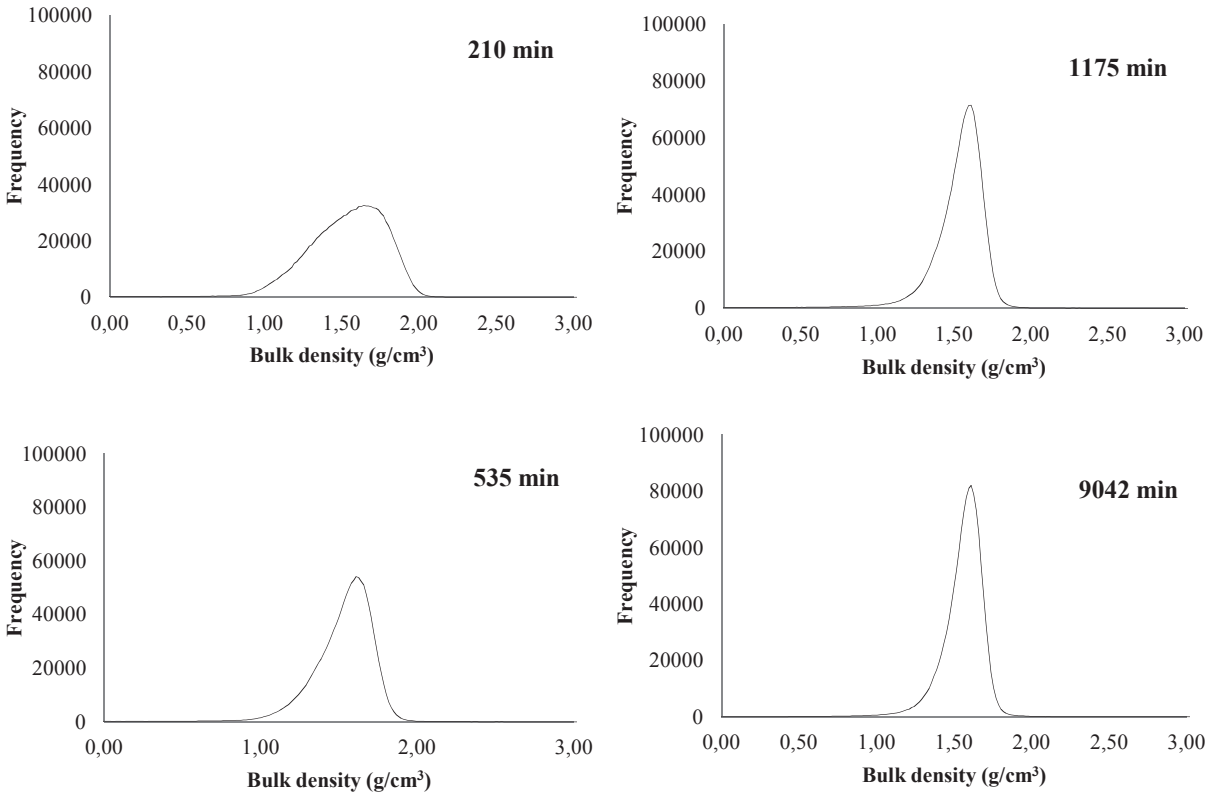

Figure 5.7: Histograms for the same four samples that were shown in Figure 4.4.

Histograms for all the ten samples have been evaluated in details and it can be seen that despite the absence of high density areas, the overall bulk density of the samples increase over time. An average bulk density versus time for all the 10 samples is shown on Figure 5.8. There is a clear relationship between the time and the increase of bulk density for the bentonite seal. A mathematical model which describes this relationship is found and can be represented by:

$$b(t) = b_{inf} - \left(b_{inf} - b_0\right) \cdot \left(\frac{\{t+t_0\}}{t_0}\right)^{-a} \quad (5.3)$$

where t is the time (min), t_0 is the initial time (in this case t_0 = 0.11 min), $b(t)$ is the bulk density at time t. b_{inf} is the bulk density at infinit time, b_0 is the initial bulk density of the water/clays system, a is a fitting constants (in this case it has been approximated to 0.0051). The mathematical model used to fit the time vs. bulk density is well correlated with the experimental with a regression coefficient (r) of 0.998.

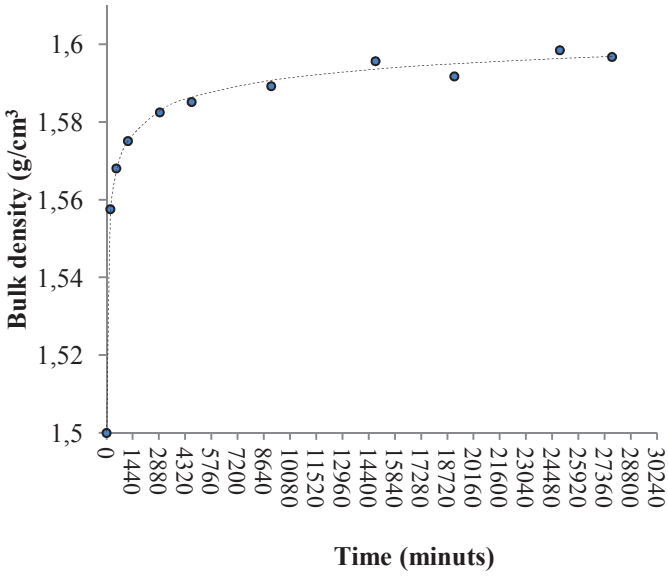

Figure 5.8: Average bulk density versus time for all the 10 samples.

5.4. Conclusion

In this work, bulk densities for whole samples have been determined from single CT images. This method is based on the assumption that hydration takes place in a confined volume, thereby allowing to setup a relationship between bulk density and water content. This relationship is necessary, since measurements of attenuation coefficients alone is not sufficient for independent determination of density and elemental composition. A natural development of the method would be to use dual energy CT, where the sample is CT scanned at two different tube voltages. This approach makes it possible to determine the density and relative water content independently at any position in the sample.

Chapter 6

Evaluation of hydraulic conductivity and channel systems

6.1. Introduction

When bentonite pellets are deposited during natural settlement, the bulk porosity is approximately 50% before the swelling process goes into action. In this case, the hydraulic conductivity through the bentonite seal must be expected to be very high. Due to the osmotic force, the hydration process of the bentonite pellets gets more pronounced over time, which means that the bentonite pellets will expand into the cavities. During this process two things can happen: i) If the waterflow, Q, through the bentonite plug is very limited, the expanding clay particles will occupy the free porespace, which means that the ratio of free porespace will decrease and consequently the hydraulic conductivity will decrease as well; ii) if the waterflow through the bentonite plug is sufficiently high, the small clay particles which are loosened and liberated from the surface of the bentonite pellet, during the hydration process, will be carried away and will not contribute to overall expansion. Consequently an erosion of the pellets will take place, which means that the porespace will remain open.

To cause this situatiation two potential scenarios are shown in Figure 6.1. During construction of the groundwater well, it is common practice to pump up water from the groundwater reservoir in order to clean up the filter section before the bentonite seal is fully evolved.

This means that the water colomn (drilling fluid) which is standing in the well is forced

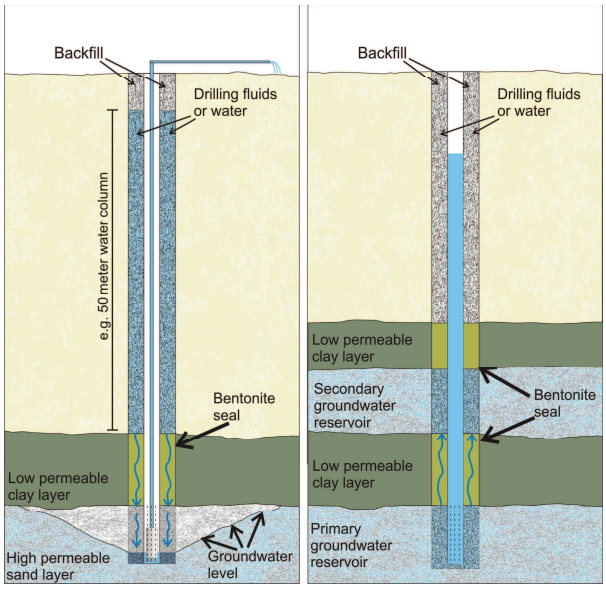

Figure 6.1: Show the two scenarious.

down and through the bentonite seal because there is no counterpressure in the upward direction from the groundwater reservoir.

Another potential scenario which could cause an upward pressure gradient is when a high pressure difference is seen between the primary and secondary groundwater reservoir. In this paper the hydraulic conductivity, *k*, of the most commonly used bentonite sealing in Denmark is studied.

The main focus is to determine the hydraulic conductivity, *k* for sealing intervals exposed to different gradients. In addition to that, the development of channel systems will be addressed. Finally the self sealing potential of a low pressure sample will be discussed. To make a quantitative evaluation of the development of channel systems in a bentonite seal, x-ray computed tomography (CT) will be used. The model to convert CT numbers into bulk densities, which was purposed in chapter 3, is used to evaluate the homogenization process. Further information about the methodology is given in subsection 3.2.1. and 4.2.2.

6.2. Hydraulic Conductivity

6.2.1. Theoretical considerations

In this study, the hydraulic conductivity, *k*, through a bentonite seal has been estimated by using the law of Darcy.

$$k = \frac{Q}{A}\left[\frac{-1}{\Delta h/\Delta l}\right] \qquad (6.1)$$

where $\Delta h/\Delta l$ is the hydraulic gradient. Δh is the difference in hydraulic head measured in mm water column just above and below the sample. By looking at Figure 4 this is illustrated by h_1 and h_2 respectively. Δl is the distande between the outlet of h_1 and h_2. In this study this distance is equvivalent to the hight of the bentonite sample. Q is the waterflow through the sample and A is the cross sectional area of the inner part of the plexiglass cylinder. Seven tests have been performed, all with different heights of the test cylinder, ranging from 1.25 m to 7.32 m.

6.2.2. Apparatus

Figure 6.2 illustrates the setup which is used in this study to measure the hydraulic conductivity, *k*. A Plexiglas cylinders with a inner diameter of 99 mm and with different heights for the different tests have been constructed. Water is loaded continously

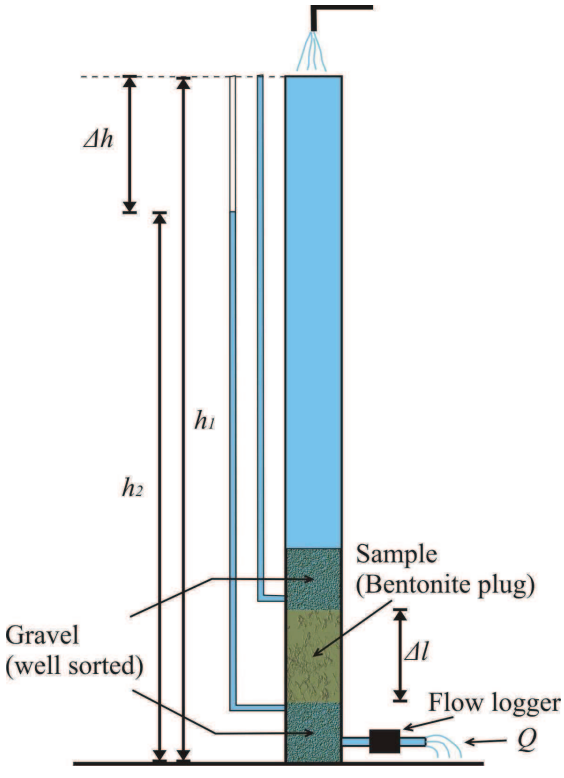

Figure 6.2: Experimental setup.

into the cylinder from the top and drained out from the bottom. Sufficient water is loaded into the cylinder, so that the hydraulic head is constant over time. Around the water outlet at the bottom of the cylinder, coarse grained gravel with high permeability has been placed. On top of that, the bentonite sample has been placed. The sample consists of bentonite pellets as described in details in Appendix III. In each test approximately 50 cm of sample has been used. In order to keep the volume of the bentonite sample constant when it starts to swell, another layer of coase grained gravel has been placed on top of the sample. Water is then transported downward through the sample. The only propelling force is the pressure gradient from the water itself.

6.2.3. Results

The hydraulic conductivity, k (cm/s), versus time, t (min) has been plotted in ae diagram (Figure 6.3). Seven experiments have been conducted, each with different heights of the water column. Note the logarithmic scale on the y-axis. The height has been measured from the water outlet to the top of the test tube (Figure 6.2).

As can be seen from Figure 6.3, the results can be divided into two main groups. The bentonite samples which have only been subjected to a water pressure equivalent to maximum 2.25 metres of water column, have a relatively smooth and decreasing shape over time. In the following those samples will be denoted “low pressure samples”. Over time it must be expected that the sealing

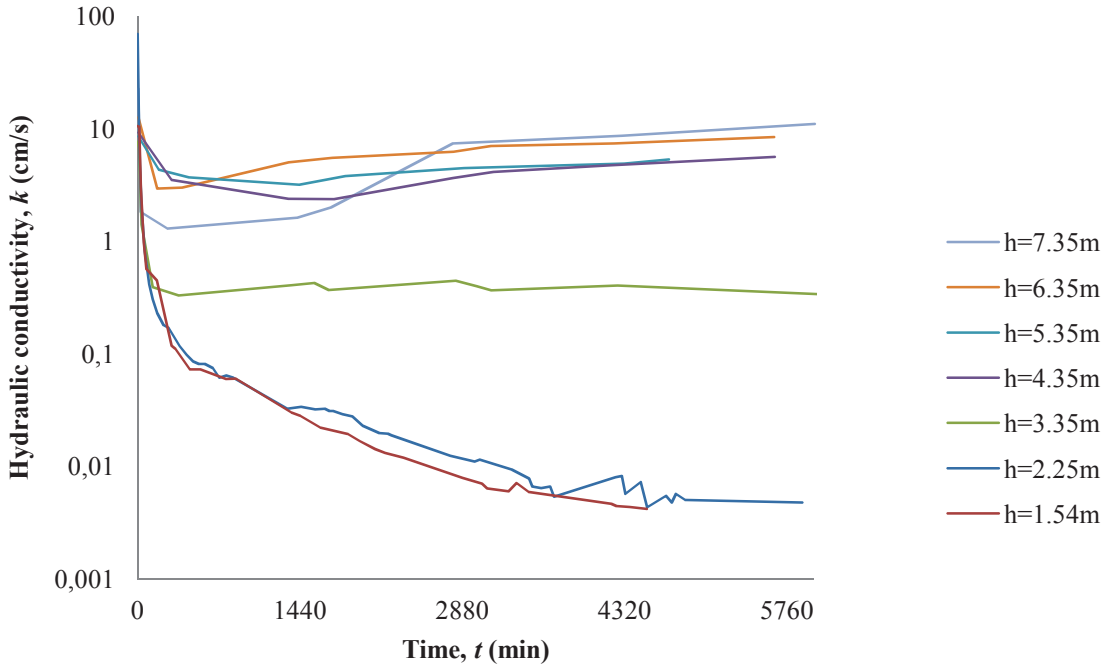

Figure 6.3: Results of the hydraulic conductivity test. Note the logarithmic scale on the y-axis.

potential increase further, which means that the hydraulic conductivity, k, will reach values which are very close to 0.

Samples which have been subjected to a water pressure above 4.35 metres of water column, has a marked different shape. A general trend of the curves is seen. Within the first 1440 minutes (24 h) a marked decrease in the hydraulic conductivity, k, is seen, which is followed by a gentle increase in values over time. In the following, those samples will be denoted “high pressure samples”. The relatively low hydraulic conductivity, k, within the first 1440 minutes in the high-pressure samples is probably due to the nature of swelling of the bentonite pellets. When the surface of the bentonite pellets is exposed to water it will start to swell, which means that a lot of small clay fragments or debris will be liberated from the surface of the pellet. The amount of liberated debris is relatively large at the beginning of the swelling process, which means that the water flow, Q, through the sample is not sufficient to remove the liberated debris completely out of the sample. After a period of maximum 1440 minutes, the water flow exceeds the amount of debris liberated from the surface of the pellets, which mean that the water flow is capable to transport the liberated fragments out of the system. The hydraulic conductivity, k, starts to increase again. From this point on, the increase of erosion of the pellets will be more pronounced. If the pressure conditions remain constant over time it must be expected that the bentonite sample will disintegrate and be removed completely. One bentonite sample which has been subjected to a water pressure equivalent to 3.35 metres of water column indicates the transition zone between the two regimes which have been discussed above.

6.3. Channel Systems

During the hydraulic conductivity tests it was observed that the water flow, Q, through the samples tends to use a specific set of preferred pathways at the rim of the sample. Some of the initial cavities or pathways, in which the water flow for some reason have been small, tend to close completely. The preferred pathways of the water flow must be expected to be those in which a high initial water flow through the sample is seen.

This effect is expected to be self-perpetuating to the point where only very few, high-potential channel systems are left. Figures 6.4 and 6.5 show the development of such channel systems in a low pressure sample and a high pressure sample, respectively.

In the low-pressure sample it can visually be observed that the channelsystem tends to be more narrow over time. In this case the sample has been subjected to a water pressure equivalent to 2.25 metres of water column. This observation is in very good agreement with the data presented in Figure 6.3 for h=2.25 m. Here it is seen that the hydraulic conductivity, k, is going towards 0 over time. In Figure 8 the channel system for a high-pressure sample is seen. This sample has been subjected to a water pressure equivalent to 6.35 metres of water column. As can be observed, the channel-system tends to broaden its path way over time. In this case as well, this observation is in a good agreement with the data presented in Figure 6.3 for h=6.35 m.

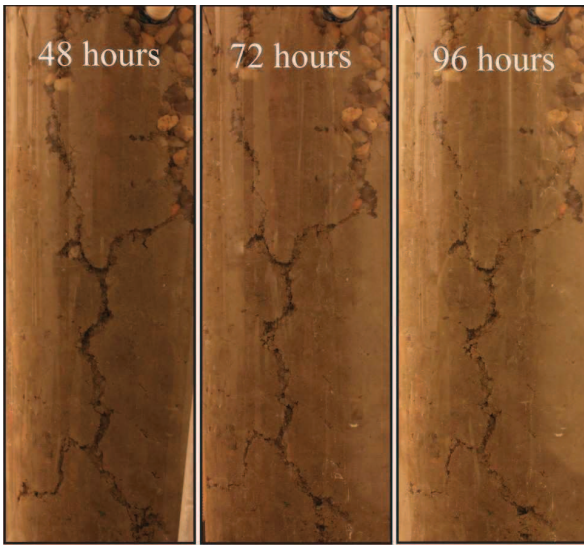

Figure 6.4: A low-pressure sample which has been subjected to a water pressure equivalent to 2.25 metres of water column. As can been seen, a preferred pathway has been created after less the 48 hours. From visual inspection of the tree photos, it can be seen that the pathway becomes more narrow over time.

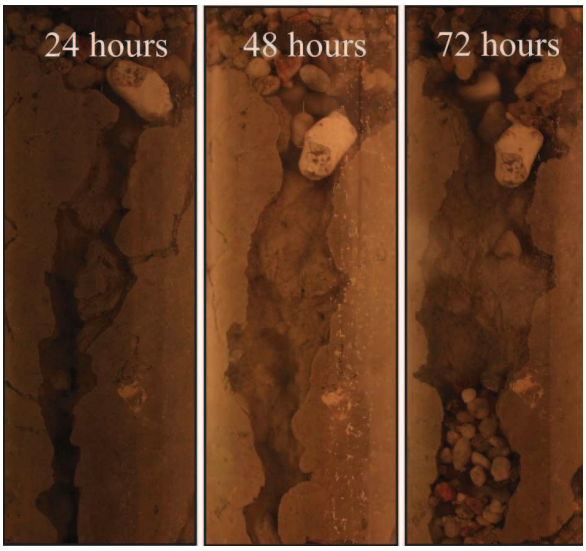

Figure 6.5: A high-pressure sample which has been subjected to a water pressure equivalent to 6.35 metres of water column. As can been seen, a preferred pathway has been created after less the 24 hours. From visual inspection of the tree photos, it can be seen that the pathway becomes wider over time.

6.3.1. Density variation of high-pressure sample

To examine the internal structure of a high-pressure sample, a CT scan was made. Figure 6.6 shows a slice through a high pressure sample perpendicular to direction of flow. The sample has been exposed to a water pressure equivalent to maximum 5.35 metres of water column for more

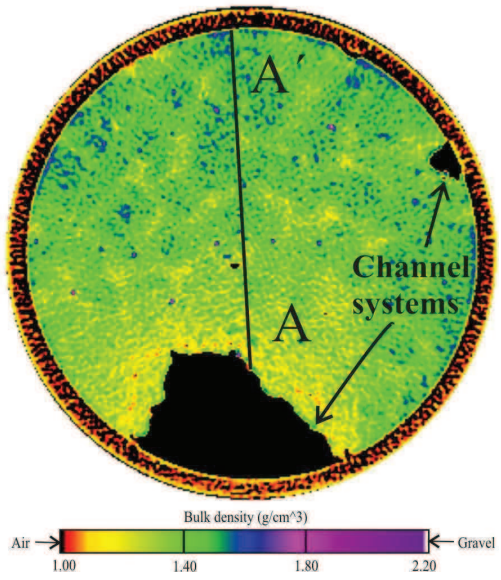

Figure 6.6: CT scan of a high pressure sample perpendicular to the flow direction. Profile A-A´ show how the density changes and become higher away from the channel. This is shown on figure 5.7.

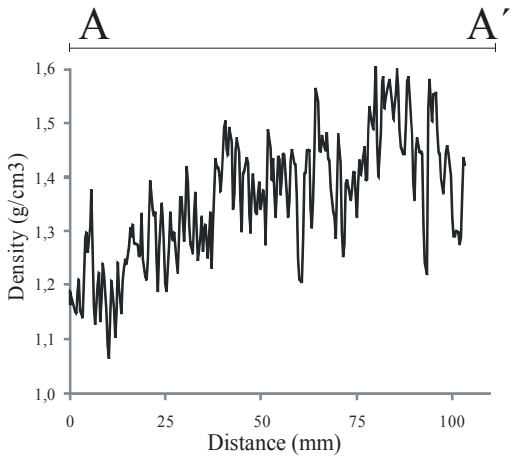

Figure 6.7: Density profile A-A´ from Figure 5.6.

than 48 hours. The black areas indicate channel systems. The colour code is directly related to density. Dark purple colours indicate densities of approximately 2.0 g/cm^3 which is the dry density of bentonite pellets. The orange/red colour indicates clay gel.

As can be seen, two channel systems are present in this sample. The channel system in the bottom of the figure has a very large surface area, which means that the velocity of the water flow through this part of the sample is very high compared to the small channel system at the upper right part of the sample. The higher velocity in the larger channel system also means that the erosional potential is bigger here. This fact has a great impact on the density variation throughout the sample. The densities of the bentonite near the large channel system are much lower compared to the rest of the sample. This is also illustrated in Figure 6.7 where a profile A-A' has been drawn through the sample. From the graph it is seen how the densities vary throughout the sample. It is clearly seen how the densities gradually increases in values away from the channel system. Near the channel system the densities are approximately 1.15 g/cm^3, and in the other end of the profile values near 1.6 g/cm^3 can be seen. In this part of the sample, much larger density variations is seen. This is due to absence of water which means that the bentonite pellets cannot use its full swelling potential. Near the channel system a more homogeneous density variation is seen.

6.3.2. Internal pathways and self-sealing potential

To investigate how the internal structure of a low pressure sample which has only been subjected to water pressure for a short period of time, a CT scan was used. After approximately 24 hours, the test was terminated and the sample was scanned. Figure 6.8 (1a and 1b) show an example of a randomly picked slice within the sample, immediately after the test has been terminated and the water has been drained out. 1a show the actual CT image and 1b show the same image after digital image analysis (DIA) has been performed. In this image the internal pathways and cavities, which are seen as black areas, are isolated.

In order to investigate the effectiveness of the self-sealing potential of the bentonite clay, the sample was scanned once more after an additional 24 hours. After the first CT scan the sample was filled with water once more, but this time there was no flow through the sample.

In this second step, water was added in the top of the sample. The water was then using the already existing pathways during the downward transport to the point in which all open pathways were completely filled with water. This means that no water entered the enclosed cavities of the sample. After the additional 24 hours, the sample was drained once more before the scanning was performed. Figure 6.8 (2a and 2b) shows the same slice after the self sealing has taken place.

A visual inspection of the figure indicates that the total number of holes has decreased and the sizes of the holes left have diminished significantly.

In order to perform a more quantitative analysis, ten slices before and after the second scan has been analysed in detail by using DIA. The results are shown in Table 6.1. Three things have been investigated with the use of DIA: number of holes, the total area of holes and the sizes of holes. In addition to that, there has been made a distinguishing between; if the holes were located at the rim of the sample (direct contact with the plexiglas tube) or in the middle of the sample.

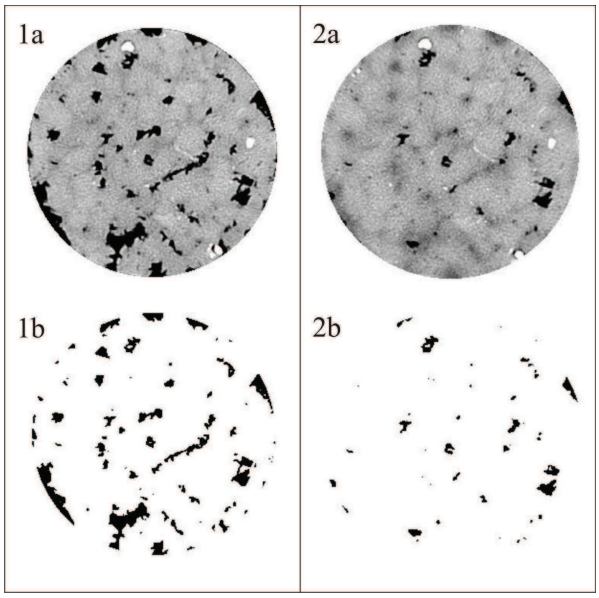

Figure 6.8: Show how the internal channel system evolves over a time period of 24 hours.

Table 6.1. Show the total number of holes, the total area which is occupied by the holes and the sizes of holes. The total number in the divided into the fraction at the middle and the fraction which is in contact with the border.

Number of holes

	Before	After	Decrease (%)
total	81.86	63.43	22.51
middle	59.57	47.14	20.87
border	22.29	16.29	26.92

Total area of holes

	Before	After	Decrease (%)
total	445.49	189.01	57.57
middle	228.94	116.06	49.31
border	216.55	72.95	66.31

Sizes of holes

	Before	After	Decrease (%)
total	5.46	2.97	45.60
middle	3.86	2.46	36.27
border	9.72	4.48	53.91

By looking at the number of holes, it can be seen that the majorities of holes is located in the middle of the sample. This is the case both before and after the second scan. Thus the biggest changes (decrease in values) is seen at the rim of the sample. The same pattern is seen when looking at the total area of holes and the sizes of holes. This fact is indicating that water flow is more pronounced in this area and that the absence of water in the middle part of the sample means that cavities will not evolve further.

It can be concluded that when a bentonite seal is subjected to a pressure gradient it can be subdivide into two zones regarding macroporosity: One zone near the rim of the seal where the cavities are actually connected with each other, so that a net transport of water can take place, and a middle zone where the cavities are isolated from each other.

Chapter 7

Recommendations

Based on the results obtained in this Ph.D. thesis, the following two main recommendations must be offered.

1. Bentonite pellets which are produced with the purpose for sealing off grondwater well, should be produced in such a way that they obtain a uniform size and with a Feret diameter d_F of approximately 10 mm.

   As stated in Section 2.1, a typical sample of bentonite pellets contains a wide range of particle sizes. During the transport phase down through the bore hole, a particle segregation of pellets travelling in a bundle will take place. In this way, the pellets are deposited according to their size and in a predictable pattern. This has been accounted for in Section 2.3.2. Small pellets will be packed more densely than larger pellets, which will lead to a higher bulk density. Basically it is agreed that the higher the bulk density in a bentonite clay, the higher the swelling pressure will be. It is also agreed that there is a clear connection between the bulk density and the hydraulic conductivity. The higher bulk density the lower hydraulic conductivity. The present research indicates that this assumption is only partly right when it comes to bentonite clay in the form of pellets.

   By the work presented in this thesis, it is shown that a sorted sample with the exact same bulk density as in an unsorted sample will obtain a much higher swelling pressure (Figure 3.11). An explanation to why this is the case is offered in Section 3.4. To obtain a maximum sealing potential in the furture, it is therefore important that bentonite pellets will be procuced in such a way that they obtain a uniform size and with a Feret diameter d_F of approximately 10 mm.

2. Immediately after construction of a groundwater well, the macroporosity of the clay deposition is in the order of approximately 48%. It is common but not good practic to start pumping in order to clean the filter section for debris and other kinds of impurities at this point. The recommentations in this area say that the pumping should not be started within the first 24 hours. Four argumentations will be offered in this Ph.D. thesis in favour of the existing recommendation.

   In Chapter 6 it was explained what could happen if a high waterflow through a bentonite sealing was present during the first phase of expansion of the pellets (in Section 6.2.4 the results of the hydraulic conductivity test are presented). During the hydration, small clay particles are loosened and liberated from the surface of the bentonite pellets and if the waterflow is sufficently high, those particles will be carried away and in this way will not contribute to the overall expansion. Two possible scenarios which could cause this situation are explained in Section 6.2 (Figure 6.1).

   As explained preveously, the macroporosity of the clay deposit is in the order of approximately 48% immediately after the deposition has taken place. From Figure 5.3. it can be seen that after 24 hours (1440 min), the macroporosity has dropped to approximately 2%. Computed tomography (CT) has been used to evaluate the degree of homogenization (for further explination see section 5.3.3.). In this work the degree of homogenization is expressed as a function of standard deviation of the density contrast through a profile versus time (Figure 5.5.). The result is seen in Figure 5.6. A marked decrease in standard deviation is seen within the first 24 hours. In other words: The degree og homogenization will increase very fast within the firste 24 hours. This mean that no weak or low density zones are present after 24 hours.

   Because of the suction of water into the sample, a marked increase in the overall bulk density is also seen within the first 24 hours (as stated previously there is a clear connection between the bulk density and the hydraulic conductivity). The higher bulk density the lower hydraulic conductivity. The increase in bulk density of the samples will of couse lead to an increase in the swelling pressure.

   By looking at the swelling pressure for both unsorted and sorted samples (Subsection 3.3.2 and 3.3.3) it can be seen that approximately 72% of the average swelling potential is reached after 24 hours.

   Based on those four arguments it is most unlikely that a waterflow will be able to penetrate a bentonite seal after a periode of 24 hours with neutral water gradient. The existing recommendation is therefore supported strongly with those new arguments.

References

Agus, S. S., and Schanz, T. (2008): A method for predicting swelling pressure of compacted bentonites. Acta Geotechnica. Vol. 3, pp. 125–137.

Andersen, S. A. 1937a: De vulkanske Askelag i Vejgennemskæringen ved Ølst og deres Udbredelse i Danmark. *Danm. geol. Unders.* (2) 59, 50 pp.

Anderson, S.H., Gantzer, C.J., Boone, J.M. and Tully, R.J., (1988). Rapid nondestructive bulk density and soil-water content determination by computed tomography. Soil Sci. Soc. Am. J. Vol. 52. Pp. 35-40.

Anderson, S.H., Peyton, R. L., and Gantzer, C. J. (1990): Evaluation of Constructed and Natural Soil Macropores Using X-Ray Computed Tomography.Geoderma, Vol. 46, pp. 13-29.

Andreasen, J. O. 1999. Historien om de utætte boringer. ATV møde, utætte boringer – kan der gøres noget. pp. 43 – 51.

Avrin, D.E., Mackovski, A., Zatz, L.M. (1978). Clinical application of Compton and photo-electric reconstruction in computed tomography: preliminary results. Investigative Radiology 13. pp.217– 222.

Bates, R. L., and Jackson, J. A. (1997): Glossary of Geology. AGI, American geological institute (fourth edition).

Bohloli, B. and Pater, C. J. (2006): Experimental study on hydraulic fracturing of soft rocks: Influence of fluid rheology and confining stress. Journal of Petroleum Science & Engineering. Vol. 53. pp. 1-12.

Brüsch. W. 2004. Pesticidanvendelse i landbruget. Udarbejdet af GEUS til Dansk Planteværn.

Brüsch. W., Stockmarr, J., Kelstrup, N., Hallermund, F. V. P., Rosenberg, P. 2004. Pesticidforurenet vand i små vandforsyninger. GEUS undersøgelsesrapport 2004/9.

Bushberg. J. T., Seibert, J. A., Boone, J. M. andLeidholdt, E. M (2001): The Essential Physics of Medical Imaging (2nd Revised edition). Lipincott Williams and Wilkins, chap. 13.

Bøggild, O. B. 1918: Den vulkanske Aske i Moleret samt en Oversigt over Danmarks ældre Tertiærbjærgarter. *Danm. geol. Unders.,* (2) 33,159 pp.

Cássaro, F.A.M., (1994). Tomografia de dupla energia simult-anea para caracterizacao fisica de um meio poroso deformável. Dissertacao de mestrado, EESC/USP, Sao Carlos, 119pp.

Castellanos, E., Villar M. V., Romero, E., Lloret, A., and Gens, A. (2008): Chemical impact on the hydro-mechanical behaviour of high-density FEBEX bentonite. Physics and Chemistry of the Earth. Vol. 33, pp. S516–S526.

Císlerová, M. and Votrubová, J. (2002): CT derived porosity distribution and flow domains. Journal of Hydrology. Vol. 267, pp. 186–200.

Chakraborty, J., Verma, N., and Chhabra, R.P. (2004): Wall effects in flow past a circular cylinder in a plane channel: a numerical study. Chemical Engineering and Processing 43, pp. 1529–1537.

Chabra, R. B. (1995): Wall effects on free-settling velocity of non-spherical particles in viscous media in cylindrical tubes. Powder Technology 85, pp. 83-90.

Chabra, R. B. (1996): Wall effects on terminal velocity of non-spherical particles in non-Newtonian polymer solutions. Powder Technology 88, pp. 39-44.

Chhabra, R. P., Agarwal1, S., and Chaudhary, K. (2003): A note on wall effect on the terminal falling velocity of a sphere in quiescent Newtonian media in cylindrical tubes. Powder Technology 129 (2003) 53– 58.

Chabra, R. B., Agarwal, L. and Sinha, N.,K. (1999): Drag on non-shperical particles: an evaluation of available methods. Powder Technology 101, pp. 288-295.

Císlerova, M., and Votrubová, J. (2002): CT derived porosity distribution and flow domains. Journal of Hydrology. 267. Vol 267. Pp. 186–200.

Clemmensen, A., and Thomsen, E., 2005, Palaeoenvironmental changes across the Danian-Selandian boundary in the North Sea Basin: Palaeogeography, Palaeoclimatology, Palaeoecology, v. 219, pp. 351–394.

Coulon, H. (1987). Proprie´te´s physico-chimiques de se´diments argileux franc¸ais : contribution au stockage de de´chets radioactifs. PhD thesis. Universite´ des sciences et techniques de Lille Flandres-Artois.

Curry, T.S., Dowdey, J.E., Murry, R.C. (1990). Christensen's physics of diagnostic radiology. Lea and Febiger, London. 522 pp.

Cuevas, J., Villar, M.V., Martín, M., Cobeña, J. C., and Leguey, S. (2002): Thermo-hydraulic gradients on bentonite: distribution of soluble salts, microstructure and modification of the hydraulic and mechanical behaviour. Applied Clay Science. Vol. 22, pp. 25– 38.

Dinesen, A., Michelsen, O. & Lieberkind, K. 1977: A survey of the Paleocene and Eocene deposits of Jylland and Fyn. *Danm. geol. Unders. Ser. B* 1, 15 pp.

DMU 2005: NOVANA – det nationale program for overvågning af vandmiljøet og naturen. Programbeskrivelse del 1, 2 og 3. Faglig rapport fra Danmarks Miljøundersøgelser nr. 495 og 508 samt http://www.dmu.dk/Overvågning/NOVANA/Programbeskrivelse+del+3/ DMU 2005.

Egger, H., and Brückl, E., 2006, Gigantic volcanic eruptions and climatic change in the early Eocene: International Journal of Earth Sciences, v. 95, pp. 1065–1070.

Escudiéa, R., Epsteina, N., Gracea, J.R., Bia, H.T. (2006), Effect of particle shape on liquid-fluidized beds of binary (and ternary) solids mixtures: segregation vs. mixing. Chemical Engineering Science vol. 61, pp. 1528 – 1539.

García-Gutiérreza, M., Mingarroa, M., Missanaa, T., Martína, P. L., Sedanoa, L. A., Cormenzanab, J. L. (2004): Diffusion experiments with compacted powder/pellets clay mixtures. Applied Clay Science. Vol. 26., pp. 57– 64.

Gabitto, J. and Tsouris, C. (2008): Drag coefficient and settling velocity for particles of cylindrical shape. Powder Technology 183, pp. 314-322.

Ganser, G. H. (1993): A rational approach to drag prediction of spherical and non spherical particles. Powder Technology 77, pp. 143-152.

Gingold, E.L., Hasegawa, B.H. (1992). Systematic bias in material decomposition applied to quantitative dual energy X-ray imaging. Medical Physics. Vol. 19. Pp. 25– 33.

Gillham, R.W. and Cherry, J.A. 1982. Contaminant migration in saturated unconsolidated geologic deposits. In: T.N. Narasimhan (Editor), Recent Trends in Hydrogeology, GSA Special Paper 189. Geol. Soc. Am., Boulder, CO, pp. 31-62.

Graversen, P., Klint, K. E. S., Jacobsen, O. S., Harrar, W. G., Felding, G., Jørgensen, P., Fomsgaard, I., og Spliid, N. H. Transport af vand og pestesider i opsprækket moræneler. Det strategiske Miljøforskningsprogram. Temanummer fra Grundvandsgruppen, nr. 42. pp.6-9.

Grim, R. G. (1962): Clay mineralogy. Applied Clay Mineralogy. Vol. 135, pp. 890-898

Grim, R. G. (1968): Clay mineralogy, 2nd. Edition. McGraw-Hill, New York. p. 596.

Grim, R. G., and Goven, N. (1978): Bentonites-Geology, Mineralogy, Properties and Uses. Elsevier, Amsterdam, p. 256.

Gry, H. 1935: Petrology of the Paleocene Sedimentary Rocks of Denmark. *Danm. geol. Unders.* (2) 61,171 pp.

Haider, A. H. and Levenspiel, O. (1989): Drag coefficient and terminal velocity of spherical and non-spherical particles. Powder Technology 58, pp. 63-70.

Hartman, M., Trnka, O. and Svoboda, K. (1994): Free settling of nonspherical particles. Ind. Eng. Chem. Res. 33, p. 1979.

Hasenpatt.R., Degen, W., and Kahr. G. (1989): Flow and diffusion in clay. Applied Clay Science, Vol 4. Pp.179-192.

Heilmann-Clausen, C , Nielsen, O. B. and Gersner, P.: Lithostratigraphy and depositional environments in the Upper Paleocene and Eocene of Denmark. *Bull. geol. Soc. Denmark,* vol. 33, pp. 287-323, Copenhagen, February, 28th, 1985.

Heilmann-Clausen, C., 2006, Chapter10, Koralrev og lerhav (except Danian) *in* G. Larsen, ed., Naturen i Danmark, Geologien. Gyldendal, Copenhagen, pp. 181–186 and 191–226.

Hoffmann, C., Alonso, E. E., and Romero, E. (2007): Hydro-mechanical behaviour of bentonite pellet mixtures. Physics and Chemistry of the Earth. Vol. 32. pp. 832–849.

Iassonov, P., Gebrenegus, T., Tuller, T. (2009): Segmentation of X-ray computed tomography images of porous materials: A crucial step for characterization and quantitative analysis of pore structures. WATER RESOURCES RESEARCH, VOL. 45. pp. 1-12.

Imbert, C. and Villar, M., V. (2006): Hydro-mechanical response of a bentonite pellet/powder mixture upon infiltration. Applied Clay Science. Vo. 32. pp. 197-209.

Illies, H. 1949: Die Lithogenese des Untereozäns in Nordwestdeutschland. *Mitt. geol. Stinst. Hamb.* 18, 6-44.

Isaacs, J., L. and Thodos, G. (1967): The Free-Settling of solid Cylindrical Particles in the turbulent Regime. The Canadian Journal of Chemical Engineering, Vol. 45, pp. 150-155.

Jacobsen, P. E. 1999. Tætte boringer – materialevalgets betydning – kan nutidens boringer sikre fremtidens boringer? ATV møde, utætte boringer – kan der gøres noget?, pp. 9 -20.

Kaiser, A.,E., Grahama, A. L., and Mondy, L. A. (2004): Non-Newtonian wall effects in concentrated suspensions. J. Non-Newtonian Fluid Mech. 116, pp. 479–488.

Kawaragi, C., Yoneda, T., Sato, T. and Kaneko, K. (2009): Microstructure of saturated bentonites characterized by X-ray CT observations. Engineering geology. Vol 106. pp. 51-56.

Ketcham, R. A., Meth, C., Hirsch, D. M., and Carlson, W. D. (2005): Improved methods for quantitative analysis of three-dimensional porphyroblastic textures. Geosphere. Vol.1. pp. 42–59.

Kemp, S. J., Wagner, D., and Harrison, H. M. (2008): Mineralogical and geochemical characterisation of bentonite samples for Dantonit Ltd. British geological survey. Laboratory operations programme commissioned report CR/08/074.

Knox, R. W. O'B. & Hariand, R. 1979: Stratigraphical relationships of the early Palaeogene ash-series of NW Europe. *J. geol. Soc. Lond.* 136 (4), 463-470.

Knox, R.W.O'B., 1996, Tectonic controls on sequence development in the Palaeocene and earliest Eocene of southeast England: implications for North Sea stratigraphy, *in* Hesselbo, S.P., and Parkinson, D.N., eds., Sequence Stratigraphy in British Geology: Geological Society Special Publication No. 103, pp. 209–230.

Kozaki, T., Sato, Y., and Nakajima, M., (1999): Effect of particle size on the diffusion behavior of some radionuclides in compacted bentonite. Journal of Nuclear Materials. Vol. 270, pp. 265-272.

Kozaki, T., Suzuki, S., Kozai, N., Sato, S., Ohashi, H. (2001). Observation of microstructures of compacted bentonite by microfocus X-ray computerized tomography (MicroCT). Journal of Nuclear Science and Technology 38, 679– 699.

Komine, H. (2004): Simplified evaluation on hydraulic conductivities of sand–bentonite mixture backfill. Applied Clay Science. Vol. 26, pp. 13– 19.

Komine, H. (2008): Theoretical Equations on Hydraulic Conductivities of Bentonite-Based Buffer and Backfill for Underground Disposal of Radioactive Wastes. Journal of Geotechnical and Geoenvironmental Engineering, Vol. 134, pp. 497-508. Engineering Geology. Vol. 114. Issue 3-4. Pp. 123-134.

Komine, H. (2010): Predicting hydraulic conductivity of sand–bentonite mixture backfill before and after swelling deformation for underground disposal of radioactive wastes.

Komine, H. (2004): Simplified evaluation for swelling characteristics of bentonites. Engineering Geology. Vol. 71, pp. 265–279.

Komine, H., Ogata, N. (1994): Experimental study on swelling characteristics of compacted bentonite. Can. Geotechnical Journal. Vol 31. Pp. 478-490.

Komine, H., Ogata, N. (1996a): Prediction for swelling characteristics of compacted bentonite. Can. Geotechnical Journal. Vol . 33. Pp. 11-22.

Komine, H., Ogata, N. (1996b): Observation of swelling behaviour of bentonite by new electron microscope. Proc. Of 2nd int congress on Environmental Geotechnics (IS-osaka*96), Vol. 1, pp. 563-568.

Komine, H., Ogata, N. (1997): Prediction for swelling characteristics of compacted bentonite: Reply. Can. Geotechnical Journal. Vol 34. Pp. 1005-1006.

Komine, H., Ogata, N. (1999). Experimental study on swelling characteristics of sand– bentonite mixture for nuclear waste disposal. Soils and Foundations. Vol. 39 (2), pp. 83– 97.

Komine, H., Ogata, N. (2003). New equations for swelling characteristics of bentonite-based buffer materials. Can. Geotech. J. 40: 460–475.

Komine, H., Ogata, N., (2004). Predicting swelling characteristics of bentonites. Journal of geotechnical and geoenvironmental engineering.

Komine, H., Yasuhara, K., and Murakami, S. (2009): Swelling characteristics of bentonites in artificial seawater. Can. Geotechnical Journal. Vol. 46. Pp. 177-189.

Laier, T. 2002. Renovering af overvågningsboringer i Roskilde amt – aldersbestemmelse af grundvand ved CFC metoden før og efter. GEUS notat.

Lajudie, A., Raynal, J., Petit, J.-C., Toulhoat, P. (1994). Clay based materials for engineered barriers: a review. Materials Research Society Symposia Proceedings of Kyoto, 221–230.

Lali, A. M., Khare, A. S., and Joshi, J. B. (1989):Behaviour of Solid Particles in Viscous Non-Newtonian Solutions: Settling Velocity, Wall Effects and Bed Expansion in Solid-Liquid Fluidized Beds. Powder Technology, 57 (1989) 39 - 50 .

Langroudi, A. A., and Yasrobi, S. S. (2009): A micro-mechanical approach to swelling behavior of unsaturated expansive clays under controlled drainage conditions. Applied Clay Science. Vol. 45, pp. 8–19.

Larsen, L.M., Fitton, J.G., and Pedersen, A.K., 2003, Palaeogene volcanic ash layers in the Danish Basin: compositions and source areas in the North Atlantic igneous province: Lithos, v. 71, pp. 47–80.

Larsen, G., 1998: Råstofkortlægning, fase 2, Bentonite, Bjerrebj, nr. 26. Svendborg Kommune

Lehmann, L.A., Alvarez, R.E., Mackovski, A., Brody, W.R., Pelc, N.J., Riederer, S.J., Hall, A.L. (1981). Generalized image combinations in dual KVP digital radiography. Medical Physics. Vol..8. pp. 659– 667.

Lloret, A., and Villar, M.V. (2007): Advances on the knowledge of the thermo-hydro-mechanical behaviour of heavily compacted ‘‘FEBEX’’ bentonite. Physics and Chemistry of the Earth. Vol. 32, pp. 701–715

Lorentzen, B. H. 1999. Undersøgelse af utætte boringer på kildeplads i Varde. ATV møde, utætte boringer – kan der gøres noget?, pp. 53 – 62.

Martínez, F. A. J., Martín, M. A., Caniego, F. J., Tuller, M., Guber, A., Pachepsky, Y., and García-Gutiérrez, C. (2010): Multifractal analysis of discretized X-ray CT images for the characterization of soil macropore structures. Geoderma. Vol. 156. Pp. 32–42.

Maugis, P., and Imbert, C. (2007): Confined wetting of FoCa clay powder/pellet mixture: Experimential and numerical modelling. Physics and Chemistry of the earth. Vol. 32. pp. 795-808.

Mees, F., Swennen, R., Van Geet, M., Jacobs, P. (Eds.). (2003). Applications of X-ray computed tomography in the geosciences, Special Publication - Geological Society of London vol. 215, 243 p.

Mesri, G., Pakbaz, M. C., and Cepeda-Diaz, A. F. (1994). Meaning, measurement and field application of swelling pressure of clay shales. Geotechnique Vol. 44(1). Pp.129–145.

Miljøstyrelsen 2007, BEK nr. 1000 af 26/7/2007. Bekendtgørelse om udførelse og sløjfning af boringer og brønde på land. Miljøministeriet, Miljøstyrelsen, j.nr. MST-420-00033.

Montes-H, G. (2005): Swelling–shrinkage measurements of bentonite using coupled environmental scanning electron microscopy and digital image analysis. Journal of Colloid and Interface Science. Vol. 284, pp. 271–277.

Monte-H, G., Duplay, J., Martinez, L. and Mendoza, C. (2003): Swelling-shrinkage kinetics of MX-80 bentonite. Applied Clay Science. Vol. 22. pp. 279-293.

Murray, H. H. (1991): Overview - clay mineral applications. Applied Clay Science. Vol. 5, pp. 379-395.

Murray, H. H. (2007): Applied Clay Mineralogy. Occurrances, Processing and Application of Kaolines, Bentonites, Palygorskite-Sepiolite, and Coon Clay. Development in clay science 2, (first edition).

Naime, J.M., 2001. Um novo metodo para estudos dinamicos, in situ, da infiltracao da agua na regiao nao-saturada do solo. Tese de doutorado, EESC/USP, Sao Carlos, 146pp.

Nielsen, O.B., 1994. Lithostratigraphy and sedimentary petrography of the Paleocene and Eocene sediments from the Harre borehole, Denmark. Aarhus Geosci. 1, 15–34.

Nitin, S., Chhabra, R. P. (2006). Sedimentation of a circular disk in power law fluids. Journal of Colloid and Interface Science 295 (2006) 520–527.

Ogata, N., Kosaki, A., Ueda, H., Asano, H., Takao, H., 1999. Execution techniques for high level radioactive waste disposal: IV. Design and manufacturing procedure of engineered barriers. Journal of Nuclear Fuel Cycle and Environment 5 (2), 103– 121 (in Japanese with English abstract).

Okagbue, C. O. (1995): Permeability of stratified sands. Geotechnical and Geological Engineering. Vol. 13. Pp. 157-168.

Oscarson, D.W. and Dixon, D.A. (1989). Elemental, mineralogical and pore-solution composition of selected Canadian clays. AECL Rep., AECL-9891. AECL, Chalk River.

Oscarson, D. W., Dixon, D. A. and Hume, H. B. (1996): Mass transport through defected bentonite plugs. Applied Clay Science. Vol. 11., pp. 127-142.

Pedrotti, A., Pauletto. E. A., Crestana, S., Holanda, F. S. R., Cruvinel, P. E., and P. M. C. Vaz. (2005): Evaluation of bulk density of Albaqualf soil under different tillage systems using the volumetric ring and computerized tomography methods. Soil & Tillage Research. Vol. 80. Pp. 115–123.

Petrovic, A.M., Siebert, J.E. and Rieke, P.E. (1982): Soil bulk density analysis in three dimensions by computed tomographic scanning. Soil Sci. Soc. Am. J., Vol. 46. Pp. 445-450.

Pires, L. F., de Macedo, J. R., de Souza, M. D., Bacchi, O. O. S., and Reichardt, K. (2002): Gamma-ray computed tomography to characterize soil surface sealing. Applied Radiation and Isotopes vol. 57. pp 375–380.

Pires, L. F., Bacchi, O. O. S., Reichardt, K., and Timm. L. C. (2005): Application of g-ray computed tomography to analysis of soil structure before density evaluations. Applied Radiation and Isotopes. Vol. 63. Pp. 505–511.

Pusch, R., 1994. Waste Disposal in Rock. Elsevier, New York.

Pusch, R. (1997): Transport phenomena in smectite clay explained by considering microstructural features. In: Mckinly, I.M., McCombie, C. M. (Eds.), Proc. MRS Scientific Basis for Nuclear Waste Management XXI vol. 506. Material Research Scoiety, Warrendale, PA, USA, pp. 439-448.

Pusch, R. (1999): Microstructural evolution of buffers. Engineering Geology. Vol 54. pp. 33-41.

Pusch, R., Bluemling, P., and Johnson, L. (2003): Performance of strongly compressed MX-80 pellets under repository-like conditions. Applied Clay Science. Vol. 23., pp. 239– 244.

Pusch, R., and Weston, R. (2003): Microstructural stability controls the hydraulic conductivity of smectitic buffer clay. Applied Clay Science. Vol. 23., pp. 35– 41.

Pusch, R., and Schomburg, J., (1999): Impact of microstructure on the hydraulic conductivity of undisturbed and artificially prepared smectitic clay. Engineering Geology. Vol. 54, pp. 167–172.

Rajitha, P., Chhabra, R. P., Sabiri, N. E., Comiti, J. (2006). Drag on non-spherical particles in power law non-Newtonian media. Int. J. Miner. Process. 78, 110– 121.

Ross, C. S., and Shannon, E. V. (1926): Minerals of Bentonite and related clays and their physical properties. Journal of Am. Ceram. Soc. Vol. 9, pp. 77-96.

Rowe, R.K., (1987). Pollutant transport through barriers. In: R.D. Woods (Editor), Geotechnical Practice for Waste Disposal.

Rutherford, R.A., Pullan, B.R., Isherwood, I. (1976a). Calibration and response of an EMI scanner Neuroradiology 11, 7 –13.

Rutherford, R.A., Pullan, B.R., Isherwood, I. (1976b). Measurement of effective atomic number and electron density using an EMI scanner. Neuroradiology 11, 15–21.

Saunders, A.D., Fitton; J.G., Kerr, A.C., Norry; M.J. and Kent, R.W., 1997, The North Atlantic Igneous Province. *In* Mahoney, J.J. and Coffin, M.F., eds, Large Igneous Provinces: Continental, Oceanic, and Planetary Flood Volcanism: AGU Geophysical Monograph, v. 100, pp. 45–93.

Schalla, R. and Walters, W. H. (1990). "Rationale for the design of monitoring well screens and filter packs" *in* Ground Water and Vadose Zone Monitoring, ASTM STP 1053, D. M. Nielsen and A. I. Johnson, Eds., American Society for testing and Materials, Philadelphia, 1990, pp. 64-75.

Schmitz, B., Heilmann-Clausen, C., King, C. Steurbaut, E., Andreasson, F.P., Corfield, R.M., and Cartlidge, J.E., 1996, Stable isotope and biotic evolution in the North Sea during the early Eocene: the Albæk Hoved section, Denmark, *in* Knox, R.W.O'B., Corfield, R.M., and Dunay, R.E., eds, Correlation of the Early Paleogene in Northwest Europe: Geological Society Special Publication, v. 101, pp. 275–306.

Schmidt, H. 1999: Udførelse og konstruktion af boringer før og nu – traditioner og regler. ATV møde, utætte boringer – kan der gøres noget?, pp. 1-7.

Sitz, P. (1997) Materialuntersuchungen für Mehrkomponentensysteme auf Ton/Bentonit Basis für Dichtung und Lastabtrag, mit hohem Rückhaltevermögen, für den langzeitsicheren Verschluß von UTD und Endlagern im Salinar. Abschlußbericht 02 C 0193 (BMBF), TU Bergakademie Freiberg, Germany

Sivakumar, V., Tan, W.C., Murray, E.J., McKinley, J.D., (2006). Wetting, drying, and compression characteristics of compacted clay. Geotechnique 56 (1), 57–62.

Skovgaard, M., Jensen, T. F., Hansen, P. B., Pedersen, O. F. (2001). Kortlægning af forureningsrisiko ved 700 boringer og brønde i Høle-Taastrup kommune. ATV møde, vintermøde om grundvandsforurening, pp. 297 -308.

Snyder, R.L. and Bish, D.L. (1989). Quantitative analysis. In: Bish, D.L., Post, J.E. (Eds), *Modern Powder Diffraction, Reviews in Mineralogy*, Volume 20, Mineralogical Society of America, USA, pp. 101-144 (Chapter 5).

Song, D., and Gupta, R. K. (2009): Wall Effects on a Sphere Falling in Quiescent Power Law Fluids in Cylindrical Tubes. Ind. Eng. Chem. Res. 48, pp. 5845–5856.

Spjeldnæs, N. 1975: Palaeogeography and faciès distribution in the Tertiary of Denmark and surtounding areas. *Norges geol. Unders.* 316, 289-311

Sridharan, A., Sreepada Rao, A., and Sivapullaiah, P. V. (1986) Swelling pressure of clays. Geotech Testing J, GTJODJ. Vol. 9(1). Pp.24–33.

Stonestrom, J.P., Alvarez, R.E., Mackovski, A. (1981). A framework for spectral artifact corrections in X-ray CT. IEEE Transactions on Biomedical Engineering Vol. 28. Pp. 128–141.

Suziki, S., Prayongphan, S., Ichikawa, Y. and Chae, B. –G. (2005): In Situ observations of the swelling of bentonite aggregates in NaCl solution. Applied Clay Science. Vol. 29. pp. 89-98.

Swamee, P., K. and Ojha, C., P. (1991): Drag coefficients and fall velocity of nonspherical particles. J. Hydraul. Eng. 117. p. 660.

Tang, C., Shi, B., Liu, C., Zhao, L., and Wang, B. (2008): Influencing factors of geometrical structure of surface shrinkage cracks in clayey soils. Engineering Geology, Vol. 101, pp. 204.217.

Thorling, L., og Jensen, O. D. 2002. Utætte boringer og punktkilder. ATV møde 1999.

Thorling, L. 2007: Grundvand, Status og udvikling 1989-2006, GEUS 2007.

Tomioka, S., Kozaki, T., Takamatsu, H., Noda, N., Nisiyama, S., Kozai, N., Suzuki, S. and Sato, S. (2008): Analysis of microstructural image of dry and water-saturated compacted bentonite samples observed with X-ray micro CT. Applied Clay Science.

Torp, S. B., Larsen, G., 1997: Råstofkortlægning, fase 1½, Bentonite, Kortlægning af plastisk ler ud fra eksisterende data. Fyns Amt nr. 1.

Van Geet, M., Bastiaens, W. and Ortiz, L. (2008): Self-sealing capacity of argillaceous rocks: Rewiev of laboratory results obtained from the SELFRAC project. Physics and Chemistry of the Earth. Vol. 33., pp. 396-406.

Van Geet, M., Volckaert, G., Bastiaens, W., Maes, N., Weetjens, E., Sillen, X., Vallejan, B. and Gens, A. (2007): Efficiency of a borehole seal by means of pre-compacted bentonite blocks. Physics and Chemistry of the Earth. Vol. 32., pp. 125-134.

Van Geet, M., Volckaert, G. and Roels, S. (2005): The use of microfocus X-ray computed tomography in characterising the hydration of a clay pellet/powder mixture. Applied Clay Science. Vol. 29., pp. 73-87.

Villar, M.V., Martín, P.L., and Barcala, J.M. (2005): Modification of physical, mechanical and hydraulic properties of bentonite by thermo-hydraulic gradients. Engineering Geology. Vol. 81, pp. 284– 297.

Villar, M.V., and Rivas, P. (1994): Hydraulic properties of montmorillonite-quartz and saponite-quartz mixtures. Applied Clay Science. Vol. 9, pp. 1-9.

Vogel, H. –J., Hoffmann, H. and Roth, K. (2005): Studies of crack dynamics in clay soil. I. Experimential methods, results, and morphological quantification. Geoderma. Vol. 125., pp. 203-211.

Vogel, H. –J., Hoffmann, H. and Roth, K. (2005): Studies of crack dynamics in clay soil. II. A physical based model for crack formation. Geoderma. Vol. 125., pp. 213-223.

Waagstein R., and Heilmann-Clausen, C. (1995): Petrography and biostratigraphy of Palaeogene volcaniclastic sediments dredged from the Faeroes shelf, *in* Scrutton, R.A. et al., eds., The tectonics, Sedimentation and Palaeoceanography of the North Atlantic Region, Geological Society Special Publication, Vol. 90, pp. 79–197.

Wang, C.H., Willis, D.L., Loveland, W.D., (1975). Characteristics of ionizing radiation. In: Wang, C.H., Willis, D.L., Loveland, W.D. (Eds.), Radiotracer Methodology in the Biological Environmental, and Physical Sciences. Prentice-Hall, Englewood Cliffs, NJ, pp. 39–74.

Wildenschild, D., Hopmans, J. W., Vaz, C. M. P., Rivers, M. L., Rikard, D,. and Christensen, B. S. B. (2002): Using X-ray computed tomography in hydrology: systems, resolutions, and limitations. Journal of Hydrology Vol. 267, pp. 285–297.

Ziegler, P.A. (1990): Geological Atlas of Western and Central Europe. Shell Internationale Petroleum Maatschappij B.V. Den Haag. pp. 239.

Ziegler, P.A., 1992. North Sea rift system. In: P.A. Ziegler (Editor), Geodynamics of Rifting, Volume I. Case History Studies on Rifts: Europe and Asia. *Tectonophysics, 208: 55-75.*

Appendix 1

Product of interest

1. Bentonite

The rock term “bentonite” is commonly used for smectite minerals and was defined by Ross and Shannon (1926) as a clay material altered from a glassy igneous material, usually volcanic ash. Grim and Goven (1978) used the term bentonite for any clay which was dominantly comprised of a smectite mineral within regards to its origin. In the Glossary of Geology Bates and Jackson (1997), bentonite is described as “*a soft plastic, rock composed essentially of clay minerals of the montmorillonite (smectite group) plus colloidal silica, and produced by devitrification and accompanying chemical alteration of a glassy igneous material, usually a tuff or volcanic ash. The rock is greasy and soap-like to the touch (without gritty feeling), and commonly has the ability to absorb large quantities of water accompanied by an increase in volume of about 8 times*”.

Smectite minerals are composed of two silica tetrahedral sheets with a central octahedral sheet and are designated as a 2:1 layer mineral (Figure 1). Water molecules and cations occupy the space between the 2:1 layers (Murray, 2007). The octahedral sheet in the smectite mineral is comprised of closely packed oxygens and hydroxyls in which aluminium, iron, and magnesium atoms are arranged in octahedral coordination. When aluminium with a positive valence of three is the cation present in the octahedral sheets, only two-thirds of the possible positions are filled in order to balance the charge. When only two-thirds of the positions are filled, the mineral is termed dioctahedral. When magnesium with a positive charge of two is present, all three positions are filled to balance the structure and the mineral are termed trioctahedral.

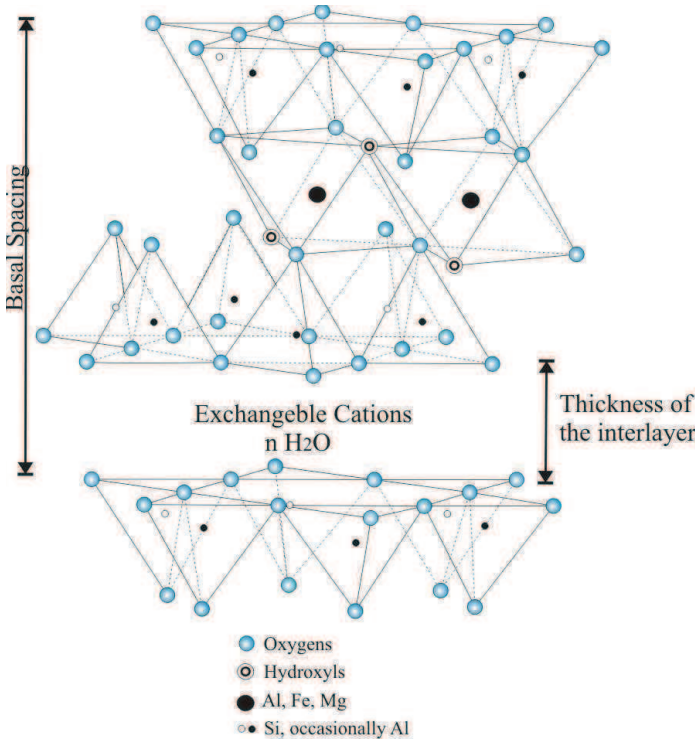

Figure 1. Diagrammed sketch of the structure of smectite.

The second structure unit in the smectite mineral is the silica tetrahedral layer in which the silicon atom is equidistant from four oxygen atoms or possible hydroxyls arranged in the form of tetrahedron with the silicon atom in the center. These tetrahedrons are arranged to form a hexagonal network repeated infinitely in two horizontal directions to form what is called the silica tetrahedral sheet (Murray, 2007). The silica tetrahedral sheet and the octahedral sheet are joined by sharing the apical oxygens or hydroxyls (Figure 1). When the octahedral sheet and the tetrahedral sheet are electrically neutral then they are held together by Van der Waals Bonds. Those forces are electrical in nature and results from the attraction of charges of opposite sign.

Both the octahedral and tetrahedral sheets can have substitutions, which creates a charge imbalance in the 2:1 layer. Alumina substitutes for silica in the tetrahedral sheet and iron and magnesium substitute for aluminum in the octahedral sheet. Grim (1962) reported that many analyses have shown that the charge imbalance in smectite is about 0.66 per unit cell. This net positive charge deficiency is balanced by exchangeable cations absorbed between the unit layers (interlayers).

The smectite group of clay minerals consists of several clay minerals, but the two most important industrially are sodium montmorillonite and calcium montmorillonite. The basal spacing of the calcium montmorillonite is 14.2 Å. Sodium montmorillonite occurs when the charge deficiency is balanced by sodium ions and water and the basal spacing is 12.2 Å (Murray, 1991). Calcium montmorillonite have two water layers in the interlayer position and sodium montmorillonite have one water layer. The water molecules that occur between the layers in smectite are called low temperature water which can be driven off by heating from 100°C to 150°C (Grim. 1968). The thickness of these water molecules between the montmorillonite layers is related to the exchangeable cation present. When sodium is the exchangeable cation, the water layer is about 2.5Å, which is one water layer and when calcium or magnesium is the exchangeable cation, then the layer is about 4.2-4.5 Å thick, which is two water layers.

2. Product of interest

The pellet which is of interest in this study is a commercially produced pellet (DantoPlug Super) which is used by many drilling companies in Denmark. The raw bentonite is mined on Tåsinge in Denmark and the pellets are produced by Dantonit. The pellet is cylindrical in its design, with an average diameter of 8 mm. The ends are irregular fractured surfaces. The color is dark brown to dark olivine green (Photo 1).

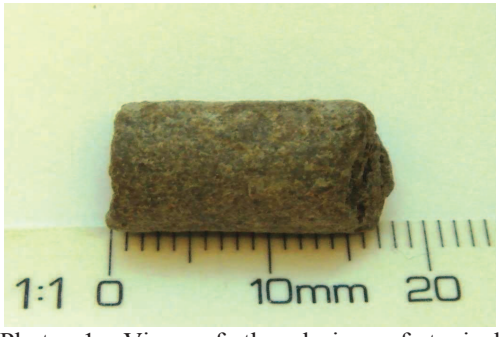

Photo 1: View of the design of typical DantoPlug Super pellet with 8 mm diameter.

3. Tåsinge Bentonite

The most important bentonite deposit in Denmark is located near Bjerreby on Tåsinge. Tåsinge is a small island in the southern part of Denmark (Figure 2). On the location the following deposits have been recognised (see Figure 3.1), starting from top:

- *Glacial deposits, Quaternary*
- *Marine clay (Ølst Fm.), Early Eocene (55.5-54 mio. years)*
- *Marine clay (Holmehus Fm.), Late Paleocene (59-57.5 mio. years)*

The clay deposits found at Bjerreby on the island of Tåsinge is late Paleocene to early Eocene of age. In time, this corresponds approximately to 59-50 million years. It should be noted that between two formations a distinct time gap (hiatus) is present (Figure 3.2.). A time gap can indicate two things. Either no depositions have occurred or the deposits have been eroded away. Either way it must be expected that the sedimentary succession described above and on Figure 3 does not show a continuous lithology change when crossing the boundaries' between two formations. Figure 3.2., show the natural succession of the different formations found in the well at Bjerreby. As can be seen, a sequence which contain Holmehus Fm. and Ølst Fm. is repeated 4 time. Neo-techtonic or Glacio-techtonic can explain this repetition. Each sequence has been forced up upon each other by the movement of ice. The deposits have been described in details by Torp and Larsen (1997) and Larsen (1998).

Figure 2: Location of Tåsinge in Denmark.

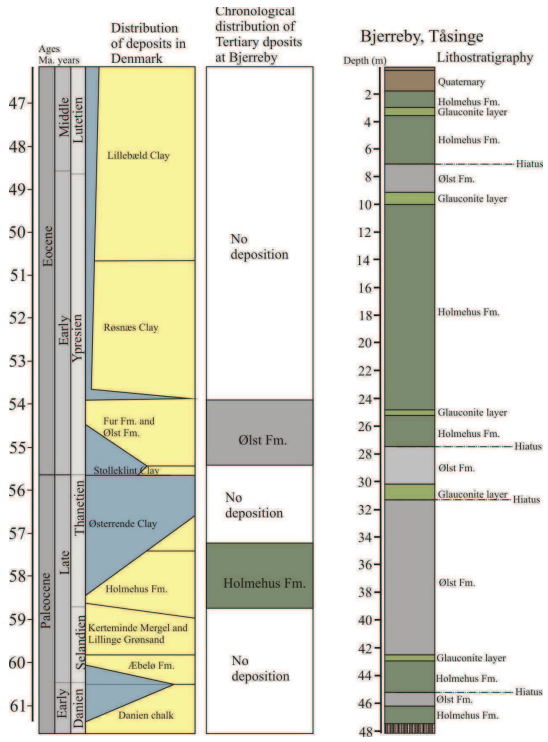

Figure 3.1 and 3.2: The chronological distribution of Tåsinge Bentonite at Bjerreby.

4. Depositional Environment

In early Mid-Paleocene (c. 61 Ma), extrusion of flood basalts started almost simultaneously in a wide area extending from the British Isles, over the Faroe Islands, East and West Greenland to Baffin Island forming first phase of the opening of the North Atlantic (Saunders et al., 1997). At the same time, a profound change to the marine clay-regime took place in the Danish area after nearly 40 million years of chalk-deposition. The cause for this shift is probably a combination of increased clay input from erosion of the uplifted Shetland Platform and the new basalt covered areas and severed connections between the North Sea Basin and the warm oceans to the south (Ziegler, 1990 and 1992; Clemmensen & Thomsen, 2005). Iilies (1949) and Spjeldnæs (1975) suggested that the remarkable absence of any coarse clastic particles in deposits so close to the Scandinavian Shield may have resulted from the presence of a thick vegetation cover on a landmass of low relief with only a moderate run-off directed to this area (Figure 4).

During the Middle and Late Paleocene, progressively deeper water and more offshore marine environments are represented by successive formations, including in Denmark the Kerteminde Marl, Ælbelø Formation and culminating in the Upper Paleocene Holmehus Formation (Heilmann-Clausen et al., 1985, and Schmitz et al., 1996). The Holmehus Clay Formation represents the first phase of very fine grained clay sedimentation in the Danish area. The regional deepening may be due to subsidence during reduced activity from the Proto-Icelandic hotspot (Knox, 1996).

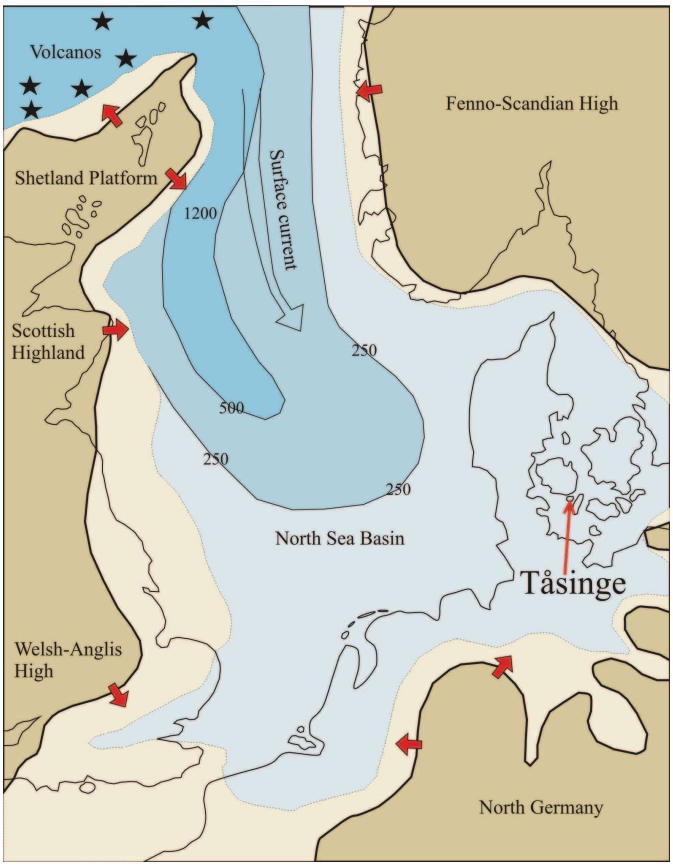

Figure 4: Paleogeography in the Late Paleocene and lower Eocene

The Paleocene – Eocene (P/E) boundary (c. 55.8 Ma) coincides with the beginning of a thermal maximum, the PETM, an extreme global warming event lasting c. 200.000 years. The second phase of the opening of the North Atlantic peaked at about the same time along the final line of opening of the NE Atlantic extruding >5 km of flood basalts in E Greenland and >2 km in the Faroe Islands. Thus during the PETM the Danish area was reduced to a stagnant, lake-like water body (Knox & Harland, 1979). The major sea-level fall was probably caused by a new updoming of the entire NE Atlantic region in connection with the second phase of increased hotspot activity (Knox, 1996; Jones & White, 2003). This event is properly responsible for

the time gap which is seen on the location on Tåsinge, between the Holmehus Clay Fm. and Ølst Clay Fm. The boundary between the Holmehus Formation and the overlying Ølst Formation is sharp and the difference in the lithology show a marked change in the depositional environment. Numerous basaltic ash beds occur in the overlying succession all over the North Atlantic–NW European region (Danish area) as far away as 1900 km from the assumed source within the North Atlantic rift zone (Egger & Bruckl, 2006). This ash series, the 'positive series' of Bøggild (1918) is best known from NW Denmark where it is well exposed in a 60 m thick diatomite, the Fur Formation (Heilmann-Clausen, 2006).

The Ølst Clay Fm. which is seen on Tåsinge is deposit at the same time as Fur Fm. The extremely violent volcanism suggests that the volcanic edifices were located in shallow water (Waagstein & Heilmann-Clausen, 1995; Larsen et al., 2003). The thickest of the ash layers are among the largest basaltic ash-falls known in geological history, and they may have contributed to the global cooling after the PETM (Egger & Brückl, 2006).

The presence of glauconite indicates that the boundary probably coincides with a period of submarine non-deposition. The oldest part of the Ølst Formation, a thick laminated clay sequence devoid of evidence for benthonic life, was deposited over a long period when anoxic conditions prevailed in the bottom waters. The laminae indicate water depths just below wave base (relatively shallow). An increased amount of clastic silt particles in the oldest part of the Ølst Formation seems to reflect the regressive conditions which occurred at that time in northwestern Europe. Duing the Early Eocene (Ypresian) the sea level rose gradually. The existence of thick and abundant ash layers in the upper part of the Ølst and Fur Formations shows that the most intensive volcanism in the Danish area must have taken place during the deposition of these units. The large amount of smectite in the Late Paleocene and Eocene sediments is believed to be derived mainly from weathering of pyroclastic rocks, resulting from this volcanism. The smectites in the Cenozoic North Sea sediments are generally believed to originate from transformation of volcanic ash from eruptions during the late Paleocene and early Eocene, related to the opening of the north Atlantic Ocean between Norway and Greenland. The proportion of smectite generally decreases upwards from the Lower Eocene sediments (Nielsen, 1994).

5. Lithology

In the following, a general short description of the lithology and distribution of the deposits mentioned above will be given, starting with the oldest deposits.

Holmehus Fm.

Non-calcareous, greenish, brownish and dark reddish, very fine-grained clay. The clay is almost exclusively composed of smectite, and the very minor sand fraction consists mainly of diagenetic products. The maximum known thickness is approximately 12 m in the LB 38 borehole at northern Lillebælt and in the Viborg 1 borehole in central Jutland (Heilmann-Clausen et al., 1985). The Holmehus Fm. is widely distributed in the Upper Paleocene of Denmark, as is evident from borehole material specified in Gry (1935) and Dinesen et al. (1977).

Ølst Fm.

A sequence of clays interbedded with beds and laminae of volcanic ash, partly argillized. The clays are sandy, silty and non-calcareous. The colour is mainly dark grey. The clay is finely laminated in the lower part, while in the upper part both laminated and structureless intervals are present (Heilmann-Clausen et al., 1985). The volcanic ash beds are graded sandy and clayey silts of blackish or grey colour. The ash beds, numbered from -1-1 to -H20 (Andersen 1937a), are closely spaced and their total thickness is approximately equal to the thickness of the clay in between, while the layers below are usually widely spaced and inconspicuous. The Ølst Formation is known throughout the distribution area of the Danish Paleocene. The thickness varies between 29 m and 9.3 m. In the western Limfjord area the Ølst Formation, is replaced by the Fur Formation (Heilmann-Clausen et al., 1985).

6. Mineralogical and geochemical characterisation

Mineralogy and geochemical analyses has been performed by the British Geological Survey (Kemp et al., 2008). The full rapport is found in Appendix 2.

Both the raw Tåsinge bentonite and the final bentonite product have been analysed. To determine the *mineralogy,* X-ray diffraction (XRD) analysis were used while *geochemistry* was to be determined using of major element X-ray fluorescence spectroscopy (XRFS). The results of whole-rock XRD analysis (mineralogy) are summarized in Table 1 and discussed below.

Table 1. Mineralogy

	Raw Tåsinge bentonite	**Bentonite pellets**
albite	6.7	6.4
calcite	<0.5	<0.5
chlorite	1.8	1.0
clinoptilolite	2.1	1.8
dolomite	nd	nd
gypsum	1.2	nd
K-feldspar	5.8	5.0
'mica'	10.0	10.6
pyrite	nd	nd
quartz	14.0	13.6
montmorillonite	58.0	61.2

XRD analysis of the samples indicates that they have a similar mineralogy and are predominantly composed of a smectite-group mineral (mean c.60%) together with minor quartz (mean c.14%), albite (mean c.7%), K-feldspar (mean c.6%) and undifferentiated mica (mean c.10%) and traces of chlorite (mean c.1%), clinoptilolite (mean c.2%) and calcite (mean <0.5%). A *d*(060) spacing of c.1.50 Å suggests that the smectite-group mineral in the samples is dioctahedral and likely to be montmorillonite. A *d*(001) spacing of c.12.2Å suggests that the interlayer cations of the montmorillonite are dominated by monovalent species such as Na+. The results of major element geochemical analysis of the samples by X-ray fluorescence spectrometry (XRFS) can be seen in Appendix 2.

The most important result in this analysis is the relative high concentration of Fe_2O_3 (approximately 9%). Since XRD analysis (Table 1) did not identify any major Fe-bearing minerals in the samples, the relatively high Fe_2O_3 concentration in these samples suggests that the smectite-group mineral is a Fe-rich species.

Appendix 2

Mineralogical and geochemical characterisation of bentonite samples for Dantonit

British Geological Survey
NATURAL ENVIRONMENT RESEARCH COUNCIL

Mineralogical and geochemical characterisation of bentonite samples for Dantonit Ltd

Laboratory Operations Programme

Commissioned Report CR/08/074

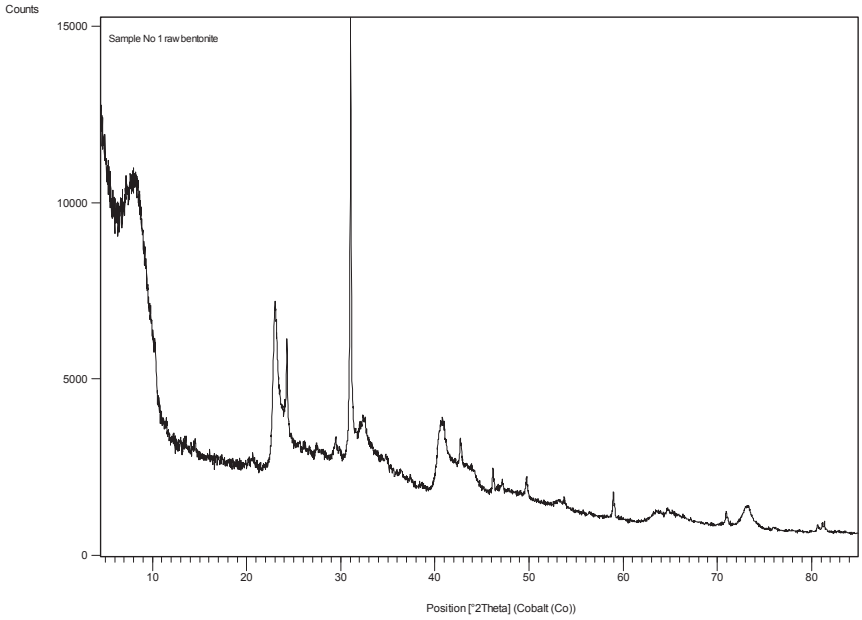

BRITISH GEOLOGICAL SURVEY

LABORATORY OPERATIONS PROGRAMME
COMMISSIONED REPORT CR/08/074

Mineralogical and geochemical characterisation of bentonite samples for Dantonit Ltd

S J Kemp, D Wagner and H M Harrison

Keywords

X-ray diffraction; X-ray fluorescence spectrometry, bentonite, smectite

Front cover

Whole-rock X-ray diffraction trace, sample no. 1 raw bentonite

Bibliographical reference

KEMP, S J, WAGNER, D AND HARRISON, H M. 2008. Mineralogical and geochemical characterisation of bentonite samples for Dantonit Ltd. *British Geological Survey Commissioned Report*, CR/08/074. 20pp.

Keyworth, Nottingham British Geological Survey 2008

BRITISH GEOLOGICAL SURVEY

The full range of Survey publications is available from the BGS Sales Desks at Nottingham and Edinburgh; see contact details below or shop online at www.thebgs.co.uk

The London Information Office maintains a reference collection of BGS publications including maps for consultation.

The Survey publishes an annual catalogue of its maps and other publications; this catalogue is available from any of the BGS Sales Desks.

The British Geological Survey carries out the geological survey of Great Britain and Northern Ireland (the latter as an agency service for the government of Northern Ireland), and of the surrounding continental shelf, as well as its basic research projects. It also undertakes programmes of British technical aid in geology in developing countries as arranged by the Department for International Development and other agencies.

The British Geological Survey is a component body of the Natural Environment Research Council.

Keyworth, Nottingham NG12 5GG

☎ 0115-936 3241 Fax 0115-936 3488
e-mail: sales@bgs.ac.uk
www.bgs.ac.uk
Shop online at: www.thebgs.co.uk

Murchison House, West Mains Road, Edinburgh EH9 3LA

☎ 0131-667 1000 Fax 0131-668 2683
e-mail: scotsales@bgs.ac.uk

London Information Office at the Natural History Museum (Earth Galleries), Exhibition Road, South Kensington, London SW7 2DE

☎ 020-7589 4090 Fax 020-7584 8270
☎ 020-7942 5344/45 email: bgslondon@bgs.ac.uk

Forde House, Park Five Business Centre, Harrier Way, Sowton, Exeter, Devon EX2 7HU

☎ 01392-445271 Fax 01392-445371

Geological Survey of Northern Ireland, Colby House, Stranmillis Court, Belfast, BT9 5BF

☎ 028-9038 8462 Fax 028-9038 8461

Maclean Building, Crowmarsh Gifford, Wallingford, Oxfordshire OX10 8BB

☎ 01491-838800 Fax 01491-692345

Sophia House, 28 Cathedral Road, Cardiff, CF11 9LJ

☎ 029–2066 0147 Fax 029–2066 0159

Parent Body

Natural Environment Research Council, Polaris House, North Star Avenue, Swindon, Wiltshire SN2 1EU

☎ 01793-411500 Fax 01793-411501
www.nerc.ac.uk

Contents

TABLES

1 Introduction

This report presents the results of mineralogical and geochemical characterisation of a suite of five bentonite samples submitted for analysis by Hasse Clemmensen, Dantonit, Denmark. The client specifically requested montmorillonite (smectite) content be assessed using X-ray diffraction (XRD) analysis while geochemistry was to be determined using a combination of major element X-ray fluorescence spectroscopy (XRFS) and carbon and sulphur analyses.

The samples were submitted in various forms from raw lump form to crushed material. Full sample details and the analyses undertaken are listed in Table 1. Although XRFS analysis was only requested for 3 of the samples, BGS were able to complete XRFS on all 5 samples due to the imposition of a minimum charge.

Table 1. Summary of samples and analyses undertaken

Incoming code	BGS MPL code	Analyses undertaken		
		XRD	XRFS	C and S
Sample No 1 raw bentonite	MPLN332	✓	✓	✓
Sample No 2 activated bentonite	MPLN333	✓	✓	✗
Sample No 3 dried activated bentonite	MPLN334	✓	✓	✗
Sample No 4 crushed bentonite 0-1mm	MPLN335	✓	✓	✓
Sample No 5 reference bentonite	MPLN336	✓	✓	✓

2 Laboratory methods

2.1 GENERAL SAMPLE PREPARATION

The samples were prepared in the BGS Sample Preparation Facility. They were firstly dried at 55°C overnight and then tema-milled to <125 μm.

2.2 X-RAY DIFFRACTION ANALYSIS

2.2.1 Preparation

In order to achieve a finer and uniform particle-size for whole-rock XRD analysis, approximately 3 g portions of the tema-milled material was micronised under acetone for 5 minutes and dried at 55°C. The dried material was then disaggregated in a pestle and mortar and back-loaded into standard stainless steel sample holders for analysis.

2.2.2 Analysis

Whole-rock XRD analysis was carried out using a PANalytical X'Pert Pro series diffractometer equipped with a cobalt-target tube, X'Celerator detector and operated at 45kV and 40mA. The micronised samples were scanned from 4.5-85°2θ at 2.76°2θ/minute. Diffraction data were initially analysed using PANalytical X'Pert Highscore Plus version 2.2a software coupled to the latest version of the International Centre for Diffraction Data (ICDD) database.

Following identification of the mineral species present in the sample, mineral quantification was achieved using the Rietveld refinement technique (e.g. Snyder & Bish, 1989) using PANalytical Highscore Plus software. This method avoids the need to produce synthetic mixtures and involves the least squares fitting of measured to calculated XRD profiles using a crystal structure databank. Errors for the quoted mineral concentrations are typically ±2.5% for concentrations >60 wt%, ±5% for concentrations between 60 and 30 wt%, ±10% for concentrations between 30 and 10 wt%, ±20% for concentrations between 10 and 3 wt% and ±40% for concentrations <3 wt% (Hillier *et al.*, 2001). Where a phase was detected but its concentration was indicated to be below 0.5%, it is assigned a value of <0.5%, since the error associated with quantification at such low levels becomes too large.

2.3 X-RAY FLUORESCENCE SPECTROMETRY

2.3.1 Preparation

The samples were dried overnight at 105°C before LOI and fusion. Fused beads for major element analysis were prepared by fusing 0.9 g sample plus 9.0 g flux (66/34 $Li_2B_4O_7$ and $LiBO_2$) at 1200°C. Loss on ignition (LOI) was determined on *c.*1 g sample heated at 1050°C for one hour.

2.3.2 Analysis

XRFS analysis was carried out using a sequential, fully automatic Philips PW2440 MagiX PRO wavelength-dispersive spectrometer, fitted with a 66 kV generator and a 4 kW rhodium end–window X-ray tube and controlled via PCs running PANalytical SuperQ (version 4.0D) XRF application software.

The work on determination of major and minor elements by XRFS by fused bead and loss on ignition (LOI) is covered under UKAS accreditation. The laboratory is a United Kingdom Accreditation Service (UKAS) accredited testing laboratory, No. 1816.

2.4 CARBON ANALYSIS

A known mass of sample was burnt in oxygen in an Exeter Analytical CE440 elemental analyser. The combustion gases were passed over suitable reagents to assure complete oxidation and removal of undesirable by-products such as sulphur, phosphorus and halogen gases. The oxides of nitrogen were converted to molecular nitrogen and residual oxygen was removed in the reduction tube. The concentrations of carbon dioxide, water vapour and nitrogen gas were measured by thermal conductivity cells. The instrument uses the concentration of these gases together with the sample weight to give a direct readout of the percentages of carbon, hydrogen and nitrogen.

2.5 SULPHUR ANALYSIS

A known mass of sample was incinerated at 1350ºC in an oxygen- enriched atmosphere in an Eltra Helios Sulphur Analyser. The sulphur in the sample was converted to sulphur dioxide and was measured by an infrared cell. The measured quantity was then converted into a percentage

3 Results

3.1 MINERALOGY

The results of whole-rock XRD analysis are summarised in Table 2 and labelled XRD traces are shown in the Appendix.

XRD analysis of samples 1-4 indicates that they have a similar mineralogy and are predominantly composed of a smectite-group mineral (mean c.60%) together with minor quartz (mean c.14%), albite (mean c.7%), K-feldspar (mean c.6%) and undifferentiated mica (mean c.10%) and traces of chlorite (mean c.1%), clinoptilolite (mean c.2%) and calcite (mean <0.5%). A *d*(060) spacing of c.1.50 Å suggests that the smectite-group mineral in samples 1-4 is dioctahedral and likely to be montmorillonite. A *d*(001) spacing of c.12.2Å suggests that the interlayer cations of the montmorillonite are dominated by monovalent species such as Na^+.

XRD analysis of the reference bentonite (sample 5) indicates a greater smectite-group mineral (c.73%) content together with minor albite (c.9%), quartz (c.6%), K-feldspar (c.4%) and undifferentiated mica (c.4%) and traces of chlorite (<0.5%), dolomite (<0.5%) and pyrite (<0.5%). A *d*(060) spacing of c.1.50 Å and a *d*(001) spacing of c.12Å suggests that the smectite-group mineral is also a montmorillonite whose interlayer cations are also dominated by monovalent species such as Na^+.

Note that the identification of clay mineral species in the samples is not definitive. Definitive identification would require isolation of a fine (typically <2 μm) fraction, the preparation of oriented mounts and the running of a diagnostic XRD testing program.

3.2 GEOCHEMISTRY

The results of major element geochemical analysis of the five samples by X-ray fluorescence spectrometry (XRFS) are summarised in Table 3. Fe_2O_3t represents total iron expressed as Fe_2O_3. SO_3 represents sulphur retained in the fused bead after fusion at 1200°C.

Because of limitations with the current software used for reporting data, the number of significant figures quoted in the attached table may not be representative of the actual uncertainty. Data should be considered accurate to no more than three significant figures.

XRFS analysis indicate very similar major element concentrations and loss on ignition (LOI) figures for samples 1-4, suggesting similar compositions. Samples 1-4 appear to be SiO_2, Fe_2O_{3t}, K_2O -rich and Al_2O_3, CaO, MgO, Na_2O –poor compared to the reference bentonite.

Since XRD analysis did not identify any major Fe-bearing minerals in samples 1-4, the relatively high Fe_2O_{3t} concentrations in these samples suggests that the smectite-group mineral is an Fe-rich species.

Total carbon for samples 1 and 4 (0.29 and 0.40%) are low compared with 2.10% for the reference bentonite (Table 4) Total sulphur values (Table 4)of 0.12% (sample 1) and 0.07% (sample 4) are also lower than the value obtained for the reference bentonite (0.18%).

4 Conclusions

Mineralogical and geochemical analyses have been completed on a suite of 5 bentonites.

- XRD analyses reveal approximately similar mineralogies for samples 1-4 with smectite contents of c.60% together with minor quartz, albite, K-feldspar and undifferentiated mica and traces of chlorite, clinoptilolite and calcite.
- XRD analysis of the reference bentonite (sample 5) indicates a higher smectite content of c.73% with minor quartz, albite, K-feldspar, calcite and undifferentiated mica and traces of chlorite, dolomite and pyrite.
- XRFS analyses and LOI figures indicate similar geochemistries for samples 1-4.
- XRFS analysis indicate that samples 1-4 are SiO_2, Fe_2O_{3t}, K_2O -rich and Al_2O_3, CaO, MgO, Na_2O –poor compared to the reference bentonite..
- Total carbon and sulphur values are lower than those obtained for the reference bentonite.

Table 2. Summary of quantitative whole-rock XRD analyses

Incoming sample name	BGS MPL code	mineral (%)										
		albite	calcite	chlorite	clinoptilolite	dolomite	gypsum	K-feldspar	'mica'	pyrite	quartz	montmorillonite
Sample No 1 raw bentonite	MPLN332	6.7	<0.5	1.8	2.1	nd	1.2	5.8	10.0	nd	14.0	58.0
Sample No 2 activated bentonite	MPLN333	6.4	<0.5	1.0	1.8	nd	nd	5.0	10.6	nd	13.6	61.2
Sample No 3 dried activated bentonite	MPLN334	6.6	<0.5	1.3	1.4	nd	nd	5.5	10.3	nd	14.2	60.5
Sample No 4 crushed bentonite 0-1mm	MPLN335	6.9	<0.5	1.8	1.6	nd	nd	6.2	10.5	nd	14.4	58.2
Sample No 5 reference bentonite	MPLN336	9.2	3.0	<0.5	nd	<0.5	nd	4.4	3.8	<0.5	6.3	72.9

KEY to Table 2

nd = not detected

*Note – clay mineral identifications are not definitive.

Table 3. Summary of XRF geochemical analysis

Incoming sample no.	BGS MPL code	SiO_2	TiO_2	Al_2O_3	Fe_2O_{3t}	Mn_3O_4	MgO	CaO	Na_2O	K_2O	P_2O_5	SO_3	Cr_2O_3	SrO	ZrO_2	BaO	NiO	CuO	ZnO	PbO	LOI	Total
		%																				
1	MPLN332	59.64	0.87	16.13	9.06	0.15	3.14	1.04	1.17	2.78	0.14	0.3	0.02	0.04	<0.02	0.06	0.02	<0.01	0.02	<0.01	6.07	100.65
2	MPLN333	58.84	0.82	15.98	9.08	0.24	3.17	1.00	2.12	2.76	0.16	0.4	0.02	0.04	<0.02	0.07	0.01	<0.01	0.02	<0.01	6.18	100.91
3	MPLN334	58.90	0.82	15.92	8.99	0.22	3.15	1.01	2.11	2.75	0.17	0.2	0.02	0.04	<0.02	0.06	0.01	<0.01	0.02	<0.01	6.09	100.48
4	MPLN335	58.95	0.82	15.98	9.02	0.13	3.17	1.07	2.11	2.76	0.19	0.2	0.02	0.05	<0.02	0.07	0.01	<0.01	0.02	<0.01	6.08	100.65
5	MPLN336	56.34	0.73	17.65	5.64	0.06	3.49	3.16	3.05	0.70	0.15	0.3	<0.01	0.02	<0.02	0.10	<0.01	<0.01	0.01	<0.01	9.37	100.77

KEY to Table3

Fe_2O_3t represents total iron expressed as Fe_2O_3.

SO_3 represents sulphur retained in the fused bead after fusion at 1200°C.

Table 4. Summary of carbon and sulphur analyses

Incoming sample name	BGS MPL code	Total sulphur	Total carbon
		%	%
Sample No 1 raw bentonite	MPLN332	0.12	0.29
Sample No 4 crushed bentonite 0-1mm	MPLN335	0.07	0.40
Sample No 5 reference bentonite	MPLN336	0.18	2.10

References

Most of the references listed below are held in the Library of the British Geological Survey at Keyworth, Nottingham. Copies of the references may be purchased from the Library subject to the current copyright legislation.

HILLIER, S., SUZUKI, K. AND COTTER-HOWELLS, J. 2001. Quantitative determination of Cerussite (lead carbonate) by X-ray powder diffraction and inferences for lead speciation and transport in stream sediments from a former lead mining area of Scotland. *Applied Geochemistry*, 16, 597-608.

SNYDER, R.L. AND BISH, D.L. 1989. Quantitative analysis. In: Bish, D.L., Post, J.E. (Eds), *Modern Powder Diffraction, Reviews in Mineralogy*, Volume 20, Mineralogical Society of America, USA, pp. 101-144 (Chapter 5).

MOORE, D M AND REYNOLDS, R C. 1997. *X-Ray Diffraction and the Identification and Analysis of Clay Minerals, Second Edition.* Oxford University Press, New York.

REYNOLDS, R C AND REYNOLDS, R C. 1996. *Description of Newmod-for-Windows™. The calculation of one-dimensional X-ray diffraction patterns of mixed layered clay minerals*. R C Reynolds Jr., 8 Brook Road, Hanover, NH.

Appendix: X-RAY DIFFRACTION TRACES:

KEY

The upper figure on each page shows the sample diffraction trace. The lower figure shows stick pattern data for the extracted sample peaks (orange) and the identified mineral standard data. Vertical axis – intensity (counts), horizontal axis - °2θ Co-Kα.

Sample No 1 raw bentonite

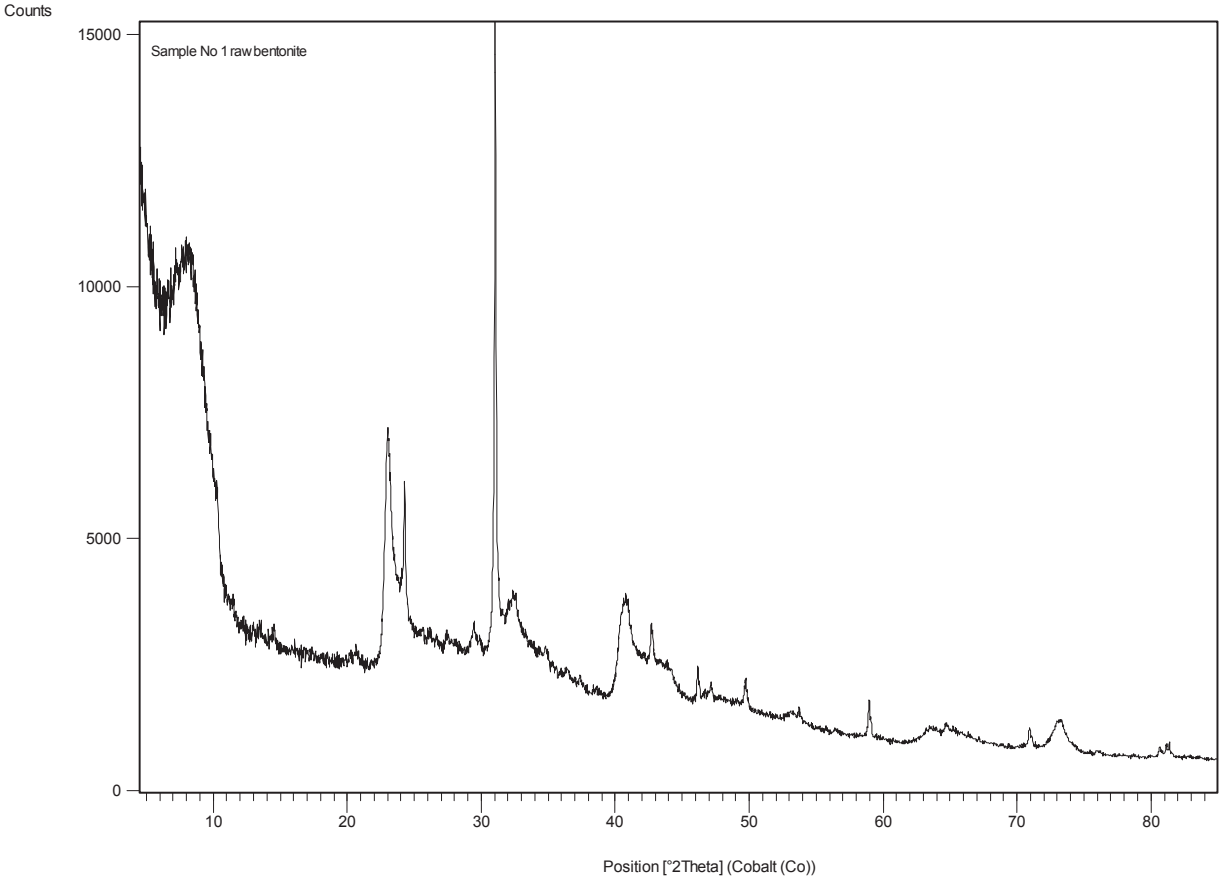

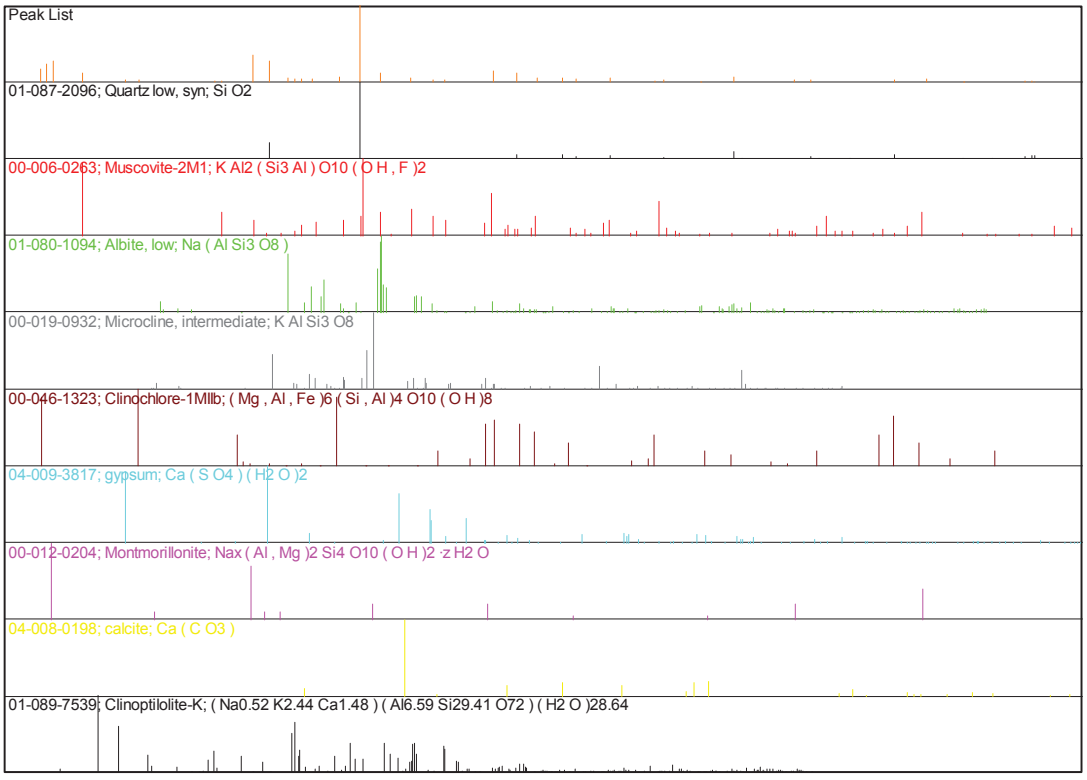

Sample No 2 activated bentonite

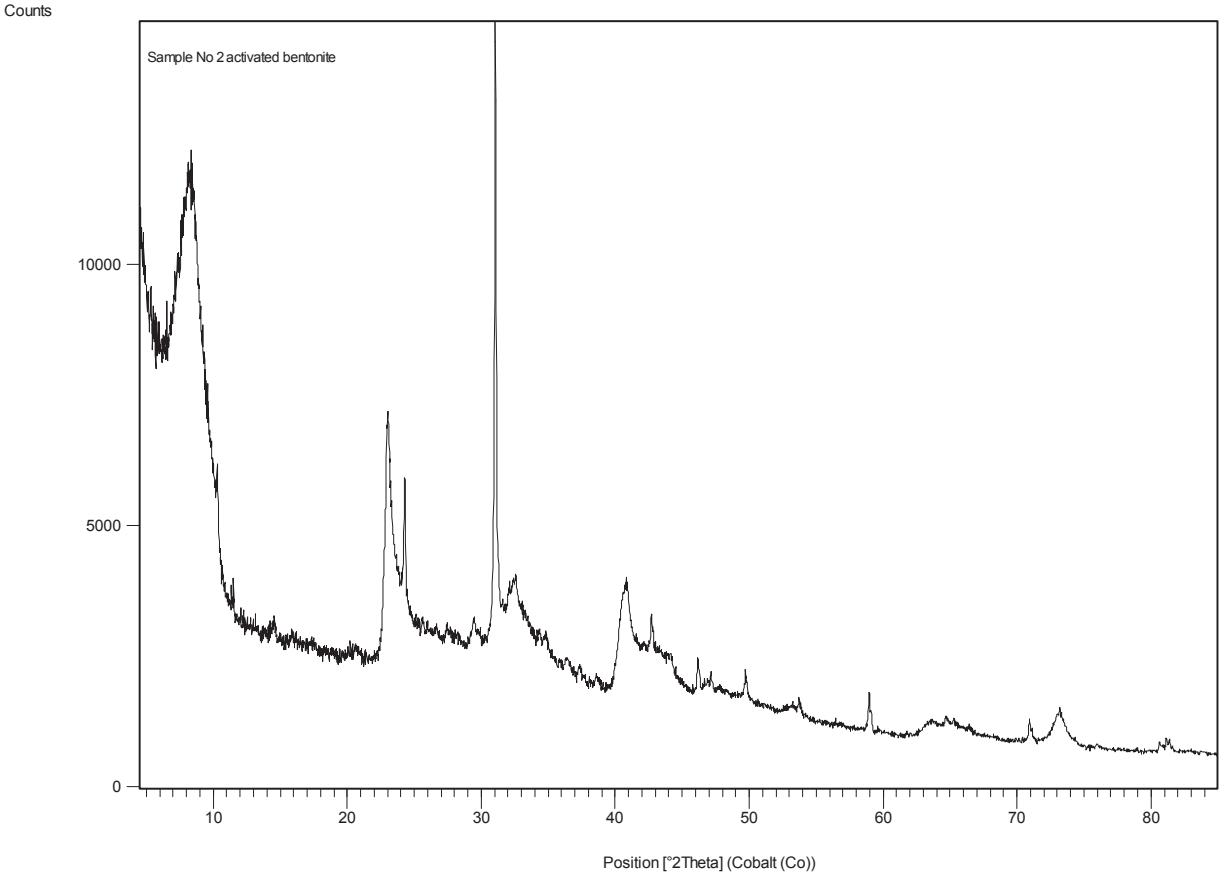

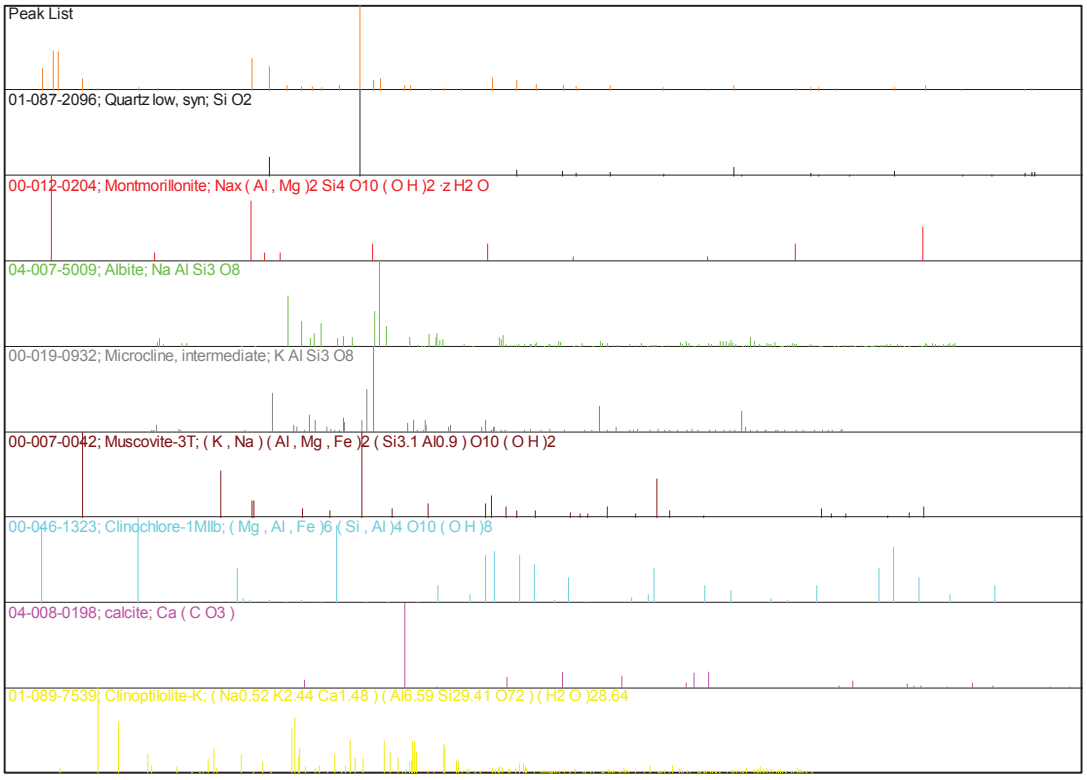

Sample No 3 dried activated bentonite

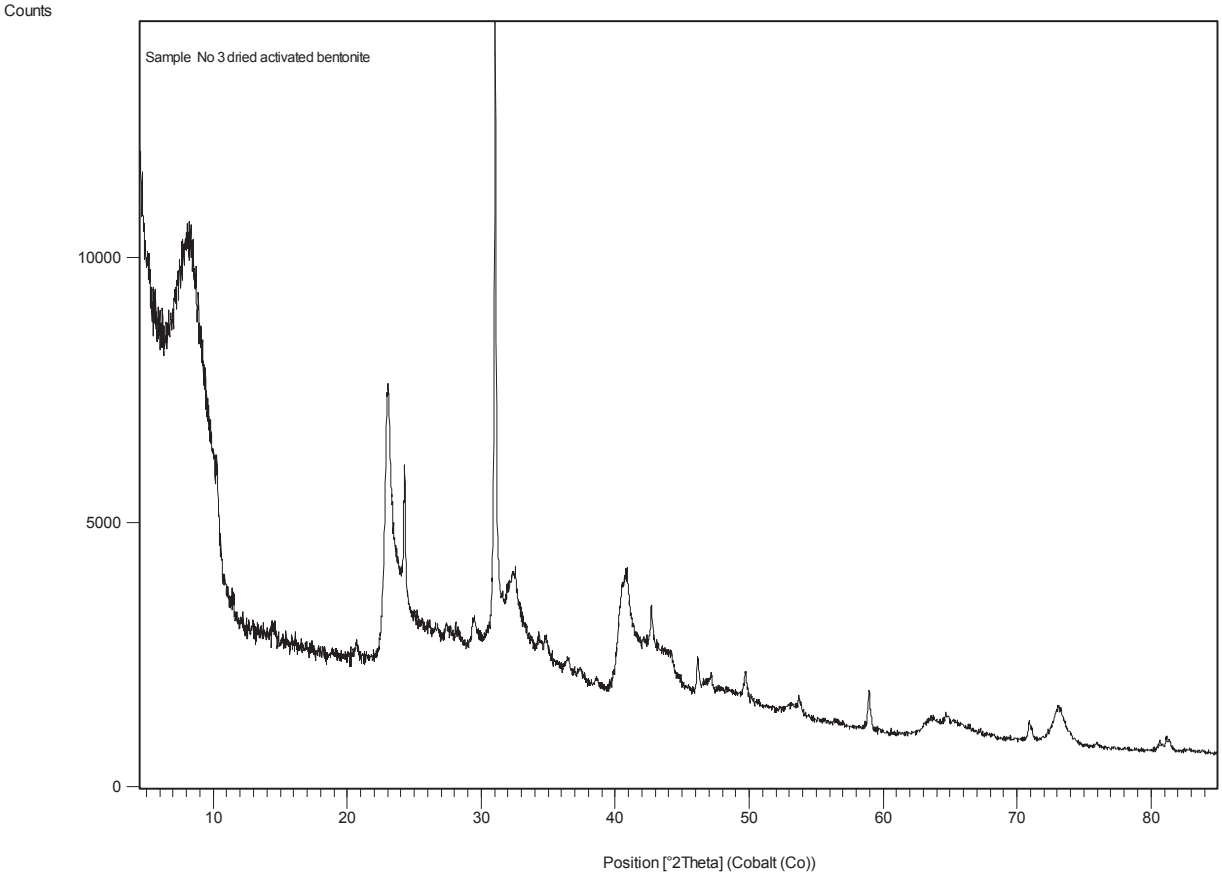

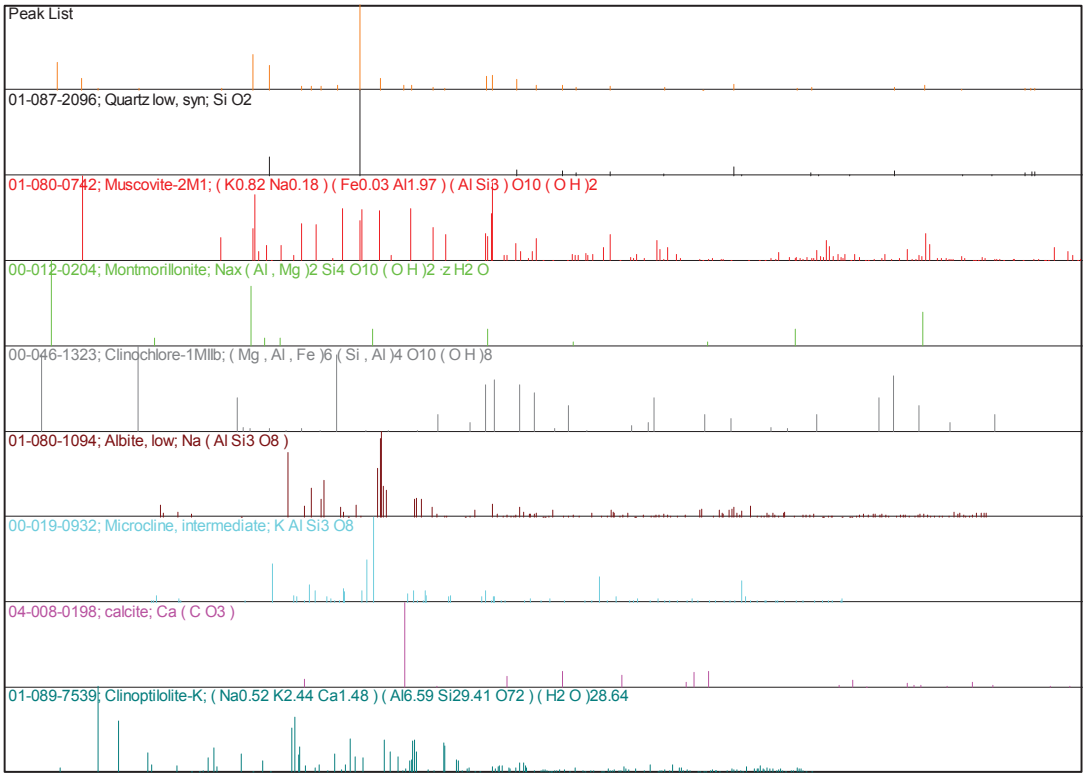

Sample No 4 crushed bentonite 0-1mm

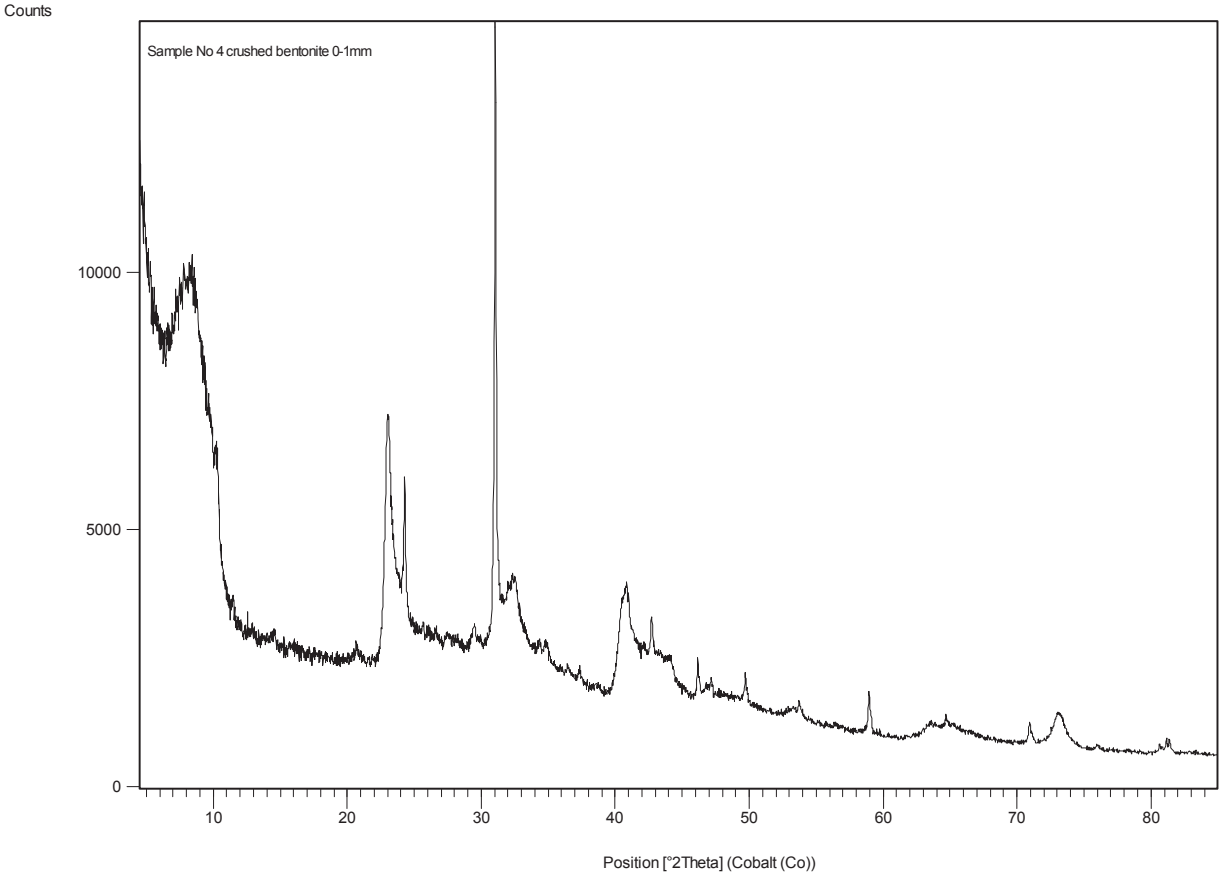

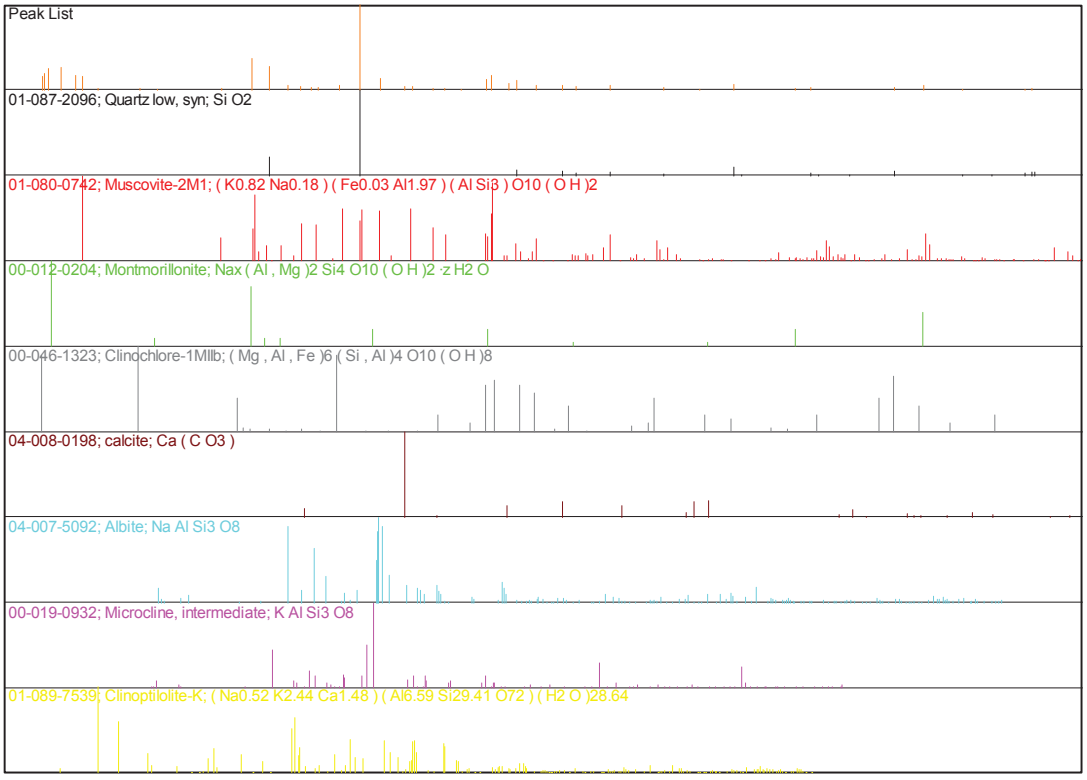

Sample No 5 reference bentonite

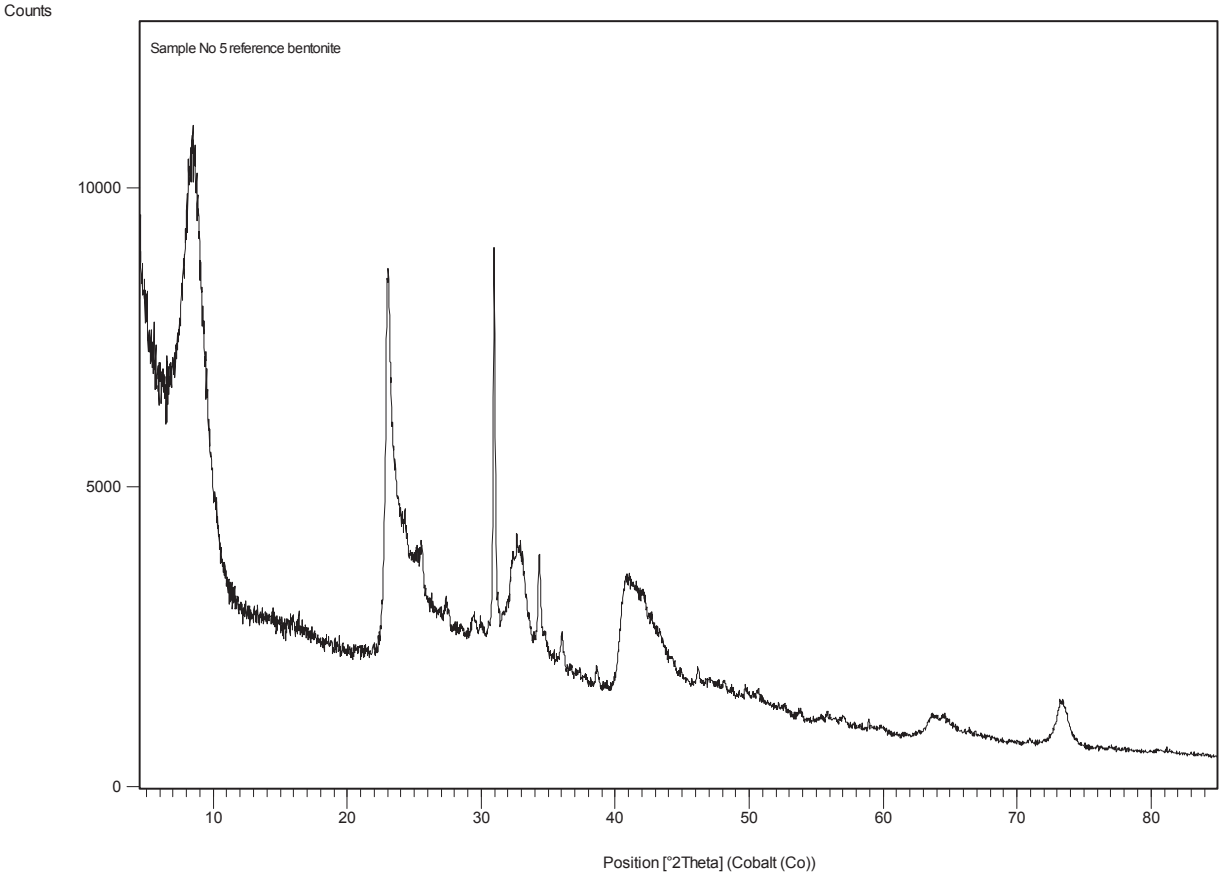

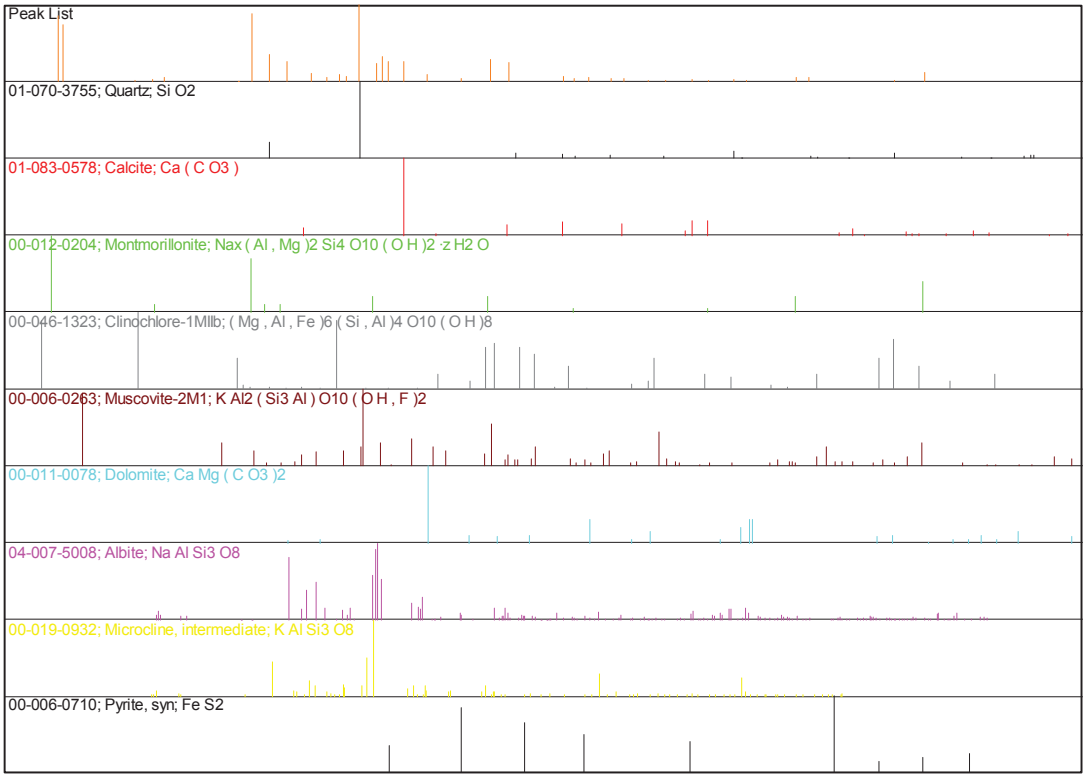

BRITISH GEOLOGICAL SURVEY

REPORT APPROVAL FORM

British Geological Survey
Kingsley Dunham Centre
Keyworth
Nottingham
United Kingdom
NG12 5GG

Tel (0115) 9363100
Fax (0115) 9363200

Report Title and Authors

Mineralogical and geochemical characterisation of bentonite samples for Dantonit Ltd

S J Kemp, D Wagner and H M Harrison

Client Name and Address	Client Report No.
Hasse Clemmensen Dantonit A/S Energivej 30 5260 Odense S	BGS Report No. **CR/08/074**
	Client Contract Ref.
	BGS Project Code **E8679, JN_08_003**
	Classification **Commercial in confidence**

Version	Status	Prepared by	Checked by	Approved by	Date
1	**-**	**S J Kemp**			

Appendix 3

Initial tests

1. Water content

The water molecules that occur between the layers in clay are called low temperature water which can be driven off by heating from 100°C to 150°C (Grim. 1968). It is defined as the ratio of the weight of water to the weight of the dry clay in the clay mass. The standard method of determining the moisture content is by over drying at 105-110 degrees Celsius over 24 hours. The low temperature water content of several samples (bentonite pellets) has been determined and they show an average water content of 25.44%.

The clay lattice also contains water which is tied very closely to the clay particles. It can only be driven off by heating to above 950°C. In this work, two samples have been subjected to increasing temperatures over time. The methods are basically the same as mentioned above (low temperature water). The weight of the sample has been measured continuously throughout the test period which lasted for 7 hours. The results are showed on figure 1.

The y-axis show the loss of mass in % and the x-axis show the temperature in °C. From 20°C to 150°C the loss in mass is approximately 25-26%, which corresponds very well with the results obtained from the low temperature water. From 150°C to 950°C an additionally decrease in loss of mass of 8.5% is seen. No loss in mass is seen in temperature above 950°C. The conclusion is that the final bentonite product contains approximately 25.44% low temperature water and approximately 8.5% high temperature water which is a total of 34 % water.

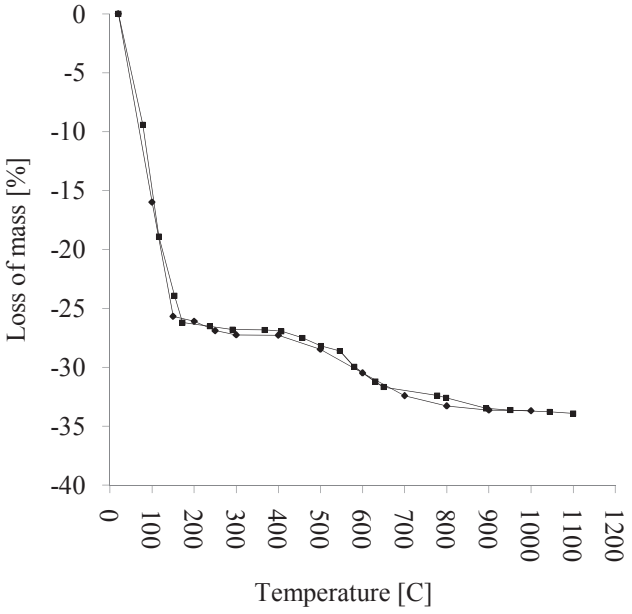

Figure 1: Show the results from the two test. 25.44 % of the water is driven off at temperatures around 100°C to 150°C. In addition to that 8.5 % of the water is driven off at temperatures between approximately 400°C to 950°C.

2. Stoichiometric composition of pellets

By summarizing section 1 (water content) and section 6 in Appendix 1, the following stoichiometric composition of pellets can be made. In section 6, it was found that the bentonite pellets contained 61.2% montmorillonite. This result was obtained after all the low temperature water has been driven off. In section 1, it was found that the bentonite pellets contained 25.44% low temperature water. If this number is added into the equation then the total amount of montmorillonite is only 45.6% and the amount of non-swelling components is 28.96%.

In addition to that, the high temperature water was found to comprise approximately 8.5% of the sample. By looking at the mineralogy (Tabel 1) it is obvious that the only place the high temperature water can be stored is in the montmorillonite. By subtracting 8.5% high temperature water from the 45.6% montmorillonite + high temperature water, we end up with a total amount of montmorillonite of 37.1% in a bentonite pellet.

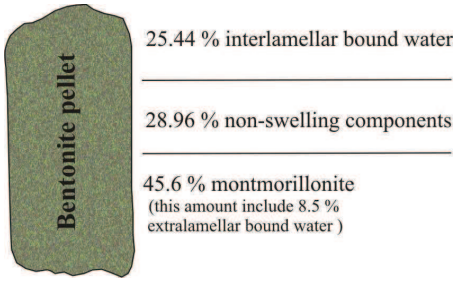

Figure 2: Schematic drawing of the composition of bentonite pellets

3. Density of material

The average density of the pellets has been determined in two different ways. The masses (m) of twenty randomly picked samples (bentonite pellets) were measured. Each sample was dropped into a test tube with water and the volume increase (V) was noted. The density (ρ) was calculated in the following way $\rho=m/V$. The mean value has been calculated to 2.02 g/cm^3 with a standard deviation of 0.07 g/cm^3. Based on geochemical data and the atomic mass of each component in the sample, it is possible to find the volume of that specific component. The density found in this way is 2.06 g/cm^3. In both cases it is assumed that the pellets contain 25.0 % interlamellar bounded water and approximately 4.6 % extralamellar bounded water.

4. Grain size distribution

The pellets used as sealing material in groundwater wells represent a great variation of grain sizes. The grain size distribution is of great importance when evaluating depositional pattern and swelling pressure.

The bentonite pellets will be sorted according to their maximal Feret diameter, d_F by using Digital Image Analysis (DIA). In general the Feret diameter is defined as the perpendicular distance between parallel tangents touching opposite sides of a given object (Figure 3).

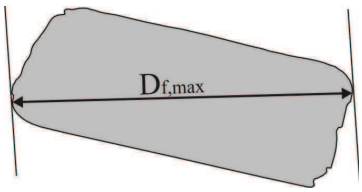

Figure. 3: Greatest Feret's Diameter (d_F), Feret's Length: The greatest distance between two parallel lines that do not intersect the image.

Methods

The grain size distribution has been performed using DIA. A high resolution Canon EOS450D camera with 12.2 megapixels was used for DIA. The photo image of the test section occupied about 2256*1504 pixels, and in all measurements the same gray level scale range 0-255, was considered. The camera was directly connected to- and controlled from a computer via a USB cable. Image processing, analysis and measurement were carried out using the free softwear, ImageJ ver. 1.43s. The aim of image processing is to obtain a binary image containing individual particle silhouettes from the original raw image.

A basic procedure of image processing includes filtering, overlapping particle segmentation, border killing, hole filling and debris removal. Digital Image Analysis consists of isolating an area of interest with ImageJ software. In this study the area of interest is always Bentonite pellets. Generally the images have a sufficient density contrast to isolate the area of interest by applying a simple gray level threshold (Figure 4A). After that, a binarization of the image was performed, in order to isolate the solid body of interest (Figure 4B). In addition each analysis was visually controlled. At Figure 4C the analyzed area has been outlined. In this process multiple parameters is registered of each particle in the image. In this study only the Feret diameter is of interest.

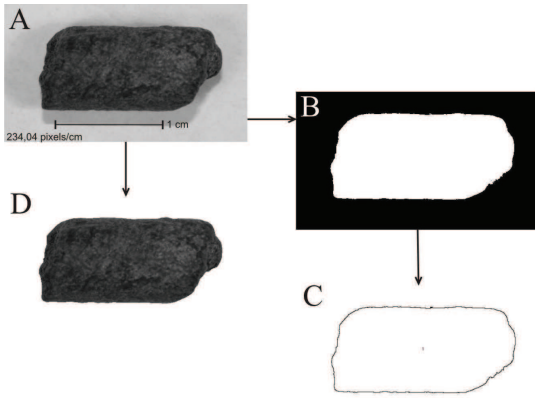

Figure 4: Digital image analysis methodology (DIA): (A) photo image, 2256x1504 pixels; (B) image binarization and isolation of the solid body of interest; (C) analyzed area has been outlined; (D) image reconstruction.

Results

The masses of fourty randomly picked pellets were measured and the pellets were photographed. By using, Digital Image Analysis (DIA) on each of the fourty images it is possible to measure the Feret diameter with great accuracy.

Figure 5 show the Feret diameter, $d_{F,}$ of the pellet versus the mass, m in the interval 8.62 mm $\leq d_F \leq$ 24.6 mm.

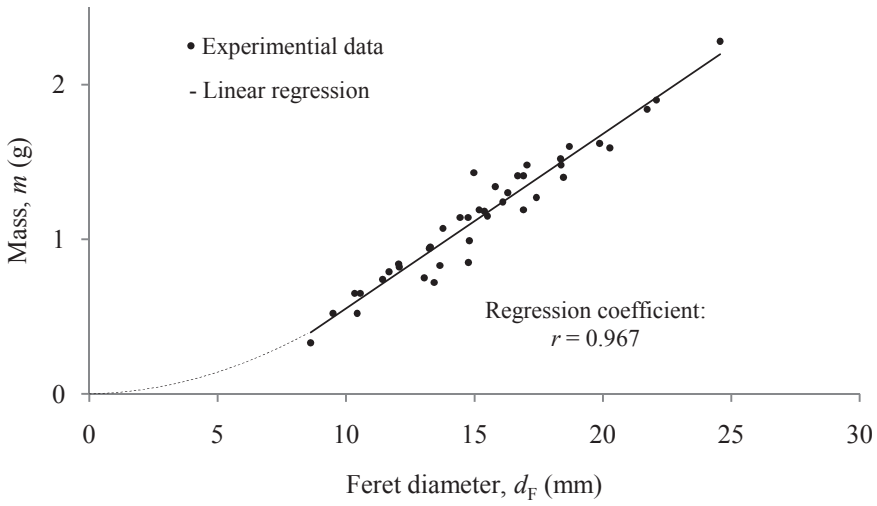

Figure 5: The Feret diameter versus the mass of the pellets. It can be seen that the relationship between the two can be expressed as a linear function.

A clear linear relationship is seen. This relationship can be represented by:

$$m = -0.58+1.13d_F \quad (1)$$

The linear model used to fit the Feret diameter vs. mass, is well correlated with the experimental data since the regression coefficient (r) estimated is close to 1. This expression must be assumed to be valid for d_F values above 24.6 mm. For d_F values below 8.62 mm and going towards 0 mm, the relationship can be expressed as a second order polynomial (dotted line on Figure 5).

Ten samples of randomly picked pellets was spread out on a sheet of white paper and within a square of 25x25 cm and then photographed and the images was analysed according to the above mentioned technique. Each sample was approximately 170g of weight. The pellets were subdivided into seven size intervals and the mass of each interval was calculated using Eq. (1). The grain size distribution is summarized in Table 1.

Table 1: Show the size distribution with respect to mass.

Size interval (cm)	Mass [%]
$0.2 < d_F \leq 0.4$	1.39
$0.4 < d_F \leq 0.6$	2.85
$0.6 < d_F \leq 1.0$	8.5
$1.0 < d_F \leq 1.5$	34.74
$1.5 < d_F \leq 1.8$	27.56
$1.8 < d_F \leq 2.0$	15.81
$2.0 < d_F \leq 2.5$	9.15

5. Bulk porosity based on grain size

A simple set of tests was made in order to examine the bulk porosity of pellets within the same size interval with respect to the feret diameter. Pellets were sorted into three groups. The first group had a maximum feret diameter of 1 cm, the second group was in the interval between 1 and 2 cm and the third group had minimum feret diameter above 2 cm. Test tubes with a known volume were then filled with pellets from each size interval. Not surprisingly the pellets from the group with a Feret diameter below 1 cm had a tendency to be packed more closely than the pellets from the groups with a larger Feret diameter which mean that more mass of material was found here. By simple calculations it was then possible to estimate the bulk porosity for the whole volume. It was found that the bulk porosity for the samples which only contained small pellets was found to be approximately 45%. The bulk porosity for the middle and large size interval was found to be approximately 50% and 58% respectively.

ISSN 1901-7294
DCE Thesis No. 29

AALBORG UNIVERSITY
Department of Civil Engineering